Robust Integrated Autopilot/Autothrottle Design

P203

Using Constrained Parameter Optimization

Uy-Loi Ly , Christopher Voth , Swamy Sanjay

Department of Aeronautics and Astronautics
University of Washington
Seattle, Washington 98195

Final Report

TABLE OF CONTENTS

LIST OF FIGURES

LIST OF TABLES

NOMENCLATURE

English Symbols

a	— bandwidth of a first-order command prefilter
a_{ij}	— ij^{th} element of the state matrix of a linear system
A	— state dynamics matrix of a linear system
B	— control input distribution matrix of a linear system
C	— state output distribution matrix of a linear system
CAS	— aircraft calibrated airspeed
D	— direct output distribution matrix of a linear system
D	— diagonal scaling matrix
D	— total aircraft drag
E	— total energy, i.e. kinetic energy plus potential energy
FPA	— aircraft flight-path angle
g	— gravitational acceleration
$G(s)$	— transfer function matrix of a linear dynamic system
h	— altitude above ground level
H	— external disturbance output distribution matrix for a linear system
j	— imaginary number defined by $j = \sqrt{-1}$
J_i	— quadratic performance index at the ith plant condition
k_1, k_2	— design parameters in velocity command variable
K	— a complex gain matrix
K	— a controller feedback gain
K_{TP}	— proportional feedback gain to the throttle
K_{TI}	— integral feedback gain to the throttle
K_{EP}	— proportional feedback gain to the elevator
K_{EI}	— integral feedback gain to the elevator
K_q	— pitch rate feedback gain to the elevator
K_θ	— pitch attitude feedback gain to the elevator
K_v	— airspeed error feedback gain to the throttle

K_h	— altitude error feedback gain to the elevator
L	— lagrangian variable
L	— turbulence scale length
m	— mass of aircraft
m	— number of controller outputs
n_{max}	— maximum number of independent controller parameters
N_p	— number of off-nominal plant models
N_R	— number of design requirements expressed in penalty functions
p	— design parameter vector in the controller matrices
p	— number of controller inputs
q	— aircraft pitch rate
Q	— output-weighting matrix in penalty function
r	— number of controller states
R	— control-input weighting matrix in penalty function
RMS	— root-mean-square
s	— time integration variable
s	— complex frequency, i.e. $s = \sigma + j\omega$
t	— time
T	— aircraft total engine thrust
T	— a similarity transformation matrix
$TECS$	— total energy control system
u	— aircraft x-axis velocity component
u	— control input to a dynamic system
v	— eigenvector of a matrix
V	— aircraft total velocity
w	— disturbance input to a dynamic system
W_i	— penalty function weighting assigned to the ith plant condition
W	— external disturbance covariance matrix
x	— state vector for a dynamic system
X	— state covariance matrix
y	— output of a dynamic system
Y	— output covariance matrix

Greek Symbols

α	— aircraft angle of attack
α	— angle between damping line and the negative real axis
α	— design destabilization factor
$\delta(t)$	— Dirac delta function
δ	— incremental control input to a linear system
ΔV	— airspeed error
Δh	— altitude error
ϵ	— accuracy of constraint on system eigenvalues
γ	— aircraft flight-path angle
Γ	— external disturbance input distribution matrix of a linear system
κ	— upper bound on the H^∞-norm of a transfer matrix
λ	— eigenvalue of a square matrix
$\mu(t)$	— unit step function defined as $\mu(t) = 0$ for $t < 0$ and $\mu(t) = 1$ for $t \geq 1$
ω_n	— undamped natural frequency
Φ	— power spectral density function of a random process
φ	— a scalar multiplier
σ	— real part of a complex number
σ	— value of constraint on real parts of eigenvalues
σ^2	— variance of a random variable
τ	— time variable
θ	— aircraft pitch attitude
ζ	— damping ratio of an eigenvalue
ζ	— value of damping constraint on system eigenvalues

Subscripts

act	— actuator model
c	— command input
c	— control input
cmd	— steady-state value of command
d	— disturbance model
ϵ	— error between commands and system outputs

f	— final value
GW	— aircraft gross weight
e	— elevator control
ec	— elevator command
ew	— disturbance input to elevator command path
i	— plant model index
i	— row index of a matrix element
i	— index of a vector element
IE	— integral of total energy rate error
IL	— integral of energy rate distribution error
m	— command model
p	— plant model
ss	— steady-state value
t	— time variable
th	— thrust per unit of aircraft gross weight
thc	— commanded thrust per unit of aircraft gross weight
thw	— disturbance input to throttle command path
Tc	— thrust command
u	— x-axis wind velocity component
w	— z-axis wind velocity component
0	— nominal plant condition
0	— initial value

Superscripts

(k)	— k^{th} performance requirement in a penalty function
$*$	— adjusted command variable in a performance index
$'$	— closed loop model

Mathematical Operators

$\lvert \cdot \rvert$	— absolute value operator
$\lVert \cdot \rVert_F$	— Frobenius norm of a matrix
$\lVert \cdot \rVert_\infty$	— infinity norm of a matrix
$E_\alpha[\cdot]$	— expectation operator for a system destabilized by a factor α

$e^{(\cdot)}$ — exponential function

$\bar{\sigma}$ — maximum singular value operator for a square matrix

$\underline{\sigma}$ — minimum singular value operator for a square matrix

sup   — supremum operator

$(\cdot)^T$ — matrix transpose

$tr(\cdot)$ — trace operator for a matrix

∂ — partial differential operator

d — ordinary differential operator

Summary

A multivariable control design method based on constrained parameter optimization has been applied to the design of a multiloop aircraft flight control system. Specifically, the design method is applied to

- Direct synthesis of a multivariable "inner-loop" feedback control system based on total energy control principles,

- Synthesis of speed/altitude-hold designs as " outer-loop" feedback/feedforward control systems around the above inner loop,

- Direct synthesis of a combined "inner-loop"and "outer- loop" multivariable control system.

The design procedure offers a direct and structured approach for the determination of a set of controller gains that meet design specifications in closed-loop stability, command tracking performance, disturbance rejection, and limits on control activities. The presented approach may be applied to a broader class of multiloop flight control systems. Direct tradeoffs between many real design goals are rendered systematic by this method following careful problem formulation of the design objectives and constraints. Performance characteristics of the optimized design have been improved over the current autopilot design on the B737-100 Transport Systems Research Vehicle (TSRV) at the landing approach and cruise flight conditions; particularly in the areas of closed-loop damping, command responses and control activity in the presence of turbulence.

Chapter 1

INTRODUCTION

Recent development in multivariable control design techniques have been focused on the improvement of controller performance and robustness to uncertainties in the plant model. Modern control system design methods such as LQG/LTR, H∞, and μ-synthesis can provide controllers with high levels of performance and robustness [Refs.1-3]. However, the controllers obtained with these techniques are usually of high order. The number of controller states is usually greater than or equal to the number of states in the plant model. Controller order must subsequently be reduced for the final design implementation. In addition, these design methods do not provide direct tradeoffs between many real design performance and robustness measures. Alternative methods based on output feedback are available [Refs.4-6] to synthesize controllers of low dimensionality. In particular, the design algorithm developed in Reference 6 provides a convenient framework for designing optimal low-order controllers. Recent extension of this method [Ref.7] and the use of constrained nonlinear optimization [Ref.8] enable designers to address conveniently those requirements, for example, eigenvalue and covariance constraints, that are not easily expressible in terms of an objective function based on quadratic performance indices.

Traditionally, classical design procedures based on single-loop closure and root-locus have been applied to the design of multiloop control systems. Designs obtained with conventional methods can have minimally achieved performance and inadequate robustness to plant model uncertainties. Tradeoffs between performance and robustness requirements are far from simple and can be time-consuming; especially when the designer lacks appropriate past design experiences or when he is faced with a non-conventional design case. Furthermore, the classical design procedures often overlook, due to their single-input/single-output nature, the intrinsic multivariable aspects of the design problem. As a result, the controllers may not contain appropriate cross-feed among individual feedback loops, and thereby limiting the maximally achievable performance.

Complexities in present automatic flight control systems (AFCS) for commercial transport aircraft are generally associated with the lack of suitable control system design integration, i.e crossfeed among different control paths. Recent work by Lambregts [Refs.9-11] on the NASA B737-100 Transport System Research Vehicle (TSRV), in improving the operation of the AFCS, has led to the development of a total energy control system (TECS) for an integrated autothrottle/autopilot design. The design philosophy incorporates fundamental aspects of the aircraft dynamics in the formulation of a multiloop controller structure. This innovative design approach has led to a controller structure that contains key cross-coupling between the elevator and throttle control loops for improved performance. Selection of the feedback gains was still performed using classical design procedures [Refs.9-14]. To satisfy multiple design requirements such as closed-loop stability, control and command bandwidths, control activities in the presence of turbulence, design robustness to modeling uncertainties, the one-loop-at-a-time iterative procedure can be overly time-consuming.

Initial design and evaluation of the TECS concept were performed on the NASA B-737-100 Transport Systems Research Vehicle (TSRV) [Refs.12-14]. Selection of the feedback gains was still a labor-intensive process even though the philosophy of TECS has inherently reduced the number of design parameters in the control-law structure. Again classical SISO design procedures without the benefits of past design experiences provides little insight into the design tradeoff; particularly when the number of constraints and design variables become large. Resulting "inner-loop" designs may possess unnecessarily high bandwidths in the control paths. Furthermore, gain scheduling to different flight conditions and robustness to plant model uncertainties pose additional complexities to the design problem; hence making the SISO design procedure lesser attractive than a direct procedure based on constrained parameter optimization.

Multivariable control design techniques could potentially provide a systematic approach to the solution for a set of feedback gains that achieve simultaneously design performance and robustness to plant model uncertainties. One such approach is provided by the unified design algorithm for robust low-order controllers [Ref.6] using constrained parameter optimization as fully implemented in the computer program SANDY. The design method has found numerous applications in flight controls [Refs.15-17] and control of flexible mechanical systems [Ref.18]. The work conducted

in this study is to demonstrate the application of the design algorithm to the synthesis of an integrated autothrottle/autopilot "inner" structure based on the TECS design philosophy. In addition, we perform autopilot designs for speed and altitude holds based on an existing optimized inner-loop and compare the results with those obtained from simultaneous redesign of both the inner (i.e TECS) and outer-loops.

The main objective of this work is the formulation of an optimal control problem addressing the same design objectives as those achieved under classical design approaches; in this case the design solution is based on direct constrained optimization. Within this formulation, a systematic approach is developed allowing the designers to achieve multiple design objectives such as damping of system modes, shaping of loop frequency responses, disturbance rejection, command tracking, and robustness to modeling uncertainties. Using this design technique, feedback gains have been obtained for the integrated autothrottle/autopilot design on the TSRV vehicle at two flight conditions. Linear analysis indicates that the design procedure using constrained optimization yields comparable and improved results in closed-loop stability, aircraft responses and control activities to turbulence, and robustness in terms of single-input/single-output gain and phase margins.

This study is divided into three parts:

1. Synthesis of an integrated autothrottle/autopilot "inner"-loop structure based on the TECS design philosophy,

2. Synthesis of airspeed-hold and altitude-hold "outer"-loops with the previously designed "inner"-loop,

3. Synthesis of an integrated autothrottle/autopilot using simultaneously design parameters from both the "inner" and "outer"-loop structures.

A systematic approach to multivariable controller design is developed allowing the designer to perform tradeoff among different performance objectives such as damping of system modes, command tracking, shaping of loop frequency responses, disturbance rejection, and robustness to modeling uncertainties. Direct tradeoffs between design criteria are conducted in a systematic manner, enabling the designer to explore the full potentials of the control system. The TECS control system designed under this

approach is found to be sufficiently insensitive to variations in the plant model, while disturbance rejection requirements to clear-air turbulence and responses to flight path, acceleration, airspeed and altitude commands are simultaneously improved.

Chapter 2

INTEGRATED AFCS DESIGN

2.1 Review of AFCS Designs

Development of automatic flight control systems (AFCS) for modern transport aircraft has resulted from the need to reduce pilot workloads and, at the same time, improve performance and fuel efficiency. The first flight control systems consisted of a pitch attitude hold system through simple feedback of pitch attitude and pitch rate to the elevator control. Speed-hold and altitude-hold modes followed soon afterwards as extentions of the basic flight control system. Design of new control modes has often proceeded with little or no consideration of existing modes in the AFCS. As a result, there is numerous replication of the basic flight-path and speed control functions in the navigation and control computer systems [Ref.10].

In recent years, the need to resolve fundamental operational and performance deficiencies of current AFCS designs has become apparent. Extensive development programs [Ref.13] have shown that the conventional AFCS design has reached a fundamental limit such that further improvements cannot be easily obtained within the existing system architecture.

The fundamental limitation resides in the traditional single-loop design approach where the throttle and elevator commands are developed separately without regard to cross-coupling effects in the longitudinal aircraft dynamics. This type of single-loop approach is evident in the underlying structure of conventional AFCS designs, Figure 2.1. Flight-path control by the autopilot is achieved through feedback to the elevator while the autothrottle independently controls speed through the throttles.

The basic AFCS structure has serious design deficiencies. In the longitudinal aircraft dynamics both the elevator and throttle controls produce responses in flight path and speed. This effect may lead to adverse cross-coupling between the autothrottle and autopilot when both feedback loops are closed. Performance and stability of the autothrottle loop may significantly degrade in the presence of the autopilot loop. In

fact, for large flight-path angle commands, the much larger control authority and bandwidth of the elevator can easily out strip the throttle's ability to maintain the commanded speed.

As a result, in 1979 NASA directed the Boeing Company to begin conceptual development of an integrated flight path and speed control system incorporating many existing design objectives while avoiding duplication of control functions. Numerous types of "energy compensation" techniques were investigated and led to the design and implementation of the so-called total energy control system (TECS) [Refs.9-11]. The total energy control concept provides an effective means of dealing with aircraft operational requirements, control nonlinearities and performance limitations [Refs.12-14].

Key features of TECS are

- Integration of vertical control modes into a single control concept designed around a fixed "inner-loop" structure,

- Use of cross-feed paths between flight path and acceleration to both the elevator and the throttles, hence formulation of a multiloop control design structure,

- Control strategies based on total energy rate and total energy distribution rate,

- Command paths for control of flight path and longitudinal acceleration.

These contrast with the conventional approach to AFCS design involving separate pitch autopilot and autothrottle designs; in which the elevator is directed to control flight path while airspeed regulation is acquired separately through the throttles.

2.2 Design Objectives

Developmental studies have been directed toward integrating numerous functions of the flight control system into a single control concept. Several important considerations in the redesign of the AFCS are

- Integration of all vertical control modes into a single control-law concept. The system should be designed around a fixed inner-loop configuration with outer-

loop control modes generating signals compatible with the inner-loop command inputs.

- Minimization of transient errors due to cross coupling between commanded inputs in the inner-loop structure. The control system should produce a "coordinated" response between the throttle and the elevator controls to command inputs.

- Elimination of functional overlaps in the AFCS design.

- Protection against exceeding aircraft performance and structural limits by providing an intelligent hierarchy in control system modes.

- Provision of overshoot-free responses to step command inputs.

- Constraint of closed-loop damping of dominant poles to an acceptable level.

- Minimization of control activities to turbulence in accordance with meeting flight-path and speed tracking requirements at each flight condition.

2.3 Review of the Total Energy Control Concept

Numerous variations of "energy compensation" techniques have been investigated for improving the simultaneous operation of the autothrottle and autopilot designs [Ref.13]. Energy compensation becomes the foundation of an integrated AFCS "inner-loop" structure in TECS. One formulation of the energy compensation technique is to develop the engine thrust command as a function of the aircraft total energy rate, while the elevator command is expressed as a function of the distribution rate between kinetic and potential energies. Key equations governing the total energy control concept were developed by Lambregts [Refs.9-11]. They are included here for completeness and to define the structure of the control system used in the constrained parameter optimization that follows.

The total energy $E(t)$ of the aircraft treated as a point mass is given by

$$E(t) = \frac{1}{2}mV(t)^2 + mgh(t) \qquad (2.1)$$

where

$$m \quad = \quad \text{mass of aircraft}$$
$$V(t) \quad = \quad \text{aircraft total velocity along the flight path}$$
$$h(t) \quad = \quad \text{altitude}$$
$$g \quad = \quad \text{gravitational acceleration}$$

The total energy rate $\dot{E}(t)$ is found by differentiating $E(t)$ in equation (2.1) with respect to time as,

$$\dot{E}(t) \approx mgV(t) \left(\frac{\dot{V}(t)}{g} + \gamma(t) \right) \tag{2.2}$$

for small flight-path angle $\gamma(t)$ in radians and assuming that the aircraft mass m is constant or slowly varying. If we write the equation for the thrust required from the equations of motion along the flight path, we have

$$T_{req}(t) = mg \left(\frac{\dot{V}(t)}{g} + \gamma(t) \right) + D(t) \tag{2.3}$$

Assuming that initial thrust is trimmed against drag and the variations in drag with time are generally slow, then it follows that the short-term thrust requirement for a desired level of total energy rate is obtained from the acceleration and flight-path angle quantities as

$$\Delta T_{req}(t) \approx \frac{\dot{E}(t)}{V(t)} \approx mg \left(\frac{\dot{V}(t)}{g} + \gamma(t) \right) \tag{2.4}$$

This implies that the aircraft total energy can be regulated directly using thrust control. However the distribution between kinetic and potential energies cannot be effectively controlled with the throttles. To distribute the total energy rate between flight path and acceleration as desired, elevator control must be used. The elevator primarily provides control of angle-of-attack and thus lift while contributing little to the aircraft total drag, thereby having little effect upon the total energy rate.

Using proportional and integral control on the total energy rate and energy rate distribution, we develop command strategies for both the thrust and the elevator controls as

$$\delta_{T_c}(s) \quad = \quad mg \left(K_{TP} + \frac{K_{TI}}{s} \right) \left(\frac{\dot{V}_c(s)}{g} + \gamma_c(s) \right) \tag{2.5}$$

$$\delta_{e_c}(s) \quad = \quad \left(K_{EP} + \frac{K_{EI}}{s} \right) \left(\frac{\dot{V}_c(s)}{g} - \gamma_c(s) \right) \tag{2.6}$$

where $\gamma_e(s) = \gamma(s) - \gamma_c(s)$ and $\dot{V}_e(s) = \dot{V}(s) - \dot{V}_c(s)$ represent the errors of flight-path angle γ and acceleration $\dot{V}$ from the commanded values γ_c and $\dot{V}_c$ respectively. The parameters K_{TP}, K_{TI}, K_{EP}, and K_{EI} are the proportional and integral feedback gains to thrust and elevator controls respectively. The basic implementation of this system is shown in Figure 2.2. The engines can be made to produce the required thrust by converting the total thrust command into an equivalent engine pressure ratio (EPR) command and closing an EPR feedback loop around the engine [Ref.11]. Notice that proportional paths on the flight path γ_c and acceleration $\dot{V}_c$ commands have been left out of the current implementation. It was found that direct feedthrough of the commanded inputs to the controls would produce undesireable overshoots. However such a problem can be resolved with proper feedforward control as evident in this study.

2.4 Analysis of the Current Total Energy Control Structure

A careful study of the TECS structure and its characteristics is crucial to the formulation of an optimal control design procedure. The NASA TSRV B-737 research aircraft was used to define linear longitudinal aircraft dynamic models at two flight conditions (Appendix E). The chosen flight conditions are listed in Table 2.1. The first flight condition FLT1 is a typical approach to landing configuration, and the second flight condition FLT2 is a cruise condition.

Table 2.2 shows the inner-loop and pitch-damper gain selection for the current design implementation on the NASA TSRV [Refs.12-14]. The gains K_θ and K_q provide feedback of pitch attitude and pitch rate for stabilization of the aircraft longitudinal rigid-body modes. Notice that the value of K_{TP} was set to zero, thus eliminating the proportional feedback path to the throttles. Classical analysis indicates that this feedback gain is not neccessary for closed-loop stability. Furthermore, by eliminating direct feedback to the throttle, the broken-loop control bandwidth and throttle activity to turbulence are reduced. Actually this restriction on K_{TP} is not needed as demonstrated in the optimal TECS design. The additional degree-of-freedom provided by the gain K_{TP} can be used to further improve stability of the phugoid and short-period modes, and to achieve better command tracking performance without increasing control activity response to turbulence.

The integral gains K_{TI} and K_{EI} were chosen to be approximately equal so as to obtain equal bandwidths in both the γ_ϵ and $\dot{V}_\epsilon/g$ feedback paths. Gain scheduling of the control system to different flight conditions is achieved through the gains K_{CAS} and K_{GW} in the elevator and throttle control loops respectively (Figure 2.2). The gain schedules are a function of calibrated airspeed (CAS) in *fps* and gross weight in *pounds* and they are given as follows,

$$K_{CAS} = \left(\frac{200}{CAS}\right)^2 \tag{2.7}$$

$$K_{GW} = mg \tag{2.8}$$

With these gain schedules the control-law when implemented will clearly be nonlinear and time-varying. However in the neighborhood of a design condition, one can still examine the responses in terms of those from a linear time-invariant system.

The TECS structure as shown in Figure 2.2 introduces an uncontrollable pole at the origin in the closed-loop system. This results from the additional integration of the aircraft acceleration variable $\dot{V}(t)$ in the control system. This means that the TECS design provides only one integral control action effective on the flight-path response and not on velocity. Integral control of the velocity variable can only be obtained through feedback of the velocity error to the inner-loop commands γ_c and $\dot{V}_c/g$, as found in an outer-loop control of a speed-hold type autopilot. Design of outer-loops for different autopilot modes (i.e speed-hold and/or altitude holds) will be discussed in chapters 7 and 8. In this section, we are primarily concerned with the redesign of the TECS "inner"-loop gains for improved performance and robustness using a procedure based on nonlinear constrained optimization.

Figure 2.3 shows frequency responses from flight-path angle and acceleration commands to the respective outputs for the closed loop system at flight condition FLT1. Note that at zero frequency the transfer function of $\dot{V}(s)/\dot{V}_c(s)$ has a gain less than one. Consequently the controller will not maintain the commanded acceleration in steady state. The TECS architecture simply cannot provide a constantly increasing thrust command (i.e. a type 2 system in the acceleration command path) when the error quantities $\dot{V}_\epsilon(t)$ and $\gamma_\epsilon(t)$ become zero, i.e. when $\dot{V}(t) = \dot{V}_c(t)$ and $\gamma(t) = \gamma_c(t)$.

Table 2.1: TSRV B-737 Flight Conditions

	Altitude (ft)	Weight (lbs)	CAS (kts)	Flaps (deg)	FPA (deg)	Gear
FLT1	1,500	80,000	120	40	-3	down
FLT2	25,000	80,000	450	0	0	up

Table 2.2: Current TECS Inner-Loop and Pitch Damper Gains

K_{TI}	K_{EI}	K_{TP}	K_{EP}	K_θ	K_q
0.4	2.52	0.0	3.36	6.0	4.0
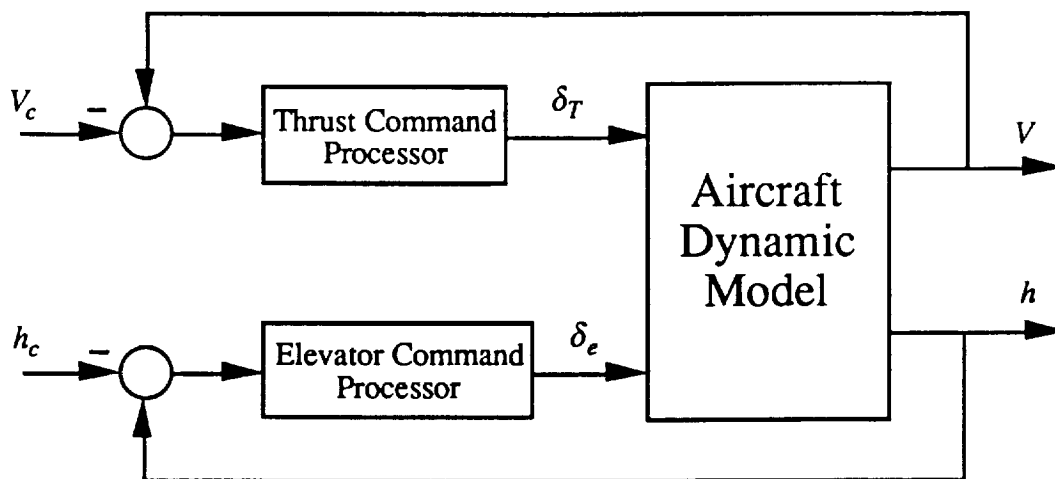
Figure 2.1: Conventional AFCS Autothrottle/Autopilot
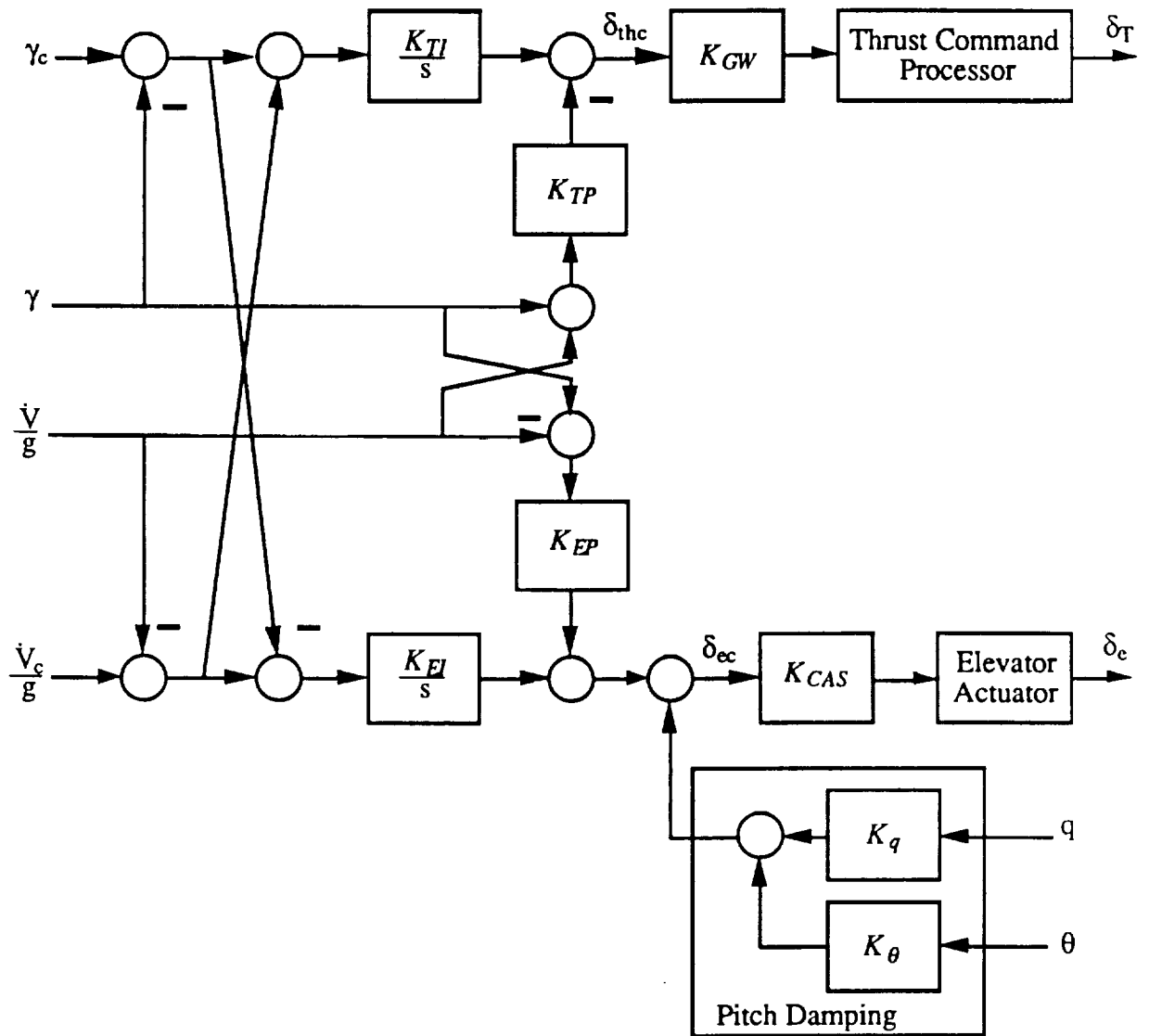
Figure 2.2: Basic Total Energy Control System
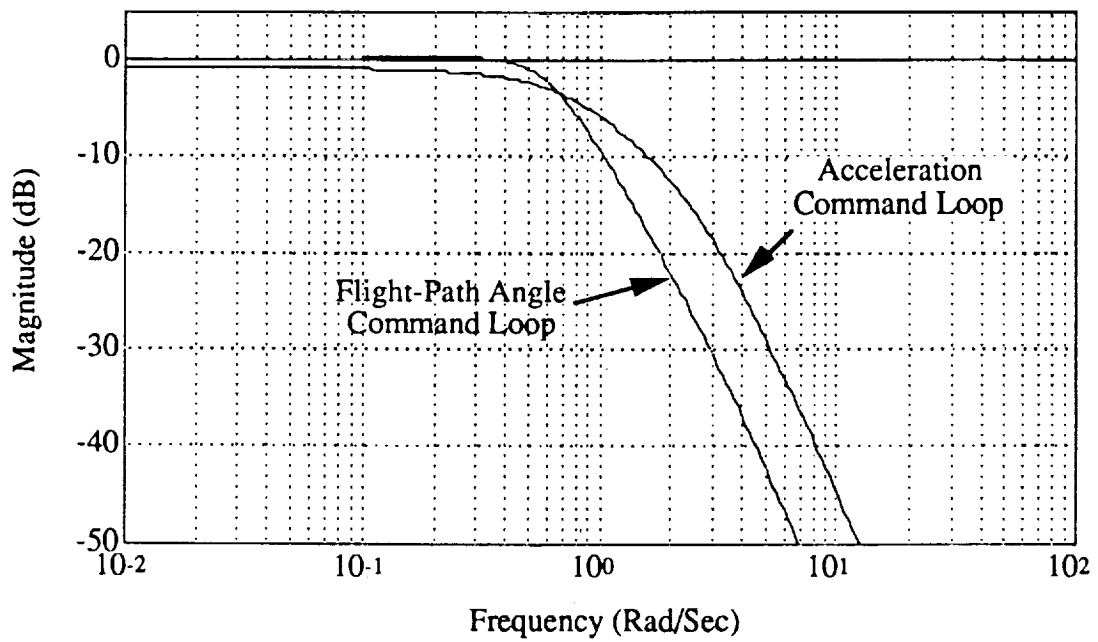
Figure 2.3: TECS Command Loop Frequency Responses

Chapter 3

OPTIMAL CONTROL DESIGN ALGORITHM USING CONSTRAINED PARAMETER OPTIMIZATION

Development of techniques for multivariable control-law synthesis is aimed at producing controllers with desired performance in command tracking and disturbance rejection along with adequate robustness to plant uncertainties. Numerous multivariable control design techniques are available such as standard linear quadratic gaussian (LQG), linear quadratic gaussian with loop transfer recovery (LQG/LTR), H^∞-optimization and μ-synthesis [Refs.1-3]. However, simple design procedures for low-order controllers addressing direct tradeoff between performance and robustness are still lacking. The procedure based on nonlinear constrained optimization as implemented in the computer program $SANDY$ [Refs.6,7,15,21] seems to offer a practical alternative amidst the abundance of multivariable robust control design schemes. In this section, we describe the formulation of models for control-law synthesis, and the definition of various performance indices and constraints used in the design algorithm.

3.1 Formulation of Models for Control-Law Synthesis

Aircraft dynamic models for linear control-law synthesis are usually obtained from the linearization of a full nonlinear model in real-time simulator about some predefined equilibrium points. A linearized plant at the ith condition is modelled as a continuous linear time-invariant system of the form

$$\dot{x}_p^i(t) = A_p^i x_p^i(t) + B_p^i u_p^i(t) + \Gamma_p^i w_p^i(t) \tag{3.1}$$

$$y_s^i(t) = C_s^i x_p^i(t) + D_s^i u_p^i(t) + \Omega_s^i w_p^i(t) \tag{3.2}$$

$$y_p^i(t) = C_p^i x_p^i(t) + D_p^i u_p^i(t) + \Omega_p^i w_p^i(t) \tag{3.3}$$

where the matrices A_p^i, B_p^i, Γ_p^i, C_s^i, D_s^i, Ω_s^i, C_p^i, D_p^i and Ω_p^i contain the plant dynamics, actuator and sensor models, disturbance and command generator filter models, etc., $(i = 1, ..., N_p)$ and N_p is the total number of design conditions. The output vector

$y_s^i(t)$ represents the sensor variables of the ith plant condition. The vector $y_s^i(t)$ in equation (3.2) contains not only the measured feedback quantities such as pitch rate, pitch attitude, airspeed, etc..., but also the tracked commands (Appendix B) which are outputs of a command generator model. This model is often imbedded as part of the augmented plant description. For example, $y_s(t) = \{q, \theta, \gamma, V, \gamma_c, V_c\}$. The output vector $y_p^i(t)$ contains those outputs used in the performance index of section 3.2 .

The design method based on nonlinear constrained optimization requires *a-priori* the setup of a predefined controller structure for both the feedback and feedforward control systems. The form of the controller is quite general. The complete arbitrariness allowed in the controller structure means that designers will have the direct responsibility to:

1. Setup a control-law with adequate number degrees of freedom so that the design algorithm will converge to a solution that meets the desired performance goals and the specified set of design constraints and,

2. Avoid overspecifying the design parameter set (especially in the case of a nonminimal state realization of the controller). This could lead to nonunique solutions or to the breakdown of the search algorithm.

A typical feedback/feedforward controller has the form

$$\dot{x}_c(t) = A_c x_c(t) + B_c u_c(t) \tag{3.4}$$

$$y_c(t) = C_c x_c(t) + D_c u_c(t) \tag{3.5}$$

where the state matrices A_c, B_c, C_c and D_c describe the form of dynamic compensation (i.e. proportional, integral, derivative, leads, lags, etc.) applied to the input vector $u_c(t)$. The controller output vector $y_c(t)$ contains the feedback controls and those output variables that are expressed as linear combination of controller states $x_c(t)$ and controller inputs $u_c(t)$. Most linear time-invariant controllers can be put into this form with individual feedback gains appearing in the elements of the state matrices A_c, B_c, C_c, and D_c. Note that a closed-loop system is formed by connecting:(1) the outputs $y_c(t)$ in equation (3.5) of the controller state model to the inputs $u_p^i(t)$ in equations (3.1)-(3.3) of the plant model and, (2) the plant output vector $y_s^i(t)$

to the input vector $u_c(t)$ of the controller state model. This action of loop closure between the plant and the controller models is automatic and carried out inside the design package SANDY.

In chapter 4 we will describe the formulation of a TECS controller using equations (3.4) and (3.5).

3.2 Description of a Design Algorithm Based on Nonlinear Constrained Optimization

As mentioned in the introduction, the design method proposed in this study is based entirely upon the minimization of a performance index for a set of closed-loop systems subjected possibly to additional design constraints such as closed-loop stability, covariance responses to process and sensor noises, and bounds on robustness measures. A nonlinear programming technique [Ref.8] implemented in the numerical library $NPSOL$ is used to solve the control problem with nonlinear design constraints.

Typical performance measures in optimal control are quadratic penalties on the closed-loop system output and control responses to random disturbances. Three types of random disturbances are considered in the design problem: initial conditions, impulse inputs and white-noise inputs. Depending on the types of disturbances, different formulations of the performance index will be used. For the ith plant condition, the performance index to initial conditions or impulse inputs has the form

$$J_i(t_f) = \frac{1}{2} \int_0^{t_f} e^{2\alpha_i t} E[y_p^{iT}(t)Q^i y_p^i(t) + u_p^{iT}(t)R^i u_p^i(t)]dt \tag{3.6}$$

and for white-noise inputs the performance index is

$$J_i(t_f) = \frac{1}{2} E_{\alpha_i}[y_p^{iT}(t_f)Q y_p^i(t_f) + u_p^{iT}(t_f)R^i u_p^i(t_f)] \tag{3.7}$$

where $y_p^i(t)$ and $u_p^i(t)$ are respectively the closed-loop responses of the performance and controller output variables (since $u_p^i(t) = y_c(t)$) . The operator $E_{\alpha_i}[\cdot]$ is the expected-value operator corresponding to a closed-loop system destabilized by a factor α_i. The matrices Q^i and R^i are the usual penalty weighting matrices on the system performance outputs and control inputs respectively. Evaluation of the performance index in equation (3.6) is done using the equivalence relation established in Appendix

A. The parameter α_i is used to ensure that, when a steady-state optimal solution has been found, the closed-loop system eigenvalues of the controllable modes will have real parts less than $-\alpha_i$ at the ith plant condition. The formulation of the outputs $y_p^i(t)$ in equation (3.3) is general and can be defined to include the plant states $x_p^i(t)$, the controller states $x_c(t)$ and the controller inputs $u_c(t)$. The plant states $x_p^i(t)$ are modeled in the performance outputs $y_p^i(t)$ by letting $C_p^i = I$, $D_p^i = \Omega_p^i = 0$. The controller states $x_c(t)$ and the controller inputs $u_c(t)$ are modeled through the term D_p^i in equation (3.3) and with $u_p^i = y_c$ established in the feedback connection.

Design gains from selected parameters within the controller matrices are determined such that a performance index of the form

$$J(t_f) = \sum_{i=1}^{N_p} W_i J_i \tag{3.8}$$

is minimized. Individual performance index $J_i(i = 1, N_p)$ is one of those shown in equations (3.6) and (3.7). Performance indices are evaluated to an *a-priori* selected finite terminal time t_f during the initial optimization. Efficient algorithms to evaluate the performance index $J(t_f)$ and its gradients with respect to the design parameters have been developed [Ref.6] that are comparable to those in the evaluation of the steady-state performance index (i.e based on Lyapunov solutions) in terms of computational time and accuracy. In fact, steady-state covariance responses can be accurately calculated by using a sufficiently large t_f (e.g. at least 4-times the slowest time-constant of the closed-loop system modes). The terminal time t_f is increased following each successful convergence in order to recover the steady-state solution. This gradual process of recovering the steady-state solution ensures that the final optimal solution will be a *stabilizing* one. The criterion for determining whether a steady-state solution has been reached is based on the condition that value of the optimized objective function will not vary by more than .1 percent from its previous value obtained for a smaller terminal time t_f. Experiences gathered so far seem to justify the use of a performance index based on a finite terminal time. This procedure avoids the difficulties encountered by conventional methods based on the Lyapunov equation for the steady-state covariance responses, requiring special provision to handle the case when the controller design becomes destabilizing during the search. Note that by starting with a sufficiently small terminal time t_f our design method can even

be initiated with a controller design guess that is not stabilizing.

The performance index J given in equation (3.8) enables designers to incorporate classical measures of design robustness or sensitivity to plant modeling uncertainties of the following types,

1. Gain and phase margins in the control and sensor paths,

2. Roll-off in the broken-loop frequency responses evaluated at the control and sensor feedback paths,

3. Sensitivity of the closed-loop eigenvalues and the closed-loop performance measures to perturbation in the plant model parameters.

The first and second items are useful measures of robustness to unmodelled dynamics. The third item is a measure of robustness to uncertainties in the coefficients of the plant model.

As seen in equation (3.8), our design algorithm for robust low-order controllers [Ref.6] involves an objective function that combines together several quadratic penalties of closed-loop system responses at different plant conditions. A simultaneous control-law synthesis to a set of multiple plant conditions allows the direct inclusion of robustness measures of type 3 into the design objective. Design to robustness measures of types 1 and 2 can be handled through the use of frequency-weighted performance functions and H^∞-norm bounds on selected system transfer function matrices [Refs.7,19].

Specifically, robustness to plant parameter uncertainties or variation in design condition is achieved by using a set of quadratic performance indices that encompass, in addition to the one at the nominal design condition (i=1), other off-nominal design conditions weighted by the design parameters W_i ($i = 2, ..., N_p$) as in equation (3.8). To impose design robustness to unmodeled dynamics, one may define additional plant conditions that have performance indices representing penalties on control and sensor loop responses to high-pass noises injected separately into the control and sensor paths, or on the H^∞-norm of desired system transfer function matrices.

Design for command following and tracking problems is done by formulating synthesis models and performance indices that penalize transient responses of the errors

between the actual and the commanded outputs. The commanded outputs (e.g filtered step, ramp, sinusoidal functions) are derived from a command generator model, a part of the augmented plant model, by using a combination of initial conditions and impulse inputs. If proportional and integral controls are desired in the feedback design, it is crucial that formulation of the design performance index reflects the need for an integral control action. The integral gains in the controller matrices tend to become ineffective (i.e converge to small values) when the objective function consists of responses to gaussian random disturbances of zero mean. In general, integral control requirements must be defined in terms of a performance index that penalizes transient error responses of the controlled variables in the presence of parameterized random disturbance inputs where the generating time functions have nonzero constant steady-state components. That is, integral action is meaningful in the optimal design when it is used to compensate plant responses in the presence of parameterized random *constant* disturbances.

Many types of parameterized random commands, such as impulse, step, and ramp inputs, are derived from responses of linear time-invariant shaping filters to random initial conditions or to impulse inputs of random magnitudes (Appendix B, section B.1). Outputs of these filters are interpreted as parameterized random commands whose magnitude y_{cmd} is a random vector with zero mean $E[y_{cmd}] = 0$ and covariance $E[y_{cmd}y_{cmd}^T] = Y_{cmd}$. Elements of the magnitude vector y_{cmd} are uncorrelated when its covariance matrix Y_{cmd} is diagonal.

Random disturbances, such as Dryden or approximate Von Karman turbulences, are outputs of stable linear shaping filters excited by white-noise inputs $w(t)$ (Appendix B, section B.2) with zero mean $E[w(t)] = 0$ and covariance $E[w(t)w^T(\tau)] = W_p\delta(t - \tau)$.

Design requirements which cannot be easily handled through a quadratic performance index are enforced through linear constraints, nonlinear constraints, and direct bounds on the design parameters. Nonlinear constraints on the closed-loop stability, performance, and robustness are defined as follows,

- Closed-loop stability of selected eigenvalues:

$$\zeta_i \geq \zeta_{i\,min}, (i = 1, ..., n) \tag{3.9}$$

$$\sigma_i \leq \sigma_{i\,max}, (i = 1, ..., n) \tag{3.10}$$

where ζ_i is the damping ratio and σ_i is the real part of the ith eigenvalue. Formulation of these non-linear constraints is described in Appendix C.

- Closed-loop mean-square responses:

$$\sigma^2_{p_i\,min} \leq \lim_{t_f \to \infty} E[y^2_{p_i}(t_f)] \leq \sigma^2_{p_i\,max} \tag{3.11}$$

where the parameters $\sigma^2_{p_i\,min}$ and $\sigma^2_{p_i\,max}$ define respectively the allowable lower and upper bounds on the mean-square response of the ith plant output y_{p_i} to random disturbances.

- Desired H^∞-norm bounds on closed-loop performance variables:

$$\kappa_{min} \leq \|G_{yw}(j\omega)\|_\infty \leq \kappa_{max} \tag{3.12}$$

where $\|G_{yw}(j\omega)\|_\infty = \sup_\omega \bar{\sigma}\left(G_{yw}(j\omega)\right)$ and $G_{yw}(s)$ is the transfer function matrix of the closed-loop system between the plant disturbance inputs $w(s)$ and the plant outputs $y_p(s)$.

Chapter 4

TECS PROBLEM FORMULATION

4.1 Formulation of Synthesis Models

The NASA B-737 TSRV aircraft [Refs.12,13,24] is used in this study of a total energy control system design based on nonlinear constrained parameter optimization. Longitudinal aircraft models are generated for the landing-approach and cruise flight conditions described in tables E.1 and E.2 (Appendix E). The linearized aircraft dynamic models have the form

$$\dot{x}_p(t) = A_p x_p(t) + B_p u_p(t) + \Gamma_p w_p(t) \tag{4.1}$$

$$y_p(t) = C_p x_p(t) + D_p u_p(t) + \Omega_p w_p(t) \tag{4.2}$$

where $x_p(t)$ contains the aircraft rigid-body states, $u_p(t)$ the elevator and throttle control inputs, $w_p(t)$ the wind components and the command inputs, and $y_p(t)$ the measurement and the performance criterion outputs. The aircraft models are subsequently augmented with appropriate linear control actuation models of the form

$$\dot{x}_{act}(t) = A_{act} x_{act}(t) + B_{act} u_{act}(t) \tag{4.3}$$

$$u_p(t) = C_{act} x_{act}(t) + D_{act} u_{act}(t) \tag{4.4}$$

Turbulence and command generation models are described by

$$\dot{x}_d(t) = A_d x_d(t) + B_d w_d(t) \tag{4.5}$$

$$w_p(t) = C_d x_d(t) + D_d w_d(t) \tag{4.6}$$

They contain the commonly used Dryden or approximate Von Karman turbulence spectra [Ref.23]. Power spectral densities for Dryden turbulence models are given by

$$\Phi_u(\omega) = \sigma_u^2 \frac{L_u}{\pi V} \frac{1}{1 + (L_u \omega / V)^2} \tag{4.7}$$

$$\Phi_w(\omega) = \sigma_w^2 \frac{L_w}{2\pi V} \frac{1 + 3 (L_w \omega / V)^2}{\left[1 + (L_w \omega / V)^2\right]^2} \tag{4.8}$$

where σ_u and σ_w are the root-mean-square intensities of turbulence (figure 4.2) with

$$\frac{\sigma_u^2}{L_u} = \frac{\sigma_w^2}{L_w} \tag{4.9}$$

The parameters L_u and L_w are turbulence scale lengths defined as a function of altitude:

- For altitude above 1750 ft: $L_u = L_w = 1750$ ft

- For altitude below 1750 ft: $L_u = 145h^{1/3}$, $L_w = h$ where h is the altitude in feet.

Aircraft rigid-body dynamics are augmented with models for the control actuators and disturbances; the latter variables contain not only the wind inputs but also the command signals (Appendix B). The resulting plant model forms a synthesis model in the form of equations (3.1)–(3.3). An automated procedure for formulating the synthesis model is implemented in a user-defined function for the MATLAB[1] control system software. A listing of the command procedure is given in Appendix F.

4.2 An Optimal Design Approach for TECS

The design algorithm for robust low-order controllers [Ref.6] implemented in the computer design package *SANDY* is applied to the design of an integrated AFCS. The total energy concept defines the "inner-loop" structure for an integrated autothrottle/autopilot control system and provides a basis for a multiloop control design. The basic TECS feedback controller shown in figure 2.2 with a pitch damper can be formulated into a controller state-space model of equations (3.4) and (3.5) as follows,

$$\begin{pmatrix} \dot{x}_{IE} \\ \dot{x}_{IL} \\ \dot{x}_{V_c} \end{pmatrix} = \begin{bmatrix} 0 & 0 & 0 \\ 0 & 0 & 0 \\ 0 & 0 & 0 \end{bmatrix} \begin{pmatrix} x_{IE} \\ x_{IL} \\ x_{V_c} \end{pmatrix} + \begin{bmatrix} -1 & -1/g & 0 & 0 & 1 & 1/g \\ 1 & -1/g & 0 & 0 & -1 & 1/g \\ 0 & 0 & 0 & 0 & 0 & 1 \end{bmatrix} \begin{pmatrix} \gamma \\ \dot{V} \\ q \\ \theta \\ \gamma_c \\ \dot{V}_c \end{pmatrix}$$

$$\tag{4.10}$$

---

[1] MATLAB is a trademark of The MathWorks, Inc.

$$
\begin{pmatrix} \delta_{thc} \\ \delta_{ec} \\ V_c^* \end{pmatrix} = \begin{bmatrix} K_{GW}K_{TI} & 0 & 0 \\ 0 & K_{CAS}K_{EI} & 0 \\ 0 & 0 & k_1 \end{bmatrix} \begin{pmatrix} x_{IE} \\ x_{IL} \\ x_{V_c} \end{pmatrix}
$$

$$
+ \begin{bmatrix} -K_{GW}K_{TP} & -K_{GW}K_{TP}/g & 0 & 0 & 0 & 0 \\ K_{CAS}K_{EP} & -K_{CAS}K_{EP}/g & K_{CAS}K_q & K_{CAS}K_\theta & 0 & 0 \\ 0 & 0 & 0 & 0 & k_2 & 0 \end{bmatrix} \begin{pmatrix} \gamma \\ \dot{V} \\ q \\ \theta \\ \gamma_c \\ \dot{V}_c \end{pmatrix}
$$

$$
\tag{4.11}
$$

Proportional and integral gains K_{TP}, K_{EP}, K_{TI} and K_{EI} along with the pitch damper gains K_q and K_θ and the additional gains k_1 and k_2 are design parameters in the controller state matrices. The gain schedule parameters K_{GW} and K_{CAS} are assumed fixed at each plant condition and their contribution to the overall feedback gains can be absorbed into the other feedback gains. The design parameters are selected from the minimization of a performance index J of the form

$$
J = \sum_{i=1}^{N_P} W_i J_i \tag{4.12}
$$

where

$$
J_i = \sum_{k=1}^{N_R} J_i^{(k)} (i = 1, ..., N_P) \tag{4.13}
$$

and W_i is a weighting factor assigned to the performance index J_i at the ith plant condition. Within each individual plant condition, performance indices $J_i^{(k)}$ ($k = 1, ..., N_R$) are used to address N_R different control design requirements. Design requirements defined in $J_i^{(k)}$ may be conflicting. Compromises among the conflicting requirements are usually made in the final design solution through iterative adjustment in the penalty weighting matrices.

In the optimal TECS design problem, the objective function at each flight condition is made up of at most *three* different performance indices $J_1^{(k)}(k = 1, 2, 3)$,

$$
J_1 = \sum_{k=1}^{3} J_1^k \tag{4.14}
$$

The first performance index $J_1^{(1)}$ is formulated to address design requirements in command tracking performance. It is given by

$$J_1^{(1)} = \lim_{t_f \to \infty} \frac{1}{2} \int_0^{t_f} E[Q_1(\gamma(t) - \gamma_c(t))^2 + Q_2(V(t) - V_c^*(t))^2]dt \qquad (4.15)$$

This performance index is evaluated to parameterized random filtered step commands in $\dot{V_c}$ and γ_c with $\dot{V_c}(t) = V_{co}ae^{-at}\mu(t)$ and $\gamma_c(t) = \gamma_{co}(1 - e^{-at})\mu(t)$ where $\mu(t)$ is the unit-step function. The parameter a determines the bandwidth of both the acceleration and the flight-path commands. In this design case, we use $a = 1.2rad/sec$, a typical value for flight-path and velocity command bandwidths. The variables V_{co} and γ_{co} are random parameters with zero means and covariances $E[V_{co}^2] = \sigma_{V_c}^2 = 1.0(fps)^2$ and $E[\gamma_{co}^2] = \sigma_{\gamma_c}^2 = 1.0(deg)^2$. The command $V_c(t)$ is computed simply as the integral of the acceleration command $\dot{V_c}(t)$, i.e.

$$V_c(t) = \int_0^t \dot{V_c}(\tau)d\tau \qquad (4.16)$$

The quantity $V_c^*(t)$ is an output of the controller model given in equation (4.11). It is used in the criterion output $V(t) - V_c^*(t)$ and is defined as a linear combination of the commanded velocity $V_c(t)$ and flight-path angle $\gamma_c(t)$, namely

$$V_c^*(t) = k_1 V_c(t) + k_2 \gamma_c(t) \qquad (4.17)$$

The parameter k_1 depicts the achieved level of commanded velocity in steady-state. Recall that the TECS design structure in figure 2.2 does not include feedback of velocity error, hence it is a type 0 system in the velocity variable V. Thus, in steady-state the aircraft velocity $V(t)$ does not settle to the command value $V_c(t)$, and the parameter k_1 is always strictly less than one (i.e $k_1 < 1$). The parameter k_2 is the amount of cross-coupling between flight-path command $\gamma_c(t)$ and aircraft steady-state velocity $V(t)$. Either parameter k_1 and/or k_2 can be set to lie within some desired values using direct bound constraints. For our design, the inequality constraint $-1 \leq k_2 \leq 1$ ensures that for one degree of flight-path angle command $\gamma_c(t)$, the change in aircraft steady-state velocity is less than one foot-per-second in magnitude. Clearly, for perfect decoupling where one does not allow changes in aircraft velocity during a flight-path angle command, k_2 would be constrained to be equal to zero. The parameters k_1 and k_2 are determined during the optimization such that bound constraints on

k_1 and k_2 are satisfied and the term $(V(t) - V_c^*(t))$ in the integrand of the performance index $J_1^{(1)}$ in equation (4.15) vanishes in the limit as $t_f \to \infty$.

The second performance index $J_1^{(2)}$ is set up to perform trade-off in the control bandwidth of the throttle loop. It is defined as

$$J_1^{(2)} = \lim_{t_f \to \infty} \frac{1}{2} E[R_1 \delta_{thc}^2(t_f)] \qquad (4.18)$$

The performance index $J_1^{(2)}$ is evaluated to a high-pass noise input in the thrust command loop [Ref.25]. The noise input is generated from the response of a first-order filter to white-noise with zero mean $E[\delta_{thw}(t)] = 0$ and covariance $E[\delta_{thw}(t + \tau)\delta_{thw}(t)] = \sigma_{thw}^2 \delta(\tau)$. The quantity $\delta_{thc}(t)$ is the thrust feedback control as shown in figure 4.1. Cut-off frequency of the high-pass filter is set approximately equal to the desired broken-loop throttle control bandwidth (i.e. $\omega_{\delta_{thw}} = 0.2$ rad/sec). Frequency-shaping of the disturbance input to the thrust command ensures that only control responses at high frequencies are penalized in $J_1^{(2)}$.

Similarly, the performance index $J_1^{(3)}$ is used to perform trade-off in the control bandwidth of the elevator loop. It is given by

$$J_1^{(3)} = \lim_{t_f \to \infty} \frac{1}{2} E[R_2 \delta_{ec}^2(t_f)] \qquad (4.19)$$

In this case, $J_1^{(3)}$ is evaluated to a high-pass noise input in the elevator command loop. Again the noise input is obtained from the response of a first-order high-pass filter to white-noise with zero mean $E[\delta_{ew}(t)] = 0$ and covariance $E[\delta_{ew}(t + \tau)\delta_{ew}(t)] = \sigma_{ew}^2 \delta(\tau)$. The quantity $\delta_{ec}(t)$ is the elevator feedback control. Cut-off frequency of the high-pass filter is approximately equal to the desired broken-loop elevator control bandwidth (i.e. $\omega_{\delta_{ew}} = 2.0$ rad/sec). Note that the elevator control has a higher bandwidth than the throttle control.

Other design considerations besides those depicted in the quadratic performance indices $J_1^{(1)}$, $J_1^{(2)}$, and $J_1^{(3)}$ are defined with the use of direct constraints. For example, desired closed-loop damping is achieved using the eigenvalue constraint defined in equation (C.41). Nonlinear damping constraints provide a direct means to achieve satisfactory damping of aircraft rigid-body modes. And covariance responses of selected outputs to clear air turbulence of Dryden spectra with RMS intensities from

the 99% probability level (figure 4.2) can be bounded using the covariance inequality constraint in equation (3.11). Nonlinear covariance constraints on control outputs ensure that the resulting optimal design has reasonable control activities to turbulence.

4.3 Control System Design Tradeoff

The design task involves a proper tradeoff among the following design performance goals:

- Damping of system eigenvalues,

- Command frequency response bandwidths,

- Broken-loop crossover frequencies in the control paths,

- Covariance responses of performance criteria,

- Command tracking/following performance,

- Disturbance rejection,

- Robustness to plant parameter uncertainties and unmodeled dynamics.

Performance objectives must be identified and established by the designer during the design tradeoff. If the desired objectives are not attainable, the NPSOL optimization [Ref.8] would most likely fail to arrive at a feasible solution, e.g. design constraints are unattainable with the specified controller structure or design constraints are too stringent and need to be relaxed.

Minimum damping of the closed-loop system eigenvalues is obtained directly through specification of the nonlinear damping constraint $\zeta \geq \zeta_{min}$. If damping requirements are too stringent then performance in other areas will be sacrificed. We found that it is generally easier to achieve the desired damping level through the use of non-linear constraints on system modes than with output penalties in the cost function. Penalties on outputs which are partially related to lightly damped modes may unnecessarily degrade other system responses. Furthermore, outputs associated with lightly damped closed-loop modes will be different for different controller designs.

Selection of desired command-loop frequency responses can be achieved through the penalties Q_1 and Q_2 in the performance index $J_1^{(1)}$. Bandwidths of individual command-loop frequency responses $\dot{V}(s)/\dot{V}_c(s)$ and $\gamma(s)/\gamma_c(s)$ relate to the ability of the system to track the respective commands. If the bandwidth in a particular command loop is too low, increasing the penalty Q_i ($i = 1, 2$) on the respective commanded output error in equation (4.15) will produce a higher bandwidth in that command path [Ref.25]. This systematic procedure enables designers to achieve satisfactory trade-off of performance in different command loops.

Crossover frequency of a loop transfer function for a system broken at a control path defines approximately the control bandwidth of that path. Selection of the control-loop crossover frequencies is accomplished through the penalties R_i ($i = 1, 2$) in equations (4.18) and (4.19). If the loop crossover frequency of a particular control path is too high, then higher penalty R_i in the respective performance index, i.e. $J_1^{(2)}$ or $J_1^{(3)}$, would lead to a design with a lower bandwidth [Ref.25]. Note that requirements for simultaneous low control-loop crossover frequency and high command-loop bandwidth are generally contradictory. Usually, decreasing control-loop crossover frequencies will inevitably result in lower command-loop bandwidths.

Upper bounds on root-mean-square (RMS) responses of selected performance criteria and control outputs to Dryden turbulence spectra may be specified to ensure adequate RMS responses. For the TECS design, throttle and elevator control activities are the two variables of primary importance. Inequality bounds are therefore placed on covariance responses of $\delta_{thc}(t)$ and $\delta_{ec}(t)$ to Dryden turbulence. The upper bounds are selected from the closed-loop control covariance responses of the current TECS design. In flight condition FLT2, one has to increase the elevator control activity in turbulence by a small amount in order to achieve the desired level of closed-loop

damping.

Design robustness in terms of closed-loop stability and performance measures to plant parameter uncertainties can be improved by using a performance index of the form given in equation (4.12), i.e.

$$J = \sum_{i=1}^{N_P} W_i J_i \qquad (4.20)$$

where each performance function $J_i(i = 2, ..., N_P)$ reflects design considerations at an off-nominal plant condition. Note that the index $i = 1$ corresponds to the nominal design condition. Stability in the presence of plant model parameter variations is defined in terms of damping constraints placed on closed-loop eigenvalues at the off-nominal plant conditions. When these constraints are satisfied, the resulting controller will then be robust to the given changes in plant conditions. However if the posed problem is overly constrained, then most likely a feasible solution cannot be found; in this case, a smaller set of uncertain plant models ought to be tried instead.

An alternative formulation for the robustness criteria is through the H^{∞}-norm bounds of selected system transfer function matrices, e.g $\|G_{yw}(j\omega)\|_{\infty}$. The H^{∞}-norm $\|G(j\omega)\|_{\infty}$ is defined as the supremum of the maximum singular value of $G(j\omega)$ for $\omega \in [0, \infty)$. From the small gain theorem, H^{∞} bounds on specific transfer function matrices give guaranteed gain and phase margins for nominally stable systems [Ref.3]. Nonlinear constraints of the form

$$\|G_{yw}(j\omega)\|_{\infty} \leq \kappa \qquad (4.21)$$

can also be specified in the extended version of the SANDY design algorithm [Ref.7] for robust stability and performance. Evaluation of this robust design procedure is left for a future study.

4.4 Gain Schedule at Other Flight Conditions

The design procedure described in section 4.3 will produce controller design gains optimal at one flight condition. Gain scheduling of the design at other flight conditions is usually required for optimum performance and may be achieved in one of three ways:

1. Design optimum controller gains at individual flight conditions separately. A gain schedule is developed for each controller gain. Usually it involves some form of curve-fitting with respect to airplane parameters such as calibrated airspeed or gross weight in the final design implementation.

2. Preselect a gain schedule for each of the control or sensor paths. Design remaining controller parameters to satisfy all requirements with the preselected gain schedule structure over the entire set of design conditions simultaneously.

3. Design a set of controller gains for a nominal flight condition. Redesign at other flight conditions based on gain scheduling a subset of controller gains. This procedure is simple and involves less computational effort in the actual implementation.

The first method is straightforward and involves doing a separate design for each flight condition. However, this may result in a gain schedule which is too cumbersome to implement. In the TECS inner-loop structure, this method would require scheduling of six separate gains.

The second approach involves deciding upon an a-priori gain schedule for the control or sensor paths, independent of the optimal design. These gains may be factored into the synthesis models at each flight condition. A single controller is then designed to satisfy all flight conditions with the pre-selected gain schedule. The design method involves defining a performance index similar to equation (4.20) that covers the entire range of flight conditions. It should be noted that this method depends upon the selection of a predefined gain schedule and provides no insight into how the gain schedule should be formulated. If the number of degrees-of-freedom is not adequately defined in the *a priori* selected controller structure, then most likely an optimal solution cannot be found that will meet all the design constraints. Thus, this method is generally not desireable since it sets the gain schedule around a predetermined structure that may be overly constrained.

A more practical approach is to select a few gains in the controller which are to be gain scheduled. These gains are often introduced at the control input paths to provide compensation for changes in control effectiveness. The procedure in the third method begins with a set of gains optimized at a nominal flight condition perceived to be the

most important. Then the gain schedule is determined by optimizing only a selected subset of gains to other flight conditions while leaving the remaining controller gains fixed at their nominal values. For example, in the TECS inner-loop structure, the scheduled parameters are K_{CAS} and K_{GW} while the gains K_{EP}, K_{TP}, K_{EI}, K_{TI}, K_{θ}, and K_q are fixed at the values optimized for the landing approach condition. The design procedure for optimizing the scheduled parameters and conducting design tradeoffs at each off-nominal flight condition is the same as described in section 4.3. This is a preferred approach since it provides insights into the level of improvement a gain schedule can offer with the selected degrees of freedom.

4.5 Issues for Numerical Convergence

Solution of the minimization problem is based upon a state-of-the-art nonlinear programming algorithm implemented in the NPSOL library [Ref.8]. Numerical conditioning of the TECS optimization problem is essential for successful convergence. Some key considerations are:

- Convergence of the performance integral. The designers must verify that the integrands of the quadratic performance index will approach zero in steady-state to the given set of input functions (i.e. white-noise, impulse, step, etc.).

- Formulation of the constrained optimization problem.

- Construction of the plant synthesis models.

Performance indices in equations (3.6) and (3.7) and their gradients with respect to the design parameters are needed for optimization. The design algorithm implemented in the computer design package $SANDY$ evaluates the performance indices and gradients to a finite terminal time t_f. In steady-state (i.e. $t_f \rightarrow \infty$), the performance index in equation (3.6) or (3.7) would become unbounded when the closed-loop system contains neutrally stable or unstable modes that are both disturbable from

the input excitation and detectable in the performance function. Selection of an appropriately small finite terminal time t_f would help avoid problems associated with lightly damped or unstable closed-loop poles in the initial phase of the numerical search.

Design optimization to step commands or constant disturbance inputs requires careful formulation of the performance index, making sure that the integrands will settle to zero in the limit as $t_f \to \infty$. Otherwise, the performance integral will be unbounded. For example, in the TECS problem formulation, the variable V_c^* given in equation (4.17) was used instead of V_c since the error $(V - V_c)$ does not approach zero in steady state for a type 0 system and the performance integral of equation (4.15) would otherwise be unbounded.

In problems dealing with constrained optimization, the possibility of having an overconstrained problem always exists. Careful formulation of the design objectives will definitely minimize problems encountered with nonlinear constraints and thereby speed up the design convergence. A helpful rule is to start the initial design with a minimal number of nonlinear constraints. Additional constraints can later be introduced in a systematic manner by order of relative importance and need. In the TECS design, damping in the aircraft rigid-body modes is of primary importance. Nonlinear constraints are henceforth used to achieve adequate closed-loop damping. Constraints on control covariance are included only when the initial design is found to be unsatisfactory.

Modern nonlinear optimization techniques as found in the NPSOL library require that design parameters be of approximately the same order of magnitude. If some parameters are significantly larger than the others, then gradients of the cost function with respect to these parameters may appear too small; consequently the true optimum may not be reached to a given level of optimality tolerance. Proper selection of physical units in both the controller and the plant synthesis model ensures that, at the start, design parameters will have the same relative magnitudes. Here in our TECS problem, we found that the quantities $\gamma(rad)$ and $\dot{V}/g$ have the same order of magnitude and the feedback gains on these variables have the same size.

Finally, it is crucial that the controller matrices in equations (3.4) and (3.5) form a minimal realization [Ref.6]. A nonminimal system will contain redundant parameters that lead to multiple local minima in the optimization. As a rule of thumb, the

maximum possible number n_{max} of independent controller parameters is, for $D_c \neq 0$,

$$n_{max} = (m + p)r + mp \qquad (4.22)$$

and for $D_c = 0$,

$$n_{max} = (m + p)r \qquad (4.23)$$

where r is the number of controller states, p is the number of controller inputs and m is the number of controller outputs. For example, in the TECS inner-loop structure as given in equation (4.11), a valid set of design parameters would be $C_c(1,1)$, $C_c(2,2)$, $D_c(1,1)$, $D_c(2,1)$, $D_c(2,3)$ and $D_c(2,4)$ while the parameters $D_c(1,2)$ and $D_c(2,2)$ are related to the above set through linear constraints, i.e $D_c(1,2) = D_c(1,1)$ and $D_c(2,2) = -D_c(2,1)$.
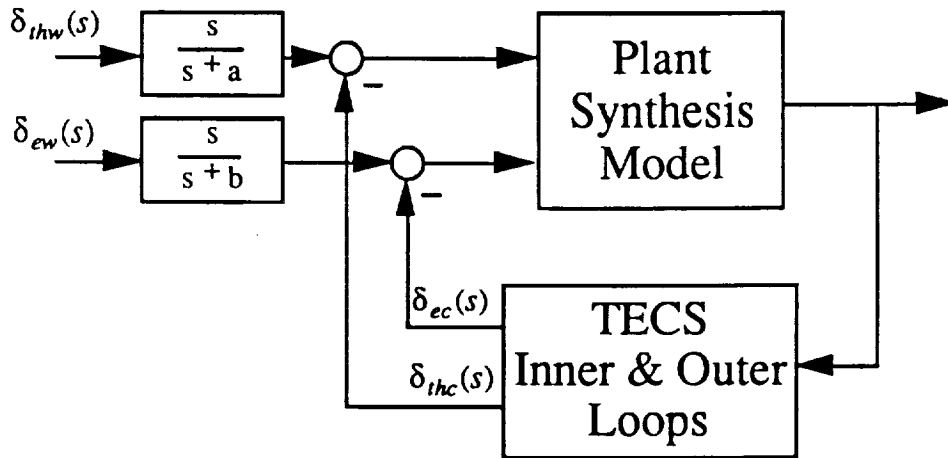
Figure 4.1: High-Pass Frequency Shaping of Control Loop Activities
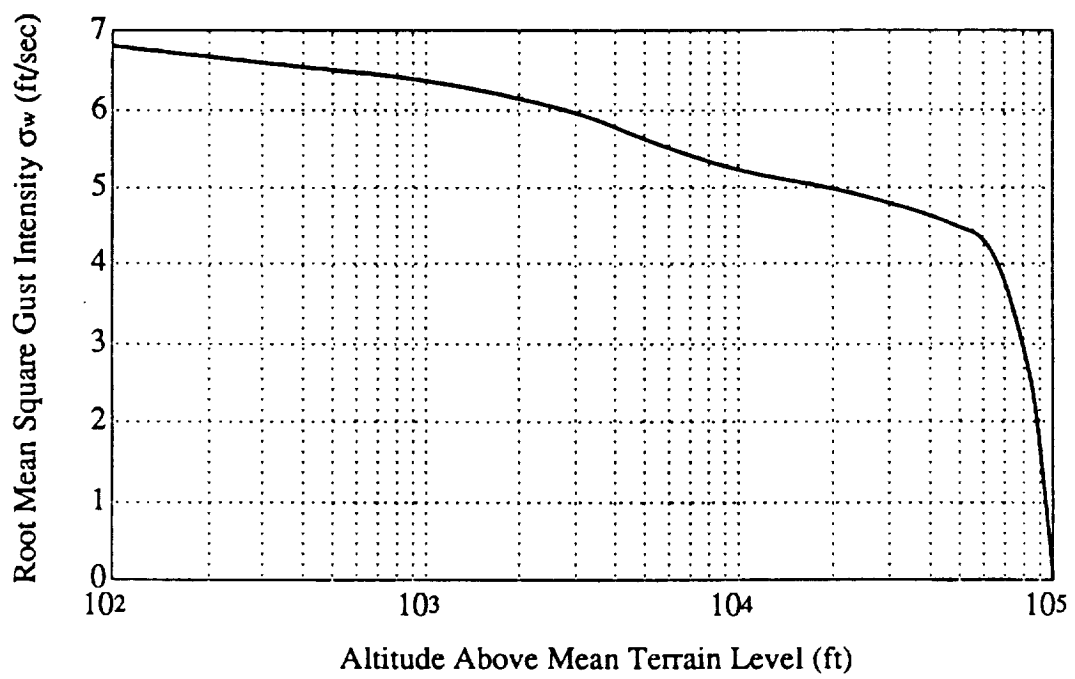
Figure 4.2: Dryden Turbulence Level as a Function of Altitude

Chapter 5

INNER-LOOP DESIGN — SYNTHESIS AND ANALYSIS

In this chapter we examine the synthesis of a TECS inner-loop design at two flight conditions FLT1 and FLT2 (Appendix E). Results presented in the following sections illustrate the application of the design procedure described in section 4.2.

5.1 Design for a Nominal Flight Condition

For AFCS designs, tight airspeed and path control is important in the presence of windshear, particularly at low altitudes and during landing approach conditions. In this respect, the landing approach flight condition FLT1 was considered most important and is selected to be the nominal design condition for the TECS inner-loop gains. These TECS gains are designed to yield optimum performance at this flight condition.

Designs at other flight conditions are synthesized around this nominal controller using the gain schedule parameters K_{CAS} and K_{GW} (figure 2.2). When optimizing the TECS inner-loop gains, the gain schedule parameters are not considered as independent parameters and must be fixed at some selected values. Without loss of generality, gain schedule at the flight condition FLT1 is selected to be the same as that of the classical design.

Design parameters in the TECS structure are determined following the procedure described in section 4.2. Arrival at a final design using constrained parameter optimization involves compromise among different design performance goals. For the landing approach flight condition FLT1, the following design objectives were used:

- The performance indices $J_1^i(i = 1, 3)$ described in equations (4.15), (4.18) and (4.19) are given below.

  (a) Command frequency response bandwidths and command tracking perfor-

mance:

$$J_1^{(1)} = \lim_{t_f \to \infty} \frac{1}{2} \int_0^{t_f} E[2(\gamma(t) - \gamma_c(t))^2 + (V(t) - V_c^*(t))^2]dt \qquad (5.1)$$

This performance index is evaluated to parameterized random filtered step commands in $\dot{V}_c$ and γ_c with $\dot{V}_c(t) = V_{co}ae^{-at}\mu(t)$ and $\gamma_c(t) = \gamma_{co}(1 - e^{-at})\mu(t)$ where $\mu(t)$ is the unit step function. The parameter a determines the bandwidth of both the acceleration and the flight-path commands. In this design case, we use $a = 1.2rad/sec$, a typical value for flight-path and velocity command bandwidths. The variables V_{co} and γ_{co} are random parameters with zero means and covariances $E[V_{co}^2] = \sigma_{V_c}^2 = 1.0(fps)^2$ and $E[\gamma_{co}^2] = \sigma_{\gamma_c}^2 = 1.0(deg)^2$.

(b) Broken-loop crossover frequency in the throttle control loop:

$$J_1^{(2)} = \lim_{t_f \to \infty} \frac{1}{2} E[10\delta_{thc}^2(t_f)] \qquad (5.2)$$

The performance index $J_1^{(2)}$ is evaluated to a high-pass noise input in the thrust command loop. The noise input is generated from the response of a first-order high-pass filter to white-noise with zero mean $E[\delta_{thw}(t)] = 0$ and covariance $E[\delta_{thw}(t+\tau)\delta_{thw}(t)] = \sigma_{thw}^2\delta(\tau)$. In this design, we choose $\sigma_{thw} = 1$. The quantity $\delta_{thc}(t)$ is the thrust feedback control as shown in figure 4.1 . Cut-off frequency of the high-pass filter is set approximately equal to the desired broken-loop throttle control bandwidth (i.e. $\omega_{\delta_{thw}} = 0.2$ rad/sec).

(c) Broken-loop crossover frequency in the elevator control loop:

$$J_1^{(3)} = \lim_{t_f \to \infty} \frac{1}{2} E[3\delta_{ec}^2(t_f)] \qquad (5.3)$$

The performance index $J_1^{(3)}$ is evaluated to a high-pass noise input in the elevator command loop. The noise input is generated from the response of a first-order high-pass filter to white-noise with zero mean $E[\delta_{ew}(t)] = 0$ and covariance $E[\delta_{ew}(t+\tau)\delta_{ew}(t)] = \sigma_{ew}^2\delta(\tau)$. In this design, we choose $\sigma_{ew} = 0.16$. The quantity $\delta_{ec}(t)$ is the elevator feedback control as shown in figure 4.1 . Cut-off frequency of the high-pass filter is set approximately equal to the desired broken-loop elevator control bandwidth (i.e. $\omega_{\delta_{ew}} = 2.0$ rad/sec).

- Stability of the closed-loop eigenvalues:
  (a) Real part of the eigenvalues must be less than zero,

$$\sigma_i \leq 0 \ (i = 1, n) \tag{5.4}$$

(b) Damping ratio of the eigenvalues must be greater than 0.7, i.e

$$\zeta_i \geq 0.7 \ (i = 1, n) \tag{5.5}$$

- Mean square responses of control activities to clear air Dryden turbulence of $\sigma_u = 6.6 fps$ and $\sigma_w = 6.3 fps$,

$$E[\delta_{thc}^2] \leq 7.56 \times 10^{-4} (lbst/lbsw)^2 \tag{5.6}$$

$$E[\delta_{ec}^2] \leq 6.735 \times 10^{-4} (rad)^2 \tag{5.7}$$

The above constraints will produce an optimal design (listed under $SANDY$ in table 5.4) with a covariance in the speed variable V exceeding that of the classical design. To remedy this design problem, we include in the next design an additional constraint on the covariance response of the speed variable as

$$E[V^2] \leq 0.5122 (fps)^2 \tag{5.8}$$

The optimal design with this additional covariance constraint is shown in tables 5.1 and 5.4 as the optimal design $SANDY^*$.

Sample of an input data file for the computer program $SANDY$ corresponding to the above design formulation at flight condition FLT1 is given in Appendix F. The data file contains the plant synthesis model, controller model, disturbance specifications, penalty weighting matrices, linear constraints, nonlinear constraints and direct bounds on parameters. The resulting optimal feedback gains and associated design parameters k_1, k_2 are summarized in table 5.1. The following paragraphs discuss design results obtained at flight condition FLT1 corresponding to the final optimized design $SANDY^*$.

In the optimal design $SANDY^*$, the proportional gain K_{TP} to the throttle, pitch damper gain K_θ and the decoupling parameter k_2 differ significantly from the classical

design. Improved performance and damping are achieved with a nonzero value of K_{TP} and a lower gain K_θ. Recall that the magnitude of the parameter k_2 represents the degree of cross-coupling between flight-path command to steady-state speed error. This value is reduced in the optimal design in comparison to the classical design. Gains in the pitch damper have been reduced while those in the proportional and integral paths to the elevator are kept at the same level as the classical design; hence maintaining the desired command bandwidth and tracking performance.

Table 5.2 gives the damping ratio and natural frequency of the closed-loop system eigenvalues. A minimum damping of 0.7 is achieved through the use of nonlinear constraints; this is an improvement over the minimum damping of 0.64 in the classical TECS design.

Figures 5.1 and 5.2 show the command and broken-loop control frequency responses of the classical and the optimized TECS designs respectively. Command and control-loop bandwidths for these designs are summarized in table 5.3. One design consideration is to have equal bandwidths in both the flight-path and acceleration command loops. Equal bandwidths in these command paths imply that transient errors in the total energy rate and energy distribution rate will decay exponentially to zero at a same time constant (i.e. *coordinated* flight-path and speed command responses). The command bandwidths for the optimal design are similar to those of the classical design. Notice that the command bandwidths are achieved with a lower bandwidth in the elevator control path.

Control-loop bandwidths give measures of control sensitivity to unmodeled high-frequency dynamics in the control paths. Lower control-loop bandwidth means less sensitivity to these types of unmodeled dynamics. The elevator loop bandwidth in the optimal design is smaller than that of the classical design at flight condition FLT1.

Figures 5.3 to 5.6 show time responses of the closed-loop systems to step commands in flight-path angle and velocity. Velocity command is derived from an acceleration command as in equation (4.16). Results to a velocity command are shown in figures 5.5 and 5.6. Both the flight-path angle and velocity commands are implemented through first-order command shaping filters with bandwidths equal to those used in the control-law synthesis (i.e. $a = 1.2$ rad/sec for both commands). Improved damping in the transient responses of flight-path angle and velocity errors is seen in figures 5.4 and 5.6. Responses to flight-path angle and velocity commands are similar

to step responses of a first-order filter. And there is less cross-coupling between the flight-path command and velocity.

Table 5.4 compares the closed-loop rms responses of the classical and the optimal designs to Dryden clear air turbulence at the 99% probability level of intensities. Results clearly illustrate the effective usage of direct bounds on the respective output covariances. By imposing inequality constraints on the control covariances, one is guaranteed at the outset that the optimal design, when converged, will have the same or lower control activities than the classical design. Furthermore, covariance responses of other aircraft variables are lower or equal to those of the classical design. In particular, the covariance response of the speed variable V is equal to the value of the classical design due to the inequality constraint defined in equation (5.8).

Conventional single-loop robustness[1] analysis gives allowable variations of gain or phase at either the control or sensor paths, while other remaining loops are closed at the nominal gains. Gain and phase margins determined from Bode or Nyquist plots yields the largest allowable variations (one-loop at a time) in loop gain and phase respectively starting from a nominally stable closed-loop system. Table 5.5 summarizes values of single-loop stability margins. Single-loop stability margins are found to be satisfactory for both the optimal and classical designs.

Multivariable robustness tests (Appendix D) based on singular values of loop return-difference matrices provide additional measures of design robustness in terms of guaranteed multivariable gain and phase margins [Ref.20]. The results may be conservative but they are applicable to *simultaneous* variation of gain and phase in each loop. Figures 5.7–5.12 show plots of minimum singular values of the return-difference and the inverse-return-difference transfer matrices respectively at both the control and sensor paths. In these plots, diagonal scaling [Ref.23] on the transfer function matrices has been used to reduce conservatism and thereby improve estimates of actual multiloop stability margins. Table 5.6 gives guaranteed multivariable stability margins in both the control actuator and sensor paths according to equations (D.8) and (D.14) of Appendix D. Both the optimal and classical designs possess similar multivariable stability margins. Note that requirements for robustness have not been

---

[1] Robustness margins are defined as the amount of allowable gain and phase *increases* prior to the onset of instability.

defined in the control-law synthesis. Systematic methods for improving design robustness are discussed in section 4.2. Robust control-law synthesis using H^∞-bounds or μ-measure will be the subject of a future study.

5.2 Determination of Gain Schedule

Gain scheduling of the TECS inner-loops is necessary in order to satisfy performance and stability requirements at other flight conditions. Gain scheduling between a landing approach condition and one other cruise condition FLT2 is considered in this study. The objective is to demonstrate the usage of nonlinear constrained optimization in the design of gain schedule. Design results are discussed in the following paragraphs. The gain schedule design is obtained by re-optimizing the gains K_{GW} and K_{CAS} in the throttle and elevator paths respectively. The TECS proportional, integral and pitch damper gains $K_{TP}, K_{EP}, K_{TI}, K_{EI}, K_q$, and K_θ are held constant at the values optimized for the landing-approach condition FLT1. Another set of design objectives are established for the cruise condition similar in form to that given in equations (5.1)-(5.8). They are as follows,

- The performance indices $J_1^i (i = 1, 3)$ described in equations (4.15), (4.18) and (4.19) are given below.

  (a) Command frequency response bandwidths and command tracking performance:

  $$J_1^{(1)} = \lim_{t_f \to \infty} \frac{1}{2} \int_0^{t_f} E[2(\gamma(t) - \gamma_c(t))^2 + 2(V(t) - V_c^*(t))^2] dt \qquad (5.9)$$

  This performance index is evaluated to parameterized random filtered step commands in $\dot{V}_c$ and γ_c with $\dot{V}_c(t) = V_{co} a e^{-at} \mu(t)$ and $\gamma_c(t) = \gamma_{co}(1 - e^{-at})\mu(t)$ where $\mu(t)$ is the unit-step function. The parameter a determines the bandwidth of both the acceleration and the flight-path commands. In this design case, we use $a = 1.2 rad/sec$, a typical value for flight-path and velocity command bandwidths. The variables V_{co} and γ_{co} are random parameters with zero means and covariances $E[V_{co}^2] = \sigma_{V_c}^2 = 1.0(fps)^2$ and $E[\gamma_{co}^2] = \sigma_{\gamma_c}^2 = 1.0(deg)^2$.

  (b) Broken-loop crossover frequency in the throttle control loop:

  $$J_1^{(2)} = \lim_{t_f \to \infty} \frac{1}{2} E[20\delta_{thc}^2(t_f)] \qquad (5.10)$$

The performance index $J_1^{(2)}$ is evaluated to a high-pass noise input in the thrust command loop. The noise input is generated from the response of a first-order high-pass filter to white-noise with zero mean $E[\delta_{thw}(t)] = 0$ and covariance $E[\delta_{thw}(t+\tau)\delta_{thw}(t)] = \sigma_{thw}^2\delta(\tau)$. Again, we choose $\sigma_{thw} = 1$. The quantity $\delta_{thc}(t)$ is the thrust feedback control as shown in figure 4.1 . Cut-off frequency of the high-pass filter is set approximately equal to the desired broken-loop throttle control bandwidth (i.e. $\omega_{\delta_{thw}} = 0.2$ rad/sec).

(c) Broken-loop crossover frequency in the elevator control loop:

$$J_1^{(3)} = \lim_{t_f \to \infty} \frac{1}{2} E[6\delta_{ec}^2(t_f)] \tag{5.11}$$

The performance index $J_1^{(3)}$ is evaluated to a high-pass noise input in the elevator command loop. The noise input is generated from the response of a first-order high-pass filter to white-noise with zero mean $E[\delta_{ew}(t)] = 0$ and covariance $E[\delta_{ew}(t+\tau)\delta_{ew}(t)] = \sigma_{ew}^2\delta(\tau)$. Again, we choose $\sigma_{ew} = 0.16$. The quantity $\delta_{ec}(t)$ is the elevator feedback control as shown in figure 4.1 . Cut-off frequency of the high-pass filter is set approximately equal to the desired broken-loop elevator control bandwidth (i.e. $\omega_{\delta_{ew}} = 2.0$ rad/sec).

- Stability of the closed-loop eigenvalues:

  (a) Real part of the eigenvalues must be less than zero,

$$\sigma_i \leq 0 \ (i = 1, n) \tag{5.12}$$

  (b) Damping ratio of the eigenvalues must be greater than 0.6, i.e

$$\zeta_i \geq 0.6 \ (i = 1, n) \tag{5.13}$$

- Mean square responses of control activities to clear air Dryden turbulence of $\sigma_u = 4.7 fps$ and $\sigma_w = 4.7 fps$,

$$E[\delta_{thc}^2] \leq 1.804 \times 10^{-5} (lbst/lbsw)^2 \tag{5.14}$$

$$E[\delta_{ec}^2] \leq 3.2 \times 10^{-3} (rad)^2 \tag{5.15}$$

It turns out that no feasible solution can be found to satisfy simultaneously the closed-loop damping constraint of at least 0.6 and an elevator control activity to turbulence less than or equal to that achieved under the classical design. Thus the covariance bound on the elevator control is set to a value *slightly* higher than the value obtained from the classical design. Note that the selected bound on the elevator control activity to turbulence still yields acceptable level of control activity to the given level of turbulence. Recall that in the gain schedule design, the optimization has only two design parameters K_{GW} and K_{CAS}. As we have demonstrated in flight condition FLT1, results of the classical design at flight condition FLT2 could similarly be achieved if we re-optimize all the inner-loop gains. Re-optimization of all the inner-loop gains at the flight condition FLT2 is presented in chapter 7 along with an altitude and speed-hold autopilot design.

Gain schedule developed for the parameters K_{GW} and K_{CAS} at the two design flight conditions and associated design parameters k_1 and k_2 are shown in table 5.7. As previously mentioned, gain schedule at the nominal flight condition FLT1 is chosen to be the same for both the optimal and classical designs.

At flight condition FLT2 the optimized gain schedule based on the inner-loop design optimized at flight condition FLT1 is quite different than the one chosen in the classical design. Design procedure for the selection of gain schedule in the classical design is usually based on closed-loop stability. It may not consider other design objectives such as tracking performance and control activities in the presence of turbulence.

Table 5.8 shows the damping ratio and the natural frequency of the closed-loop system eigenvalues. A minimum damping of 0.6 is achieved in the optimal design through the use of nonlinear constraints on the closed-loop system eigenvalues. The result is improved over the conventional TECS closed-loop damping of 0.45. It is found by increasing the minimum damping requirement that higher damping of 0.7 for all modes is not achievable with simple gain scheduling of the parameters K_{GW} and K_{CAS}. Furthermore, the covariance constraint on the elevator control activity to turbulence with upper bound set equal to the value obtained in the classical design cannot be satisfied together with a minimal damping of 0.60 using only the design parameters K_{GW} and K_{CAS}.

Figures 5.13 and 5.14 show the command and the broken-loop control frequency responses at flight condition FLT2. Command and control-loop bandwidths are summarized in table 5.9. Bandwidths in the flight-path and acceleration command loops are made nearly equal in the optimal design through adjustment of the design weighting parameters Q_1 and Q_2 in the cost function $J_0^{(1)}$. The throttle control-loop bandwidth is significantly reduced in the optimal design; however, this result comes at the expense of an increased bandwidth in the elevator control path. The increase in elevator control bandwidth did not result in significantly higher elevator control activities to turbulence as seen in table 5.10. This design result illustrates the benefit of control covariance constraints in maintaining a given level of control activities while control bandwidths are optimized (i.e. increased) for improved damping and frequency of the longitudinal modes.

Figures 5.15 to 5.18 show the time responses to step commands of the flight-path angle and velocity variables. Velocity command is developed from an acceleration command according to equation (4.16). Results associated with the velocity command are shown in figures 5.17 and 5.18. Both the flight-path angle and velocity commands are implemented through first-order command shaping filters with bandwidths equal to those used in the design synthesis (i.e. $a = 1.2$ rad/sec for both commands). Improved damping in the transient responses of flight-path angle and velocity errors is seen in figures 5.16 and 5.18. Command overshoots in flight-path angle responses have been nearly eliminated in the $SANDY^*$ design.

Table 5.10 lists the closed-loop rms responses of the optimal and classical designs to Dryden clear air turbulence at the 99% probability level of intensities. Control rms responses are constrained with nonlinear inequality bounds on the control covariances. Results indicate that the optimal design possesses significantly lower throttle activities. Nearly the same rms turbulence response in the elevator control is maintained in spite of significantly higher elevator control bandwidth.

Table 5.11 gives values of single-loop type gain and phase margins. Single-loop stability margins are found to be satisfactory for both the optimal and the classical gain schedule designs.

Figures 5.19–5.24 show respectively plots of minimum singular values of the return-difference and the inverse return-difference transfer matrices for the optimal and classical designs at both the control and sensor paths. Diagonal scaling has been

used to improve estimates of actual multivariable stability margins. Table 5.12 show guaranteed stability margins in both the control actuator and sensor paths obtained according to equations (D.8) and (D.14) in Appendix D. Note that the design robustness was achieved without direct design considerations. As pointed out in section 4.2, H^∞ bounds on appropriate loop transfer matrices can be set up to address design robustness when such an improvement is needed.

In the next chapters, we discuss the design of an altitude and speed-hold control system using the TECS controller structure as inner-loop. The objective is to demonstrate the design features and the usage of nonlinear constrained parameter optimization in autopilot designs. There are two basic approaches one can adopt in the autopilot design:

- The outer-loop design can be developed based on an existing (i.e previously designed) inner-loop TECS controller. This approach is simple and involves a fewer number of design parameters. But it does not yield the maximally achievable performance that would be possible if the inner-loop gains are re-optimized together with the outer-loop control functions. As seen in chapter 6, this method yields excessive throttle and elevator control activities to altitude command.

- The outer-loop design is integrated with the synthesis of the inner-loop control-law. This latter procedure provides a better overall control design as demonstrated in chapter 7.

Table 5.1: Inner-Loop Feedback Gains (FLT1)

Parameter	SANDY	SANDY*	Classical
K_{TP}	0.09694	0.14189	0.0
K_{EP}	3.3760	3.4312	3.36
K_{TI}	0.3499	0.3835	0.4
K_{EI}	2.4037	2.3360	2.52
K_q	3.0071	2.9788	4.0
K_θ	3.1240	3.1184	6.0
k_1	0.9194	0.9060	0.8932
k_2	-0.1633	-0.0950	0.2465

Table 5.2: Closed-Loop System Poles (FLT1)

Design	SANDY*		Classical	
Mode	ζ	ω_n (rad/sec)	ζ	ω_n (rad/sec)
Phugoid mode	0.7	0.81	0.64	0.61
Short period	0.7	2.23	0.79	3.01

Table 5.3: Command and Broken-Loop Control Bandwidths (FLT1)

Command/Control Path	Bandwidths (rad/sec)	
	SANDY*	Classical
γ_c	0.8	0.7
$\dot{V}_c$	0.7	0.8
δ_{ec}	3.1	4.3
δ_{thc}	0.37	0.37

Table 5.4: Closed-Loop RMS Responses to Turbulence (FLT1)

($\sigma_u = 6.6$ fps, $\sigma_w = 6.3$ fps)

Variable	SANDY	SANDY*	Classical
γ (deg)	0.9243	0.9025	1.0531
V (fps)	0.7915	0.7157	0.7157
n_{zcg} (g)	0.0805	0.0803	0.0800
δ_{th} (lbst/lbsw)	0.02570	0.02605	0.02725
δ_e (deg)	1.3324	1.3311	1.3324

Table 5.5: Single-Loop Type Stability Margins (FLT1)

Design	SANDY*		Classical	
Margins	Gain Margin (dB)	Phase Margin (deg)	Gain Margin (dB)	Phase Margin (deg)
Actuator Paths	$(-42, +\infty)$	-60	$(-44, +31)$	-57
Sensor Paths	$(-15, +14)$	$(-64, +62)$	$(-17, +20)$	$(-63, +74)$

Table 5.6: Guaranteed Multivariable Stability Margins (FLT1)

Design	SANDY*		Classical	
Margins	Gain Margin (dB)	Phase Margin (deg)	Gain Margin (dB)	Phase Margin (deg)
Actuator Paths	$(-14.9, +5.2)$ $(-5.3, +16.4)$	± 50.2	$(-14.8, +5.2)$ $(-5.1, +14.6)$	± 48
Sensor Paths	$(-2.8, +4.2)$	± 22	$(-3.3, +5.4)$	± 27

Table 5.7: Inner-Loop Gain Schedule and Design Parameters

Parameter	FLT1		FLT2	
	SANDY*	Classical	SANDY*	Classical
K_{CAS}	0.9322	0.9322	0.1950	0.07006
K_{GW}	80,000	80,000	67,328	80,000
k_1	0.9060	0.8932	0.9801	0.9717
k_2	-0.0950	0.2465	-0.3208	0.1795

Table 5.8: Closed-Loop System Poles (FLT2)

Design	SANDY*		Classical	
Mode	ζ	ω_n (rad/sec)	ζ	ω_n (rad/sec)
Phugoid mode	0.6	0.64	0.45	0.42
Short period	0.68	3.95	0.47	3.43

Table 5.9: Command and Broken-Loop Control Bandwidths (FLT2)

Command/Control Path	Bandwidths (rad/sec)	
	SANDY*	Classical
γ_c	0.65	0.55
$\dot{V}_c$	0.65	0.63
δ_e	4.3	2.7
δ_{th}	0.29	0.37

Table 5.10: Closed-Loop RMS Responses to Turbulence (FLT2)

$(\sigma_u = 4.7$ fps, $\sigma_w = 4.7$ fps)

Variable	SANDY*	Classical
γ (deg)	0.2095	0.2094
V (fps)	0.1369	0.2060
n_{zcg} (g)	0.0862	0.0805
δ_{th} (lbst/lbsw)	0.00355	0.004142
δ_e (deg)	0.2222	0.1667

Table 5.11: Single-Loop Type Stability Margins (FLT2)

Design	SANDY*		Classical	
Margins	Gain Margin (dB)	Phase Margin (deg)	Gain Margin (dB)	Phase Margin (deg)
Actuator Paths	$(-56, +\infty)$	-83	$(-51, +30)$	-70
Sensor Paths	$(-\infty, 21)$	$(-68, +105)$	$(-\infty, 24)$	$(-48, +124)$

Table 5.12: Guaranteed Multivariable Stability Margins (FLT2)

Design	SANDY*		Classical	
Margins	Gain Margin (dB)	Phase Margin (deg)	Gain Margin (dB)	Phase Margin (deg)
Actuator Paths	$(-15, +5.2)$ $(-5.4, +17.8)$	± 51.6	$(-11.24, +4.7)$ $(-5.4, +17.4)$	± 51.2
Sensor Paths	$(-3.6, 6.3)$	± 29.9	$(-3.1, 5.0)$	± 25.3
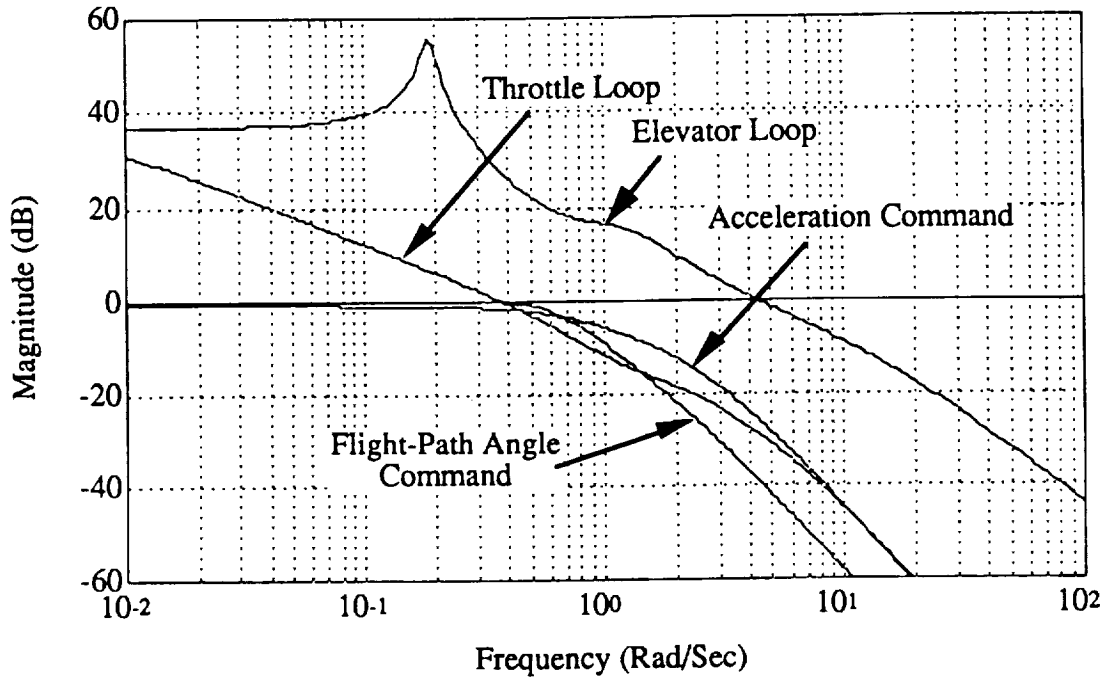
Figure 5.1: Loop Frequency Responses of Classical Design (FLT1)
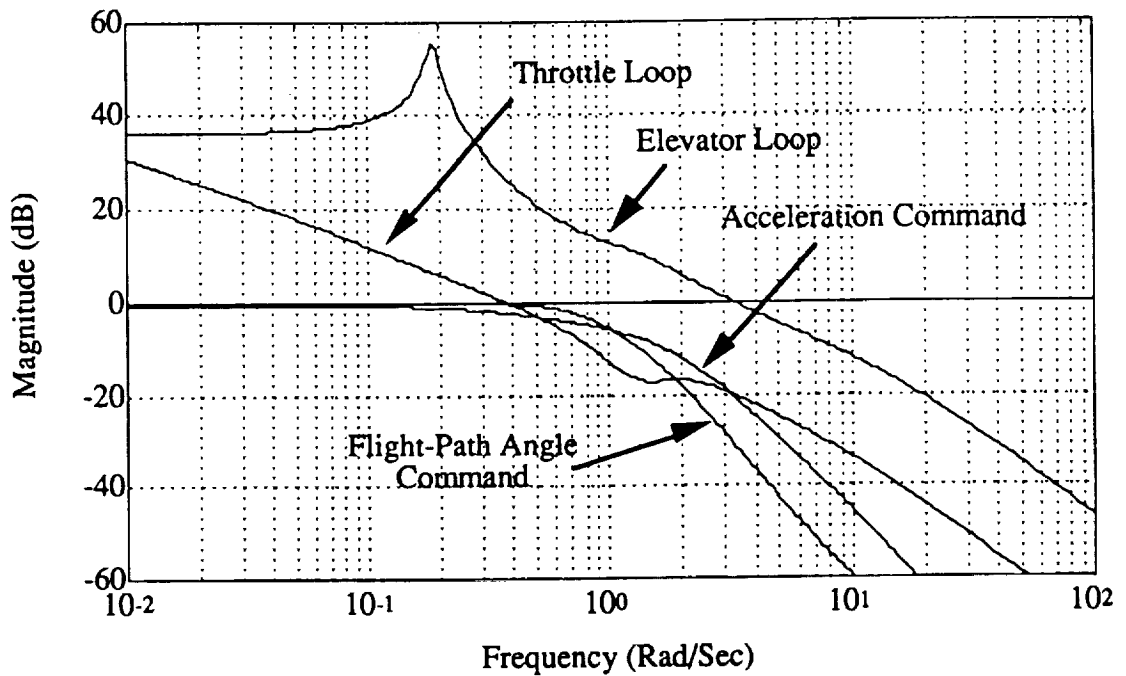
Figure 5.2: Loop Frequency Responses of Optimal Design (FLT1)
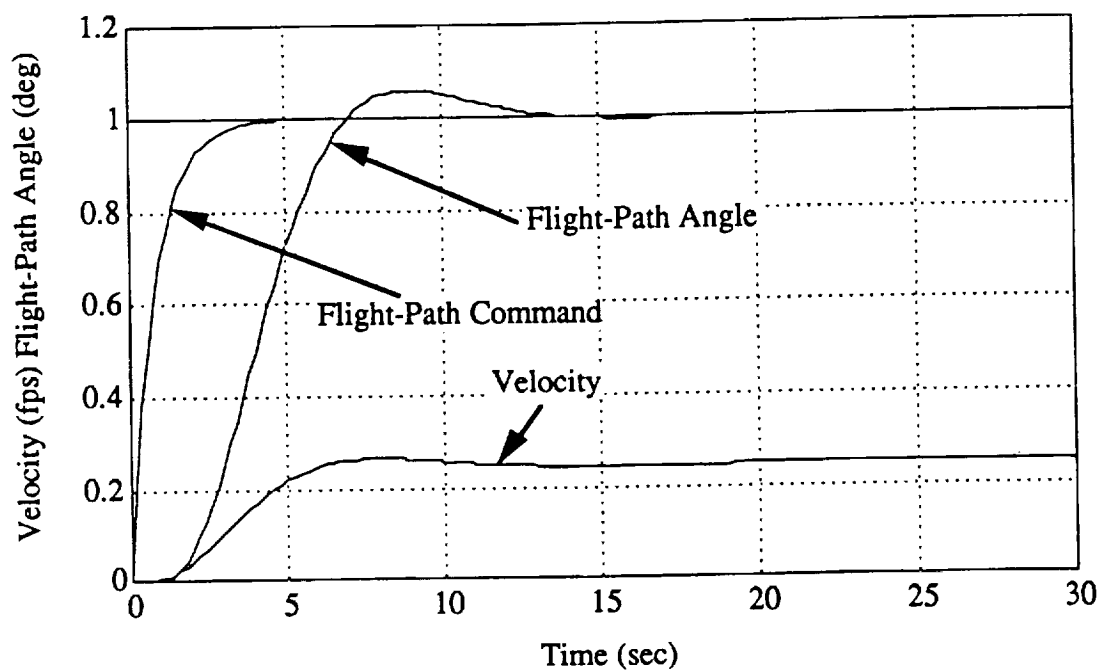
Figure 5.3: γ_c Command Responses of Classical Design (FLT1)
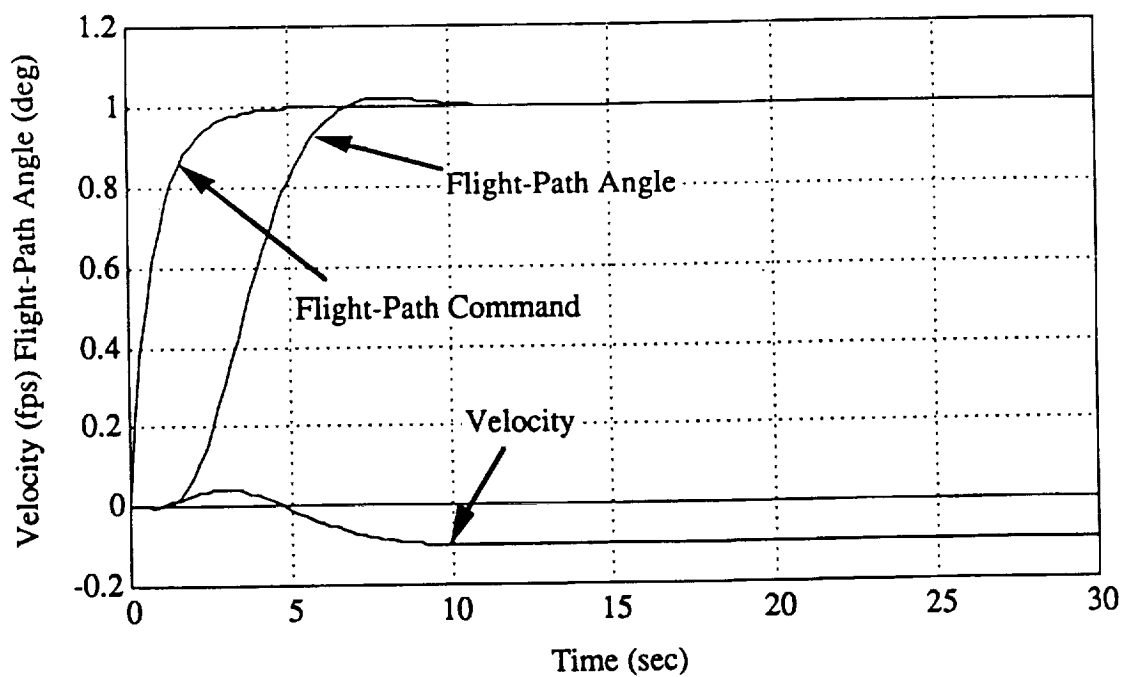
Figure 5.4: γ_c Command Responses of Optimal Design (FLT1)
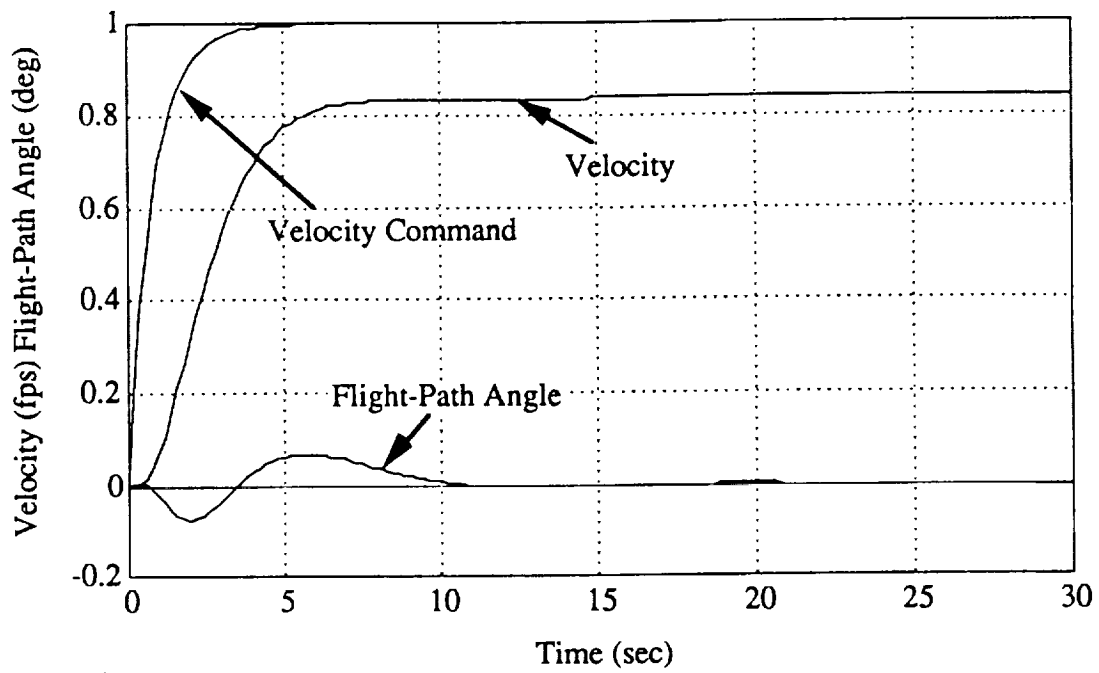
Figure 5.5: V_c Command Responses of Classical Design (FLT1)
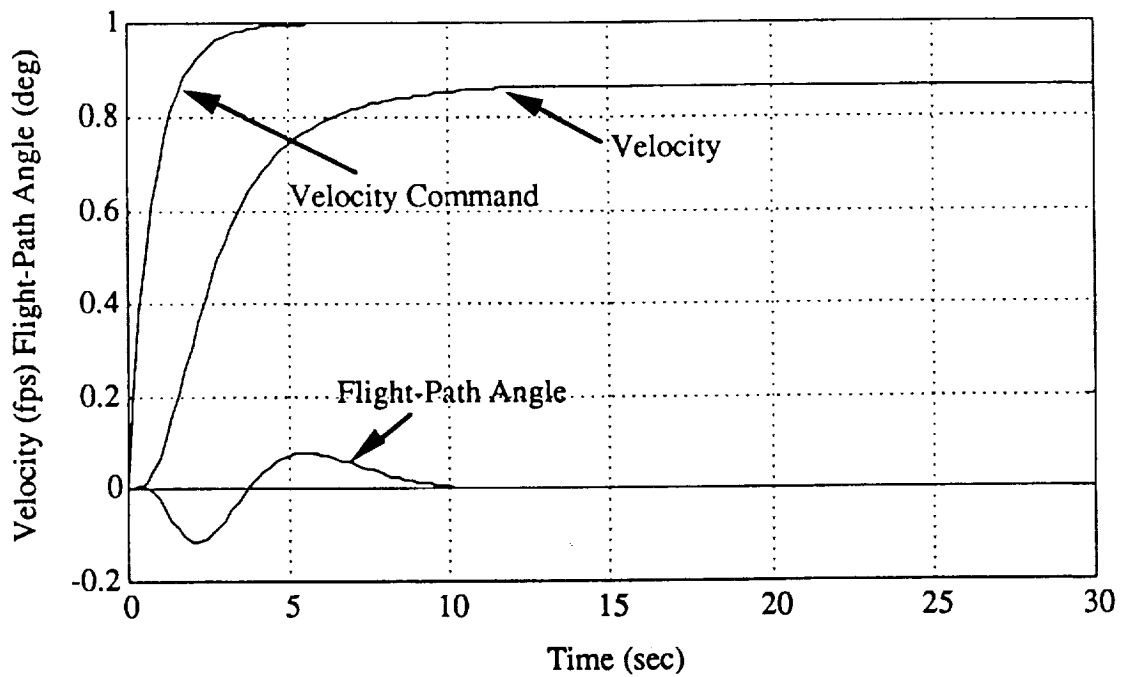
Figure 5.6: V_c Command Responses of Optimal Design (FLT1)

Minimum Singular Value of the Return-Difference Matrix

Sigma

Frequency (Rad/Sec)
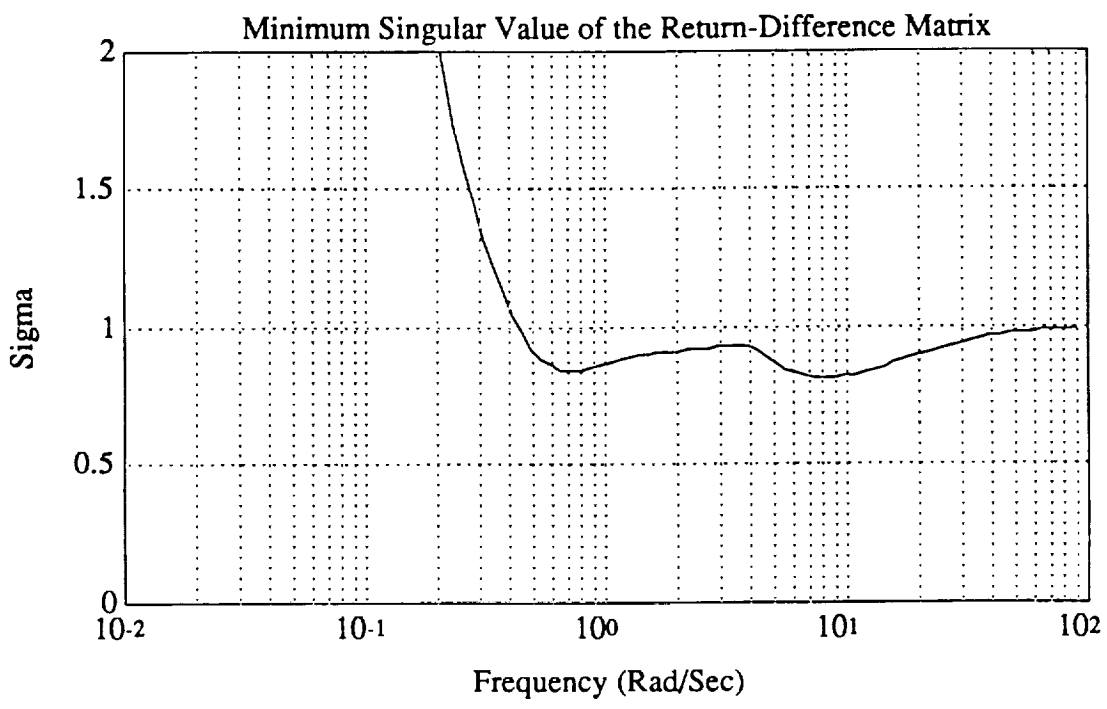
Figure 5.7: Robustness at the Control Paths of Classical Design (FLT1)

Minimum Singular Value of the Return-Difference Matrix

Sigma

Frequency (Rad/Sec)
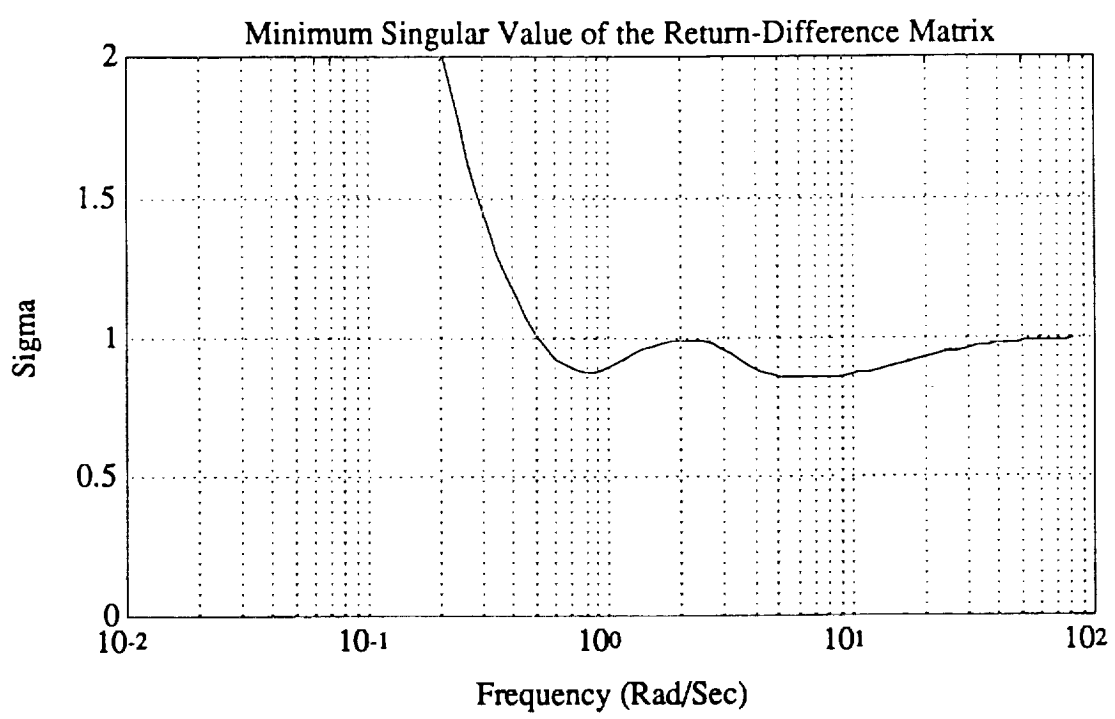
Figure 5.8: Robustness at the Control Paths of Optimal Design (FLT1)
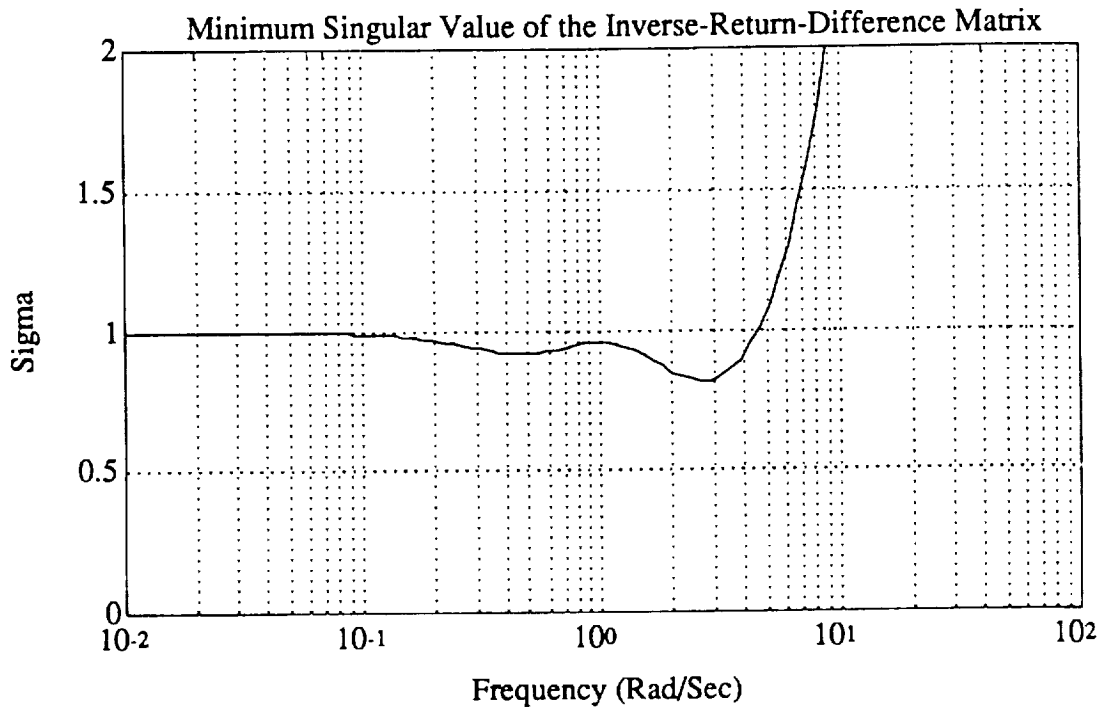
Figure 5.9: Robustness at the Control Paths of Classical Design (FLT1)
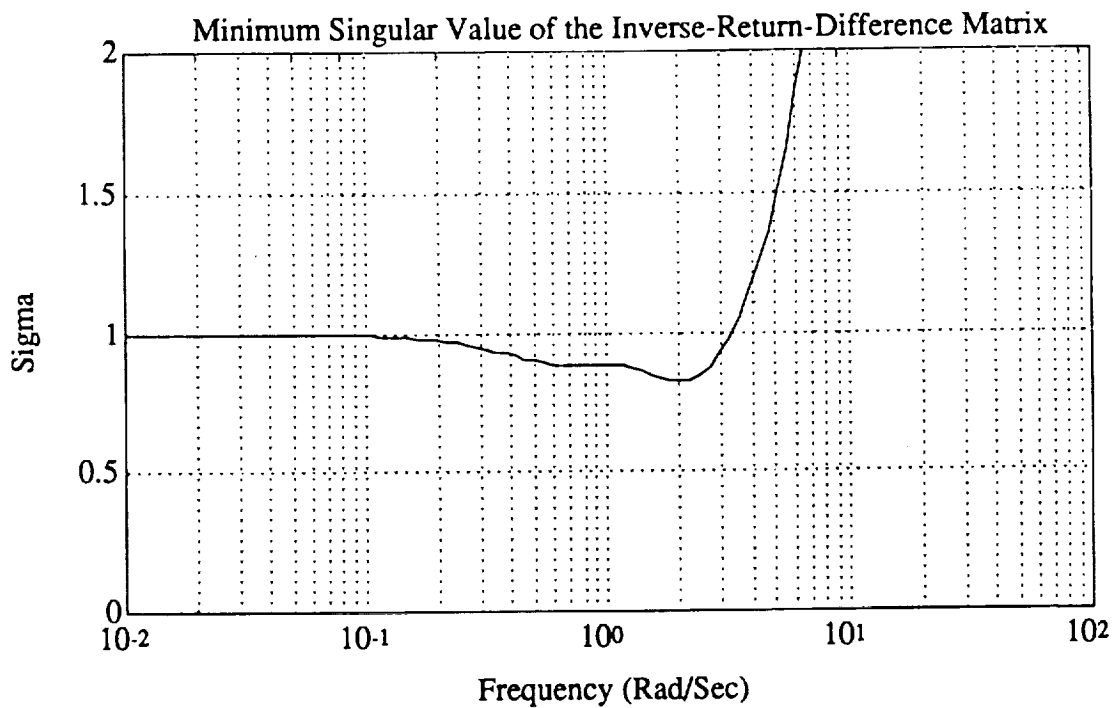
Figure 5.10: Robustness at the Control Paths of Optimal Design (FLT1)
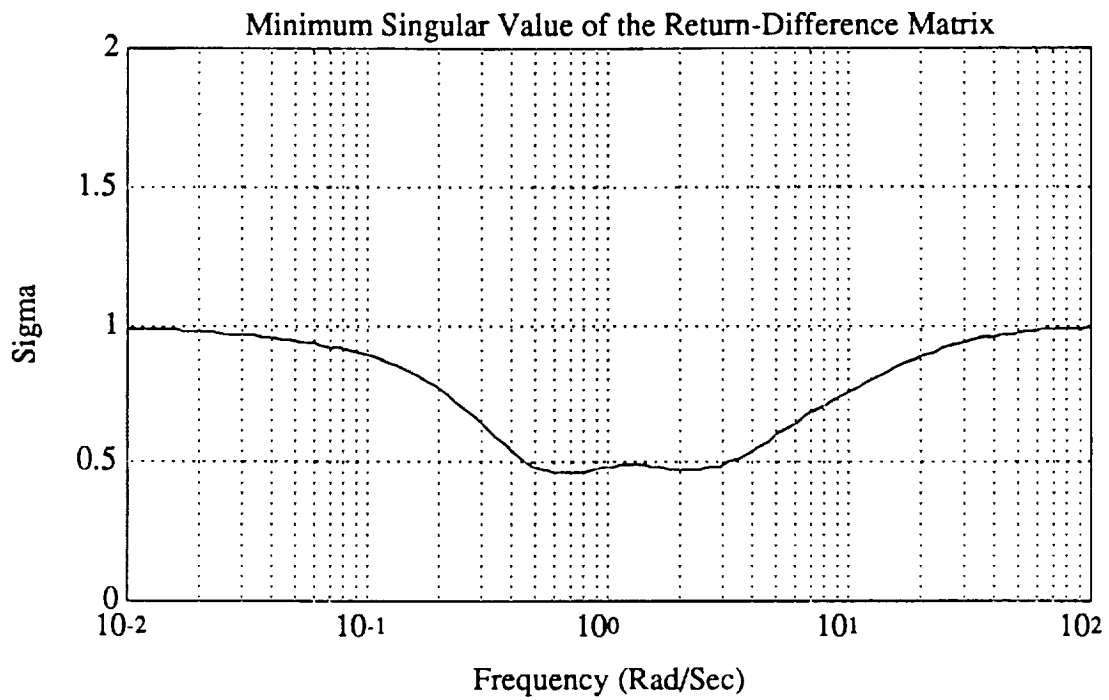
Figure 5.11: Robustness at the Sensor Paths of Classical Design (FLT1)
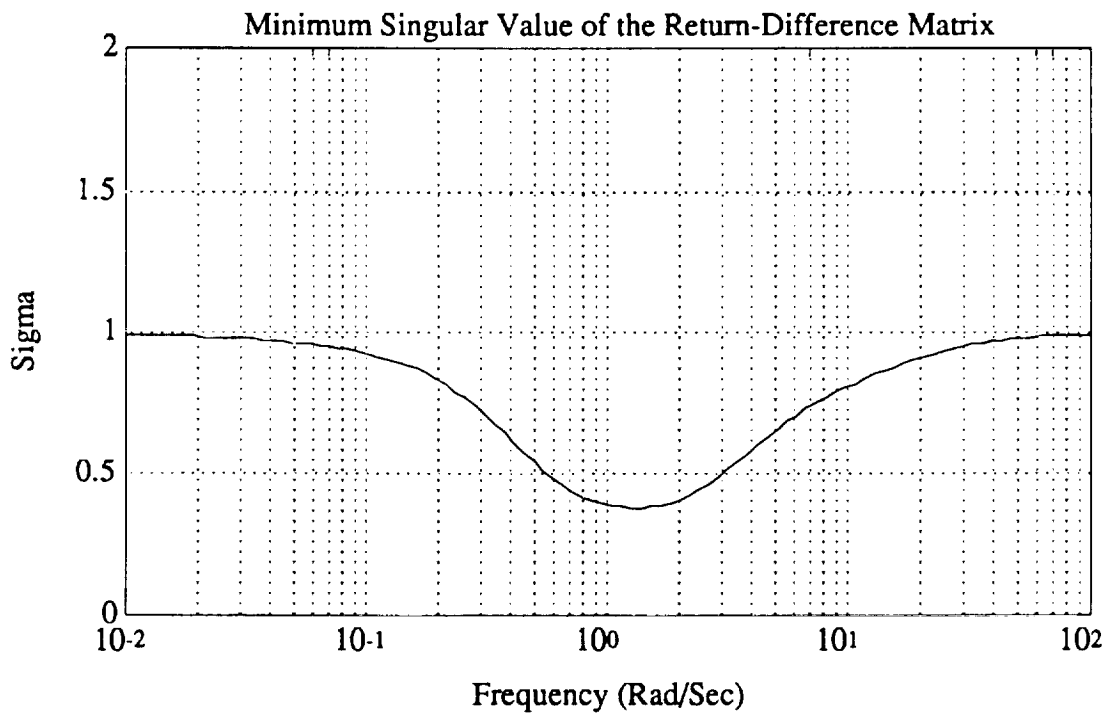
Figure 5.12: Robustness at the Sensor Paths of Optimal Design (FLT1)
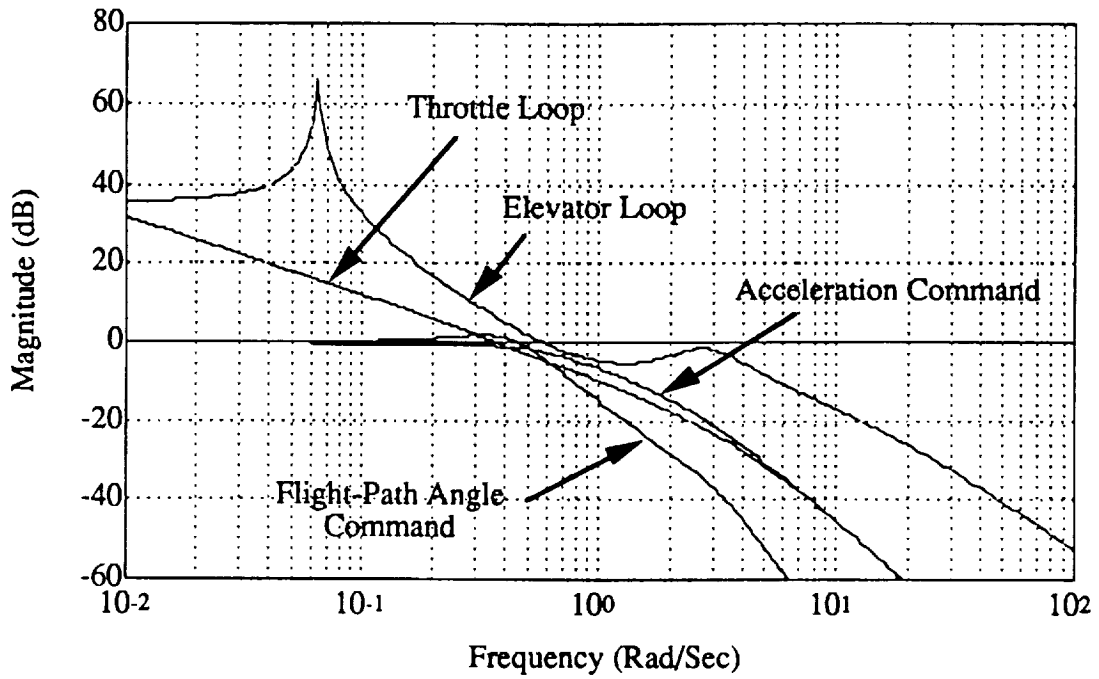
Figure 5.13: Loop Frequency Responses of Classical Design (FLT2)
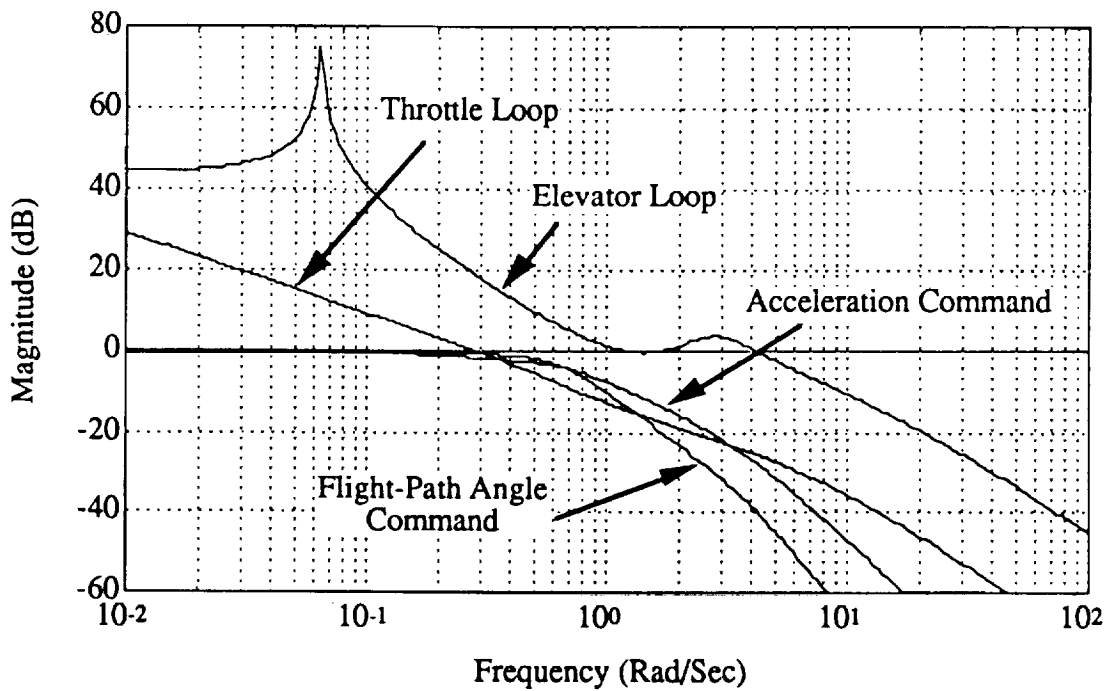
Figure 5.14: Loop Frequency Responses of Optimal Design (FLT2)
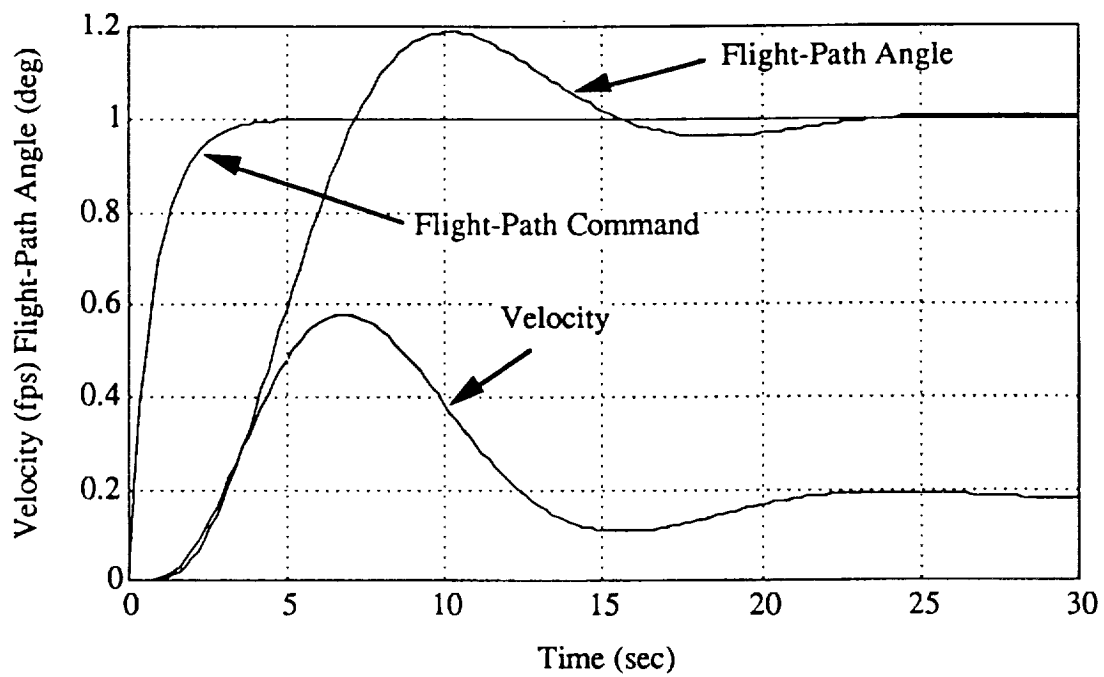
Figure 5.15: γ_c Command Responses of Classical Design (FLT2)
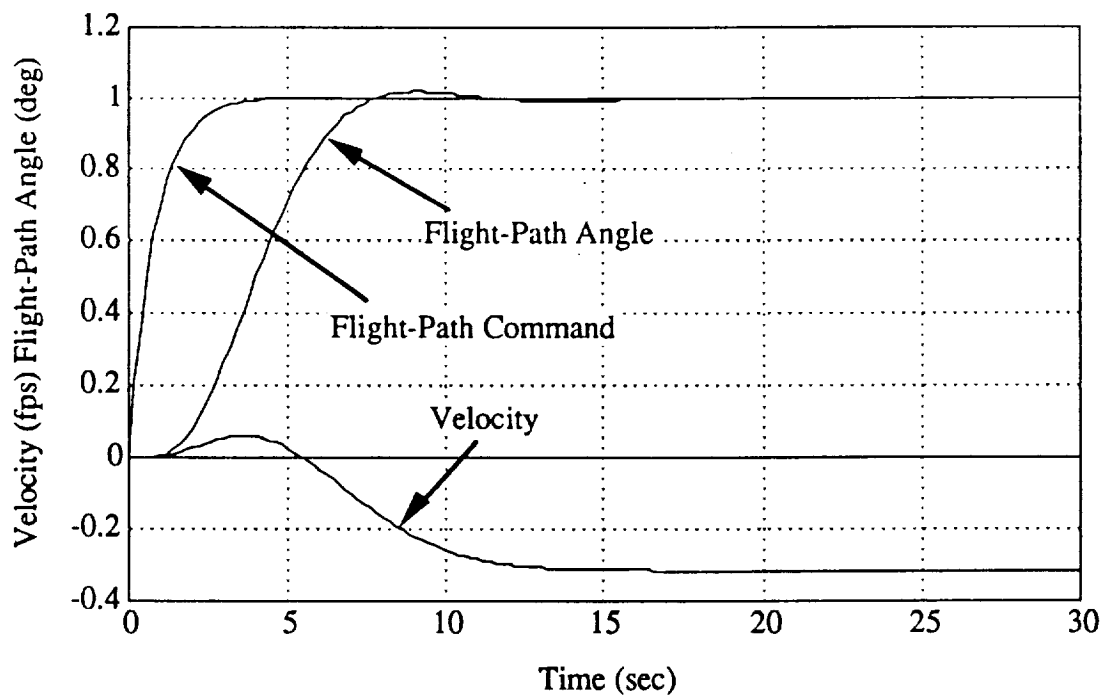
Figure 5.16: γ_c Command Responses of Optimal Design (FLT2)
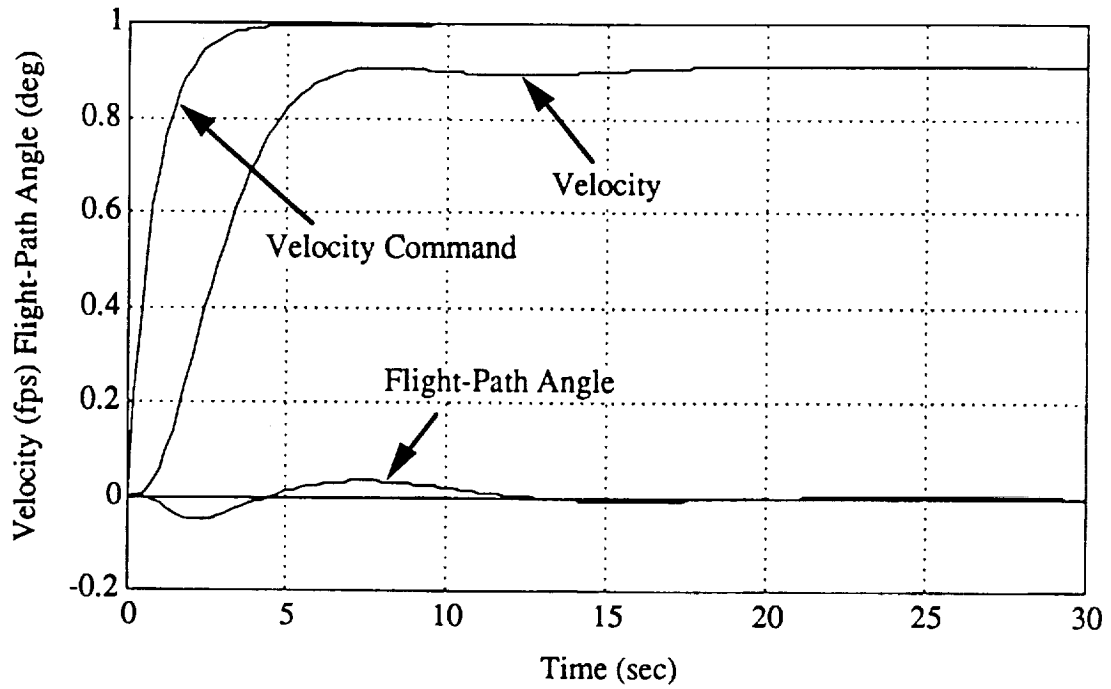
Figure 5.17: V_c Command Responses of Classical Design (FLT2)
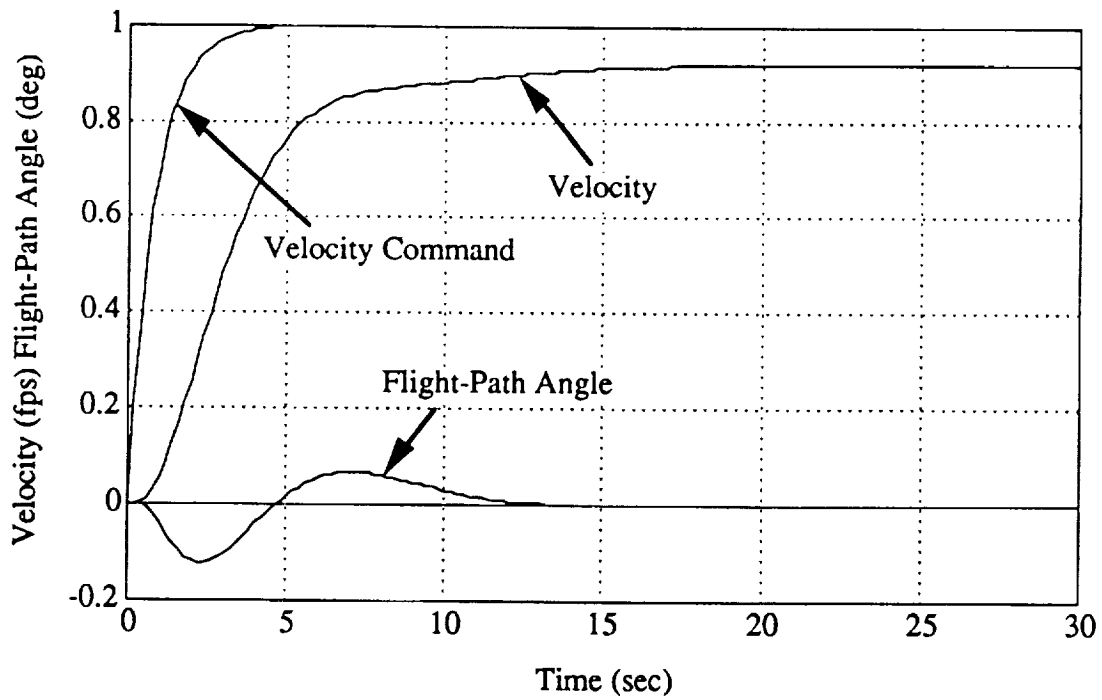
Figure 5.18: V_c Command Responses of Optimal Design (FLT2)
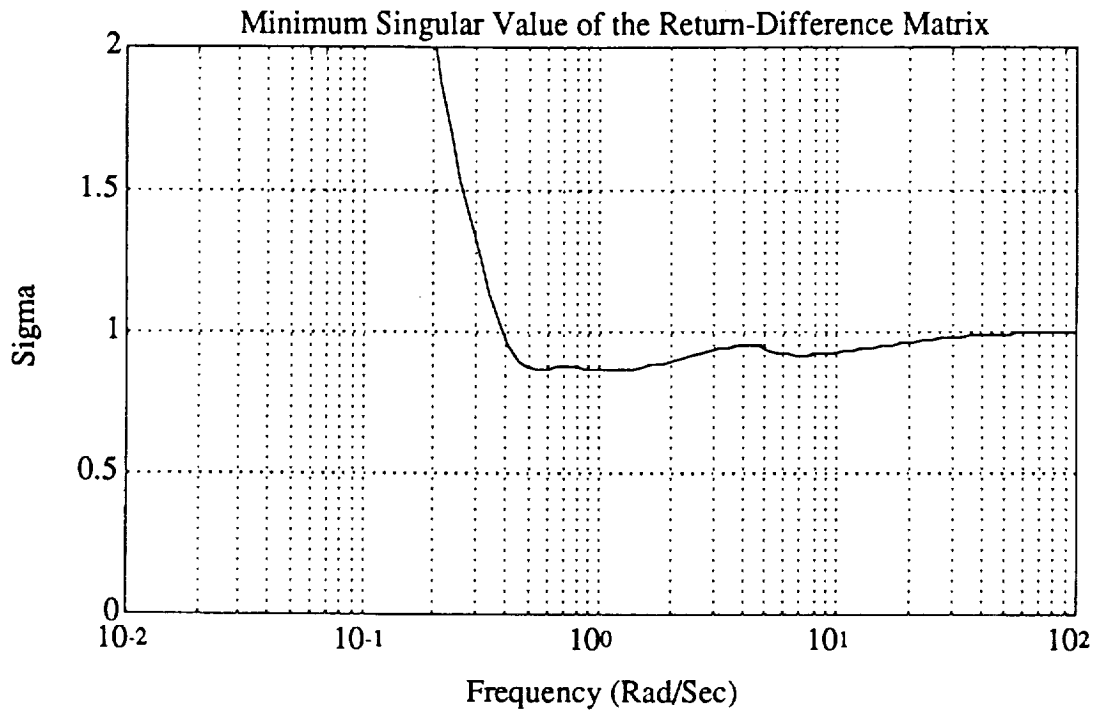
Figure 5.19: Robustness at the Control Paths of Classical Design (FLT2)
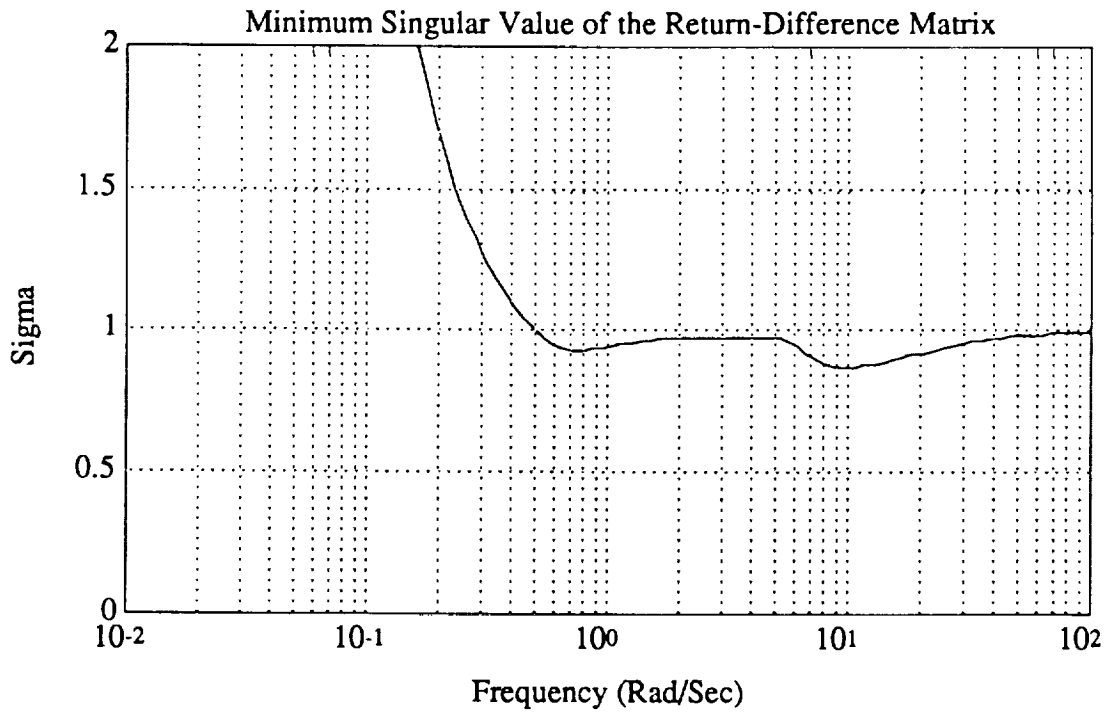
Figure 5.20: Robustness at the Control Paths of Optimal Design (FLT2)
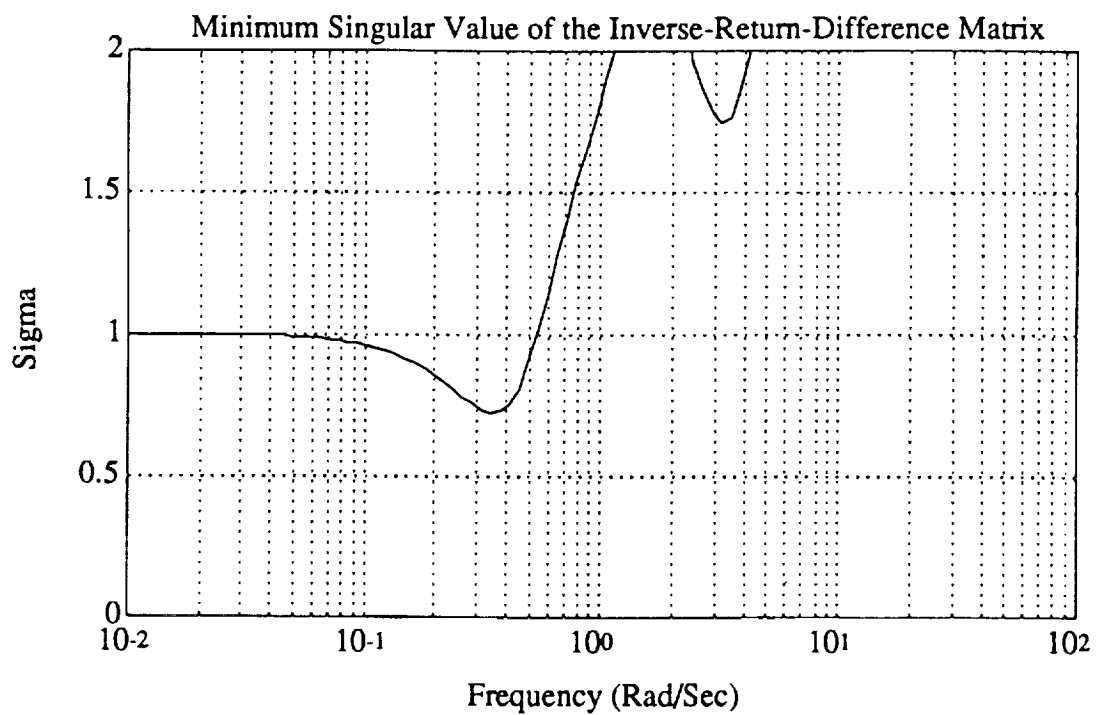
Figure 5.21: Robustness at the Control Paths of Classical Design (FLT2)
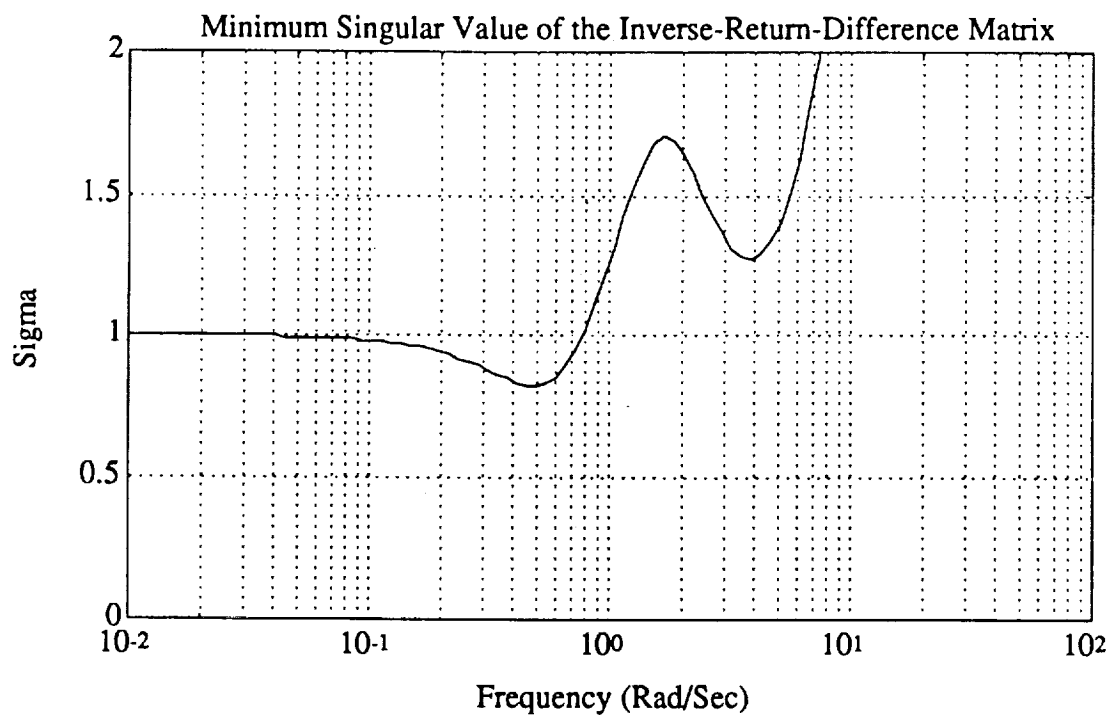
Figure 5.22: Robustness at the Control Paths of Optimal Design (FLT2)
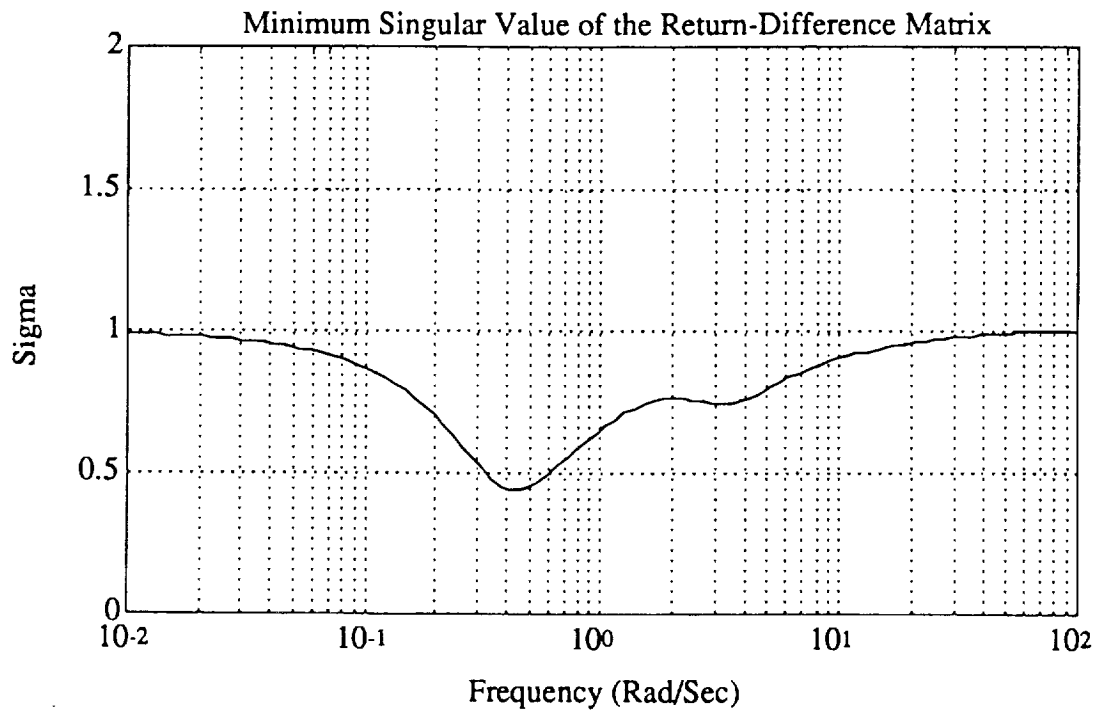
Figure 5.23: Robustness at the Sensor Paths of Classical Design (FLT2)
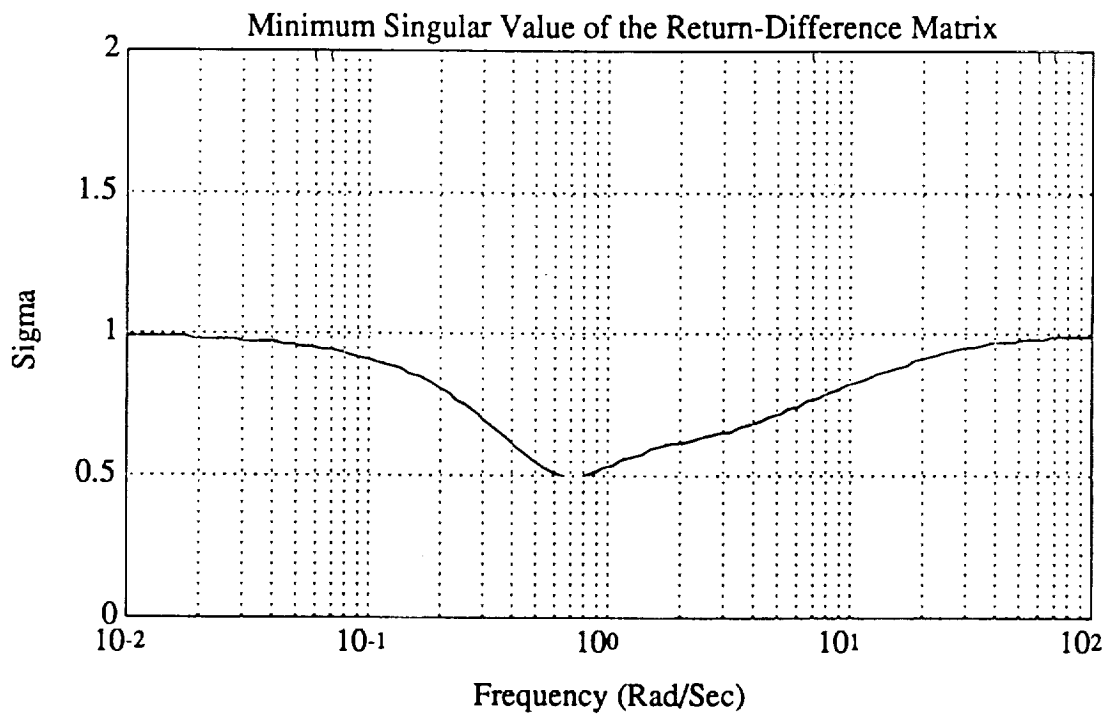
Figure 5.24: Robustness at the Sensor Paths of Optimal Design (FLT2)

Chapter 6

AIRSPEED AND ALTITUDE-HOLD AUTOPILOT AROUND AN OPTIMIZED TECS INNER LOOP

In the previous chapter, we have described the use of a total energy concept in the design of an "inner-loop" for an integrated autothrottle/autopilot control system. This controller possesses essential and physically intuitive feedback paths to achieve the following design specifications :

- Stability of closed-loop eigenvalues,

- Minimum damping ratio of eigenvalues,

- Acceptable mean square responses of control activities to turbulences,

- Command frequency response bandwiths and command tracking performance.

The following study covers the development of autopilot designs for an airspeed- and altitude-hold system using the TECS control-law as the inner loop. It was described in chapter 4 that the basic structure of the TECS controller does not include feedback of airspeed and/or altitude errors. The primary function of the inner-loop TECS (including the pitch damper) is to provide appropriate tracking bandwidths in the flight-path and longitudinal acceleration variables along with adequate closed-loop stability. To ensure that the airplane will indeed provide steady-state tracking of airspeed and altitude, we need to design an outer-loop that involves feedback of airspeed and altitude errors as shown in figure 6.1. In this chapter we present the synthesis of such an autopilot design around the existing optimal TECS inner loop discussed in chapter 5. In the next chapter 7, our design for the airspeed and altitude-hold system will also include the design parameters of the inner loop for improved tracking performance. This latter design approach for an integrated control-law synthesis covering simultaneously the inner and outer loops is clearly the preferred approach as indicated by the results of chapter 7.

In the airspeed-hold design, the airspeed error $\Delta V = V(t) - V_c(t)$ (where $V(t)$ is the actual airspeed and $V_c(t)$ is the commanded airspeed) is fedback through a feedback gain K_v to the acceleration command $\dot{V}_c$ of the TECS "inner loop" as shown in figure 6.1. While in the altitude-hold design, the altitude error $\Delta h = h(t) - h_c(t)$ (where $h(t)$ is the actual altitude and $h_c(t)$ is the commanded altitude) is fedback through a feedback gain K_h to the flight-path command γ_c. The outer-loop feedback gains K_v and K_h are selected simultaneously from the minimization of the following performance index,

$$J_1^1 = \lim_{t_f \to \infty} \frac{1}{2} \int_0^{t_f} E[Q_v(V(t) - V_c(t))^2 + Q_h(h(t) - h_c(t))^2]dt \qquad (6.1)$$

subjected to an additional damping constraint of $\zeta \geq \zeta_{min}$. The performance index J_1^1 is evaluated to parameterized random filtered step commands $V_c(t) = V_{co}(1 - e^{-at})\mu(t)$ and $h_c(t) = h_{co}(1 - e^{-at})\mu(t)$ where $\mu(t)$ is the unit-step function. The parameter a describes the bandwidth of both the airspeed and altitude commands. In this case, we use $a = 1.2 rad/sec$ similar to the bandwidths used for the inner-loop TECS design described in chapter 5. The variable V_{co} is a random variable with zero mean and covariance $E[V_{co}^2] = \sigma_{V_c}^2 = 1.0(fps)^2$. And the variable h_{co} is a random variable with zero mean and covariance $E[h_{co}^2] = \sigma_{h_c}^2 = 1.0(ft)^2$.

Note that if we have only one design parameter, say K_v in an airspeed-hold system or K_h in an altitude-hold system, then either the gain K_v or K_h can be conveniently designed by simple root locus techniques. In fact, the root-locus method is very useful even in an optimization-based design setting. It provides us valuable information on the type of trade-offs occurred in the outer-loop design when the inner-loop is fixed at an existing controller design. In particular, one can examine by root locus the degradation of closed-loop damping when we add the outer loop. Root locus plots are shown in figures 6.2 and 6.3. As we observe from these plots, increasing either K_v or K_h will eventually result in a reduction of the minimum achievable damping in the closed-loop system eigenvalues. Particularly the gain K_v has always a destabilizing effect. Therefore one can no longer expect to retain the damping achieved by the inner-loop design when the outer-loop is closed. Trade-off between minimum damping of the closed-loop eigenvalues and command tracking performance is arrived at by varying the desired minimum damping ζ_{min} and the respective penalty weightings Q_1 and Q_2 in the performance index J_1^1 of equation (6.1). For example, we have to

reduce ζ_{min} from 0.7 to 0.6 in order to achieve satisfactory tracking performance. An outer-loop design is developed for each of the two flight conditions considered in this study.

6.1 Outer-Loop Design at Flight Condition FLT1

At flight condition FLT1, the performance index J_1^1 used in the design of the outer-loop feedback gains K_v and K_h is given by

$$J_3 = \lim_{t_f \to \infty} \frac{1}{2} \int_0^{t_f} E[(V(t) - V_c(t))^2 + 0.1(h(t) - h_c(t))^2] dt \qquad (6.2)$$

subjected to a damping constraint of $\zeta \geq 0.6$. The penalties Q_v and Q_h are determined after a few design iterations and they are chosen to give comparable tracking performance between airspeed and altitude commands. For example, if transient responses in the airspeed error is large then increasing Q_v in equation 6.1 would improve the tracking of airspeed command.

The final design gains are shown in Table 6.1. The following analysis have been carried out on the final design:

- Frequency and damping ratio of closed-loop eigenvalues,

- Time responses to airspeed and altitude commands,

- Command and broken-loop control bandwidths,

- Closed-loop rms responses to turbulences,

- Single-loop type stability margins,

- Multivariable stability margins.

Notice that the inner-loop gains are fixed at the values obtained in chapter 5 for the optimal TECS controller at this flight condition. Table 6.2 gives the frequency and damping ratio of the closed-loop eigenvalues. Notice a slight reduction in the closed-loop damping as to be expected according to the root-locus plots of figure 6.2.

However in the next chapter, where the inner-loop gains are redesigned along with the outer-loop gains in an integrated manner, we are able to increase the damping back to at least 0.7.

Figure 6.4 shows the command and broken-loop control frequency responses while table 6.3 summarizes the command and broken-loop control bandwidths. The control-loop bandwidths are essentially the same as those obtained in the inner-loop design. However, as expected, the command bandwidths of the outer loop is generally lower than those of the inner loop.

Table 6.4 gives the rms responses of the closed-loop system to Dryden clear air turbulence at the 99% probability level of intensities. Results are comparable to those achieved by the optimized TECS inner-loop design.

Table 6.5 gives the single-loop type gain and phase margins at the actuator and sensor paths. The corresponding multivariable stability margins are shown in table 6.6. All these robustness results are found to be satisfactory.

Figures 6.5 and 6.6 show the time simulation to step commands in altitude of $1000 ft$ and airspeed of $10 fps$ respectively. Note that in both cases the commanded value has been reached in about 100 seconds. Evaluation of time responses to the respective commands provide insights into the iterative design procedure since these responses reflect directly the effects of varying the penalties Q_v and Q_h. It is seen that comparable performance is achieved between speed and altitude commands. One advantage of our outer-loop design is that there is small coupling between the speed and altitude variables. That is, there is little change in altitude when we apply an airspeed command and vice versa. Both the elevator and throttle control excursions in the altitude command responses are rather excessive. This is due to the fact that we have achieved a tight tracking on the altitude response and the outer loop has been synthesized around an existing (i.e fixed) inner loop.

6.2 Outer-Loop Design at Flight Condition FLT2

The discussion of the outer-loop design at the cruise condition FLT2 follows an outline similar to the one presented for the landing approach condition FLT1. At flight condition FLT2, the performance index J_1^1 used in the design of the outer-loop feedback

gains K_v and K_h is given by

$$J_3 = \lim_{t_f \to \infty} \frac{1}{2} \int_0^{t_f} E[10(V(t) - V_c(t))^2 + (h(t) - h_c(t))^2]dt \qquad (6.3)$$

subjected to a damping constraint of $\zeta \geq 0.6$.

The final design gains are shown in Table 6.7. The following analysis have also been carried out on the final design:

- Frequency and damping ratio of closed-loop eigenvalues,

- Time responses to airspeed and altitude commands,

- Command and broken-loop control bandwidths,

- Closed-loop rms responses to turbulences,

- Single-loop type stability margins,

- Multivariable stability margins.

Notice that the inner-loop gains are fixed at the values obtained in chapter 5 for the optimal TECS controller at this flight condition. Table 6.8 gives the frequency and damping ratio of the closed-loop eigenvalues. In this design, we are able to maintain the same level of closed-loop damping of 0.6 as the inner-loop gain schedule design at the flight condition FLT2. However, in the chapter 7 where we consider the re-design of the inner-loop gains together with the outer-loop gains, an improvement in closed-loop damping of 0.65 can be obtained.

Figure 6.10 shows the command and broken-loop control frequency responses while table 6.9 summarizes the command and broken-loop control bandwidths. The control-loop bandwidths are essentially the same as those obtained in the inner-loop design. However, as expected, the command bandwidths of the outer loop are generally lower than those of the inner loop.

Table 6.10 gives the rms responses of the closed-loop system to Dryden clear air turbulence at the 99% probability level of intensities. Results are similar to those achieved by the TECS inner-loop design.

Table 6.11 gives the single-loop type gain and phase margins at the actuator and sensor paths. The corresponding multivariable stability margins are shown in table 6.12. All these robustness results are found to be satisfactory.

Figures 6.11 and 6.12 show the time simulation to step commands in altitude of $1000ft$ and airspeed of $10fps$ respectively. Note that in both cases the commanded value has been reached in about 100 seconds. Evaluation of time responses to the respective commands provide insights into the iterative design procedure since these responses reflect directly the effects of varying the penalties Q_v and Q_h. It is seen that comparable performance is achieved between speed and altitude commands. One advantage of our outer-loop design is that there is small coupling between the speed and altitude variables. That is, there is little change in altitude when we apply an airspeed command and vice versa.

In this chapter we have developed a design procedure applied to the synthesis of an autopilot design using an a-priori designed inner loop. A performance index based simply on tracking errors to step commands in airspeed and altitude was used. We are able to achieve good tracking performance and adequate closed-loop damping requirements. In some situation, it may be required to re-design the inner loop at the same time one is designing the outer loop in order to accomodate more stringent requirements in closed-loop damping and control activities to turbulence. The next chapter, we consider the problem of simultaneous inner and outer loop design in an airspeed and altitude hold autopilot.

Table 6.1: Outer-Loop Gains with Existing Optimal TECS Design (FLT1)

Parameter	SANDY
K_{TP}	0.1419
K_{EP}	3.4312
K_{TI}	0.3835
K_{EI}	2.3360
K_q	2.9788
K_θ	3.1184
K_V	-7.5202 $\times 10^{-3}$
K_h	-1.1223 $\times 10^{-3}$
K_{CAS}	0.9322
K_{GW}	80,000

Table 6.2: Closed-Loop System Poles (FLT1)

Design	SANDY	
Mode	ζ	ω_n (rad/sec)
Phugoid mode	0.6	0.43
Short period	0.7	2.23
Altitude Mode	1	0.124
Integral Speed Mode	0.6	0.37

Table 6.3: Command and Broken-Loop Control Bandwidths (FLT1)

Command/Control Path	SANDY
	Bandwidths (rad/sec)
h_c	0.6
V_c	0.35
δ_{ec}	3.19
δ_{thc}	0.40

Table 6.4: Closed-Loop RMS Responses to Turbulence (FLT1)

$(\sigma_u = 6.6 \text{ fps}, \sigma_w = 6.3 \text{ fps})$

Variable	SANDY
γ (deg)	1.2491
V (fps)	0.5487
h (ft)	11.3
n_{zcg} (g)	0.09335
δ_{th} (lbst/lbsw)	0.03558
δ_e (deg)	1.6901

Table 6.5: Single-Loop Type Stability Margins (FLT1)

Design	SANDY	
Margins	Gain Margin (dB)	Phase Margin (deg)
Actuator Paths	$(-19.6, +\infty)$	-42
Sensor Paths	$(-8.3, +8.6)$	$(-43, +62)$

Table 6.6: Guaranteed Multivariable Stability Margins (FLT1)

Design	SANDY	
Margins	Gain Margin (dB)	Phase Margin (deg)
Actuator Paths	$(-8.5, +4.2)$ $(-4.4, +9.3)$	± 38.5
Sensor Paths	$(-2.2, +2.9)$	± 16.4

Table 6.7: Outer-Loop Gains with Existing Optimal TECS Design (FLT2)

Parameter	SANDY
K_{TP}	0.10895
K_{EP}	9.8268
K_{TI}	0.29446
K_{EI}	6.6903
K_q	8.5310
K_θ	8.9311
K_V	-2.1231 $\times 10^{-3}$
K_h	-2.1016 $\times 10^{-4}$
K_{CAS}	0.07006
K_{GW}	80,000

Table 6.8: Closed-Loop System Poles (FLT2)

Design	SANDY	
Mode	ζ	ω_n (rad/sec)
Phugoid mode	0.60	0.508
Short period	0.68	3.95
Altitude Mode	1	0.08578
Integral Speed Mode	0.8	0.26

Table 6.9: Command and Broken-Loop Control Bandwidths (FLT2)

Command/Control Path	SANDY
	Bandwidths (rad/sec)
h_c	0.10
V_c	0.30
δ_{ec}	4.26
δ_{thc}	0.29

Table 6.10: Closed-Loop RMS Responses to Turbulence (FLT2)

$(\sigma_u = 4.7 \text{ fps}, \sigma_w = 4.7 \text{ fps})$

Variable	SANDY
γ (deg)	0.2596
V (fps)	0.1438
h (ft)	8.1443
n_{zcg} (g)	0.09089
δ_{th} (lbst/lbsw)	0.004549
δ_e (deg)	0.2418

Table 6.11: Single-Loop Type Stability Margins (FLT2)

Design	SANDY	
Margins	Gain Margin (dB)	Phase Margin (deg)
Actuator Paths	$(-16, +\infty)$	-58
Sensor Paths	$(-12, +11.4)$	$(-50, +81)$

Table 6.12: Guaranteed Multivariable Stability Margins (FLT2)

Design	SANDY	
Margins	Gain Margin (dB)	Phase Margin (deg)
Actuator Paths	$(-11, +4.6)$ $(-5.1, +14)$	± 47
Sensor Paths	$(-2.6, +3.6)$	± 20
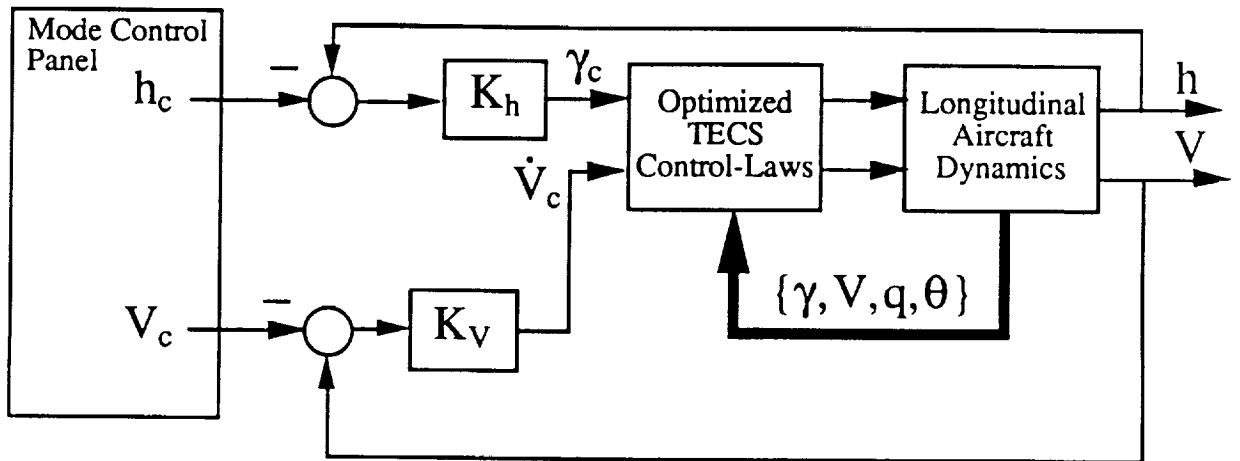
Figure 6.1: Airspeed and Altitude-Hold Design with an Optimized TECS Inner Loop
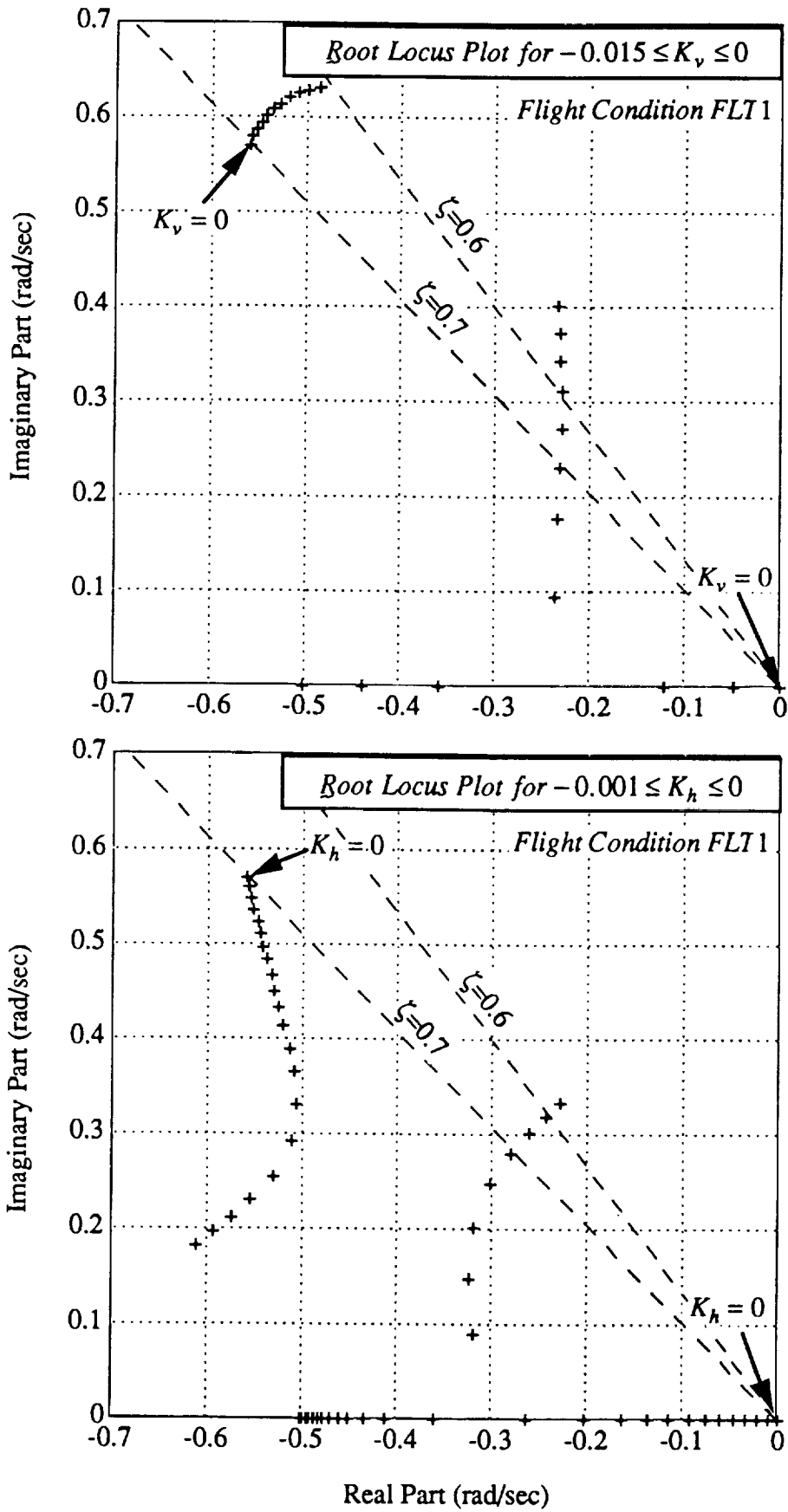
Figure 6.2: Root-Locus Plots versus Design Gains K_v and K_h (FLT1)
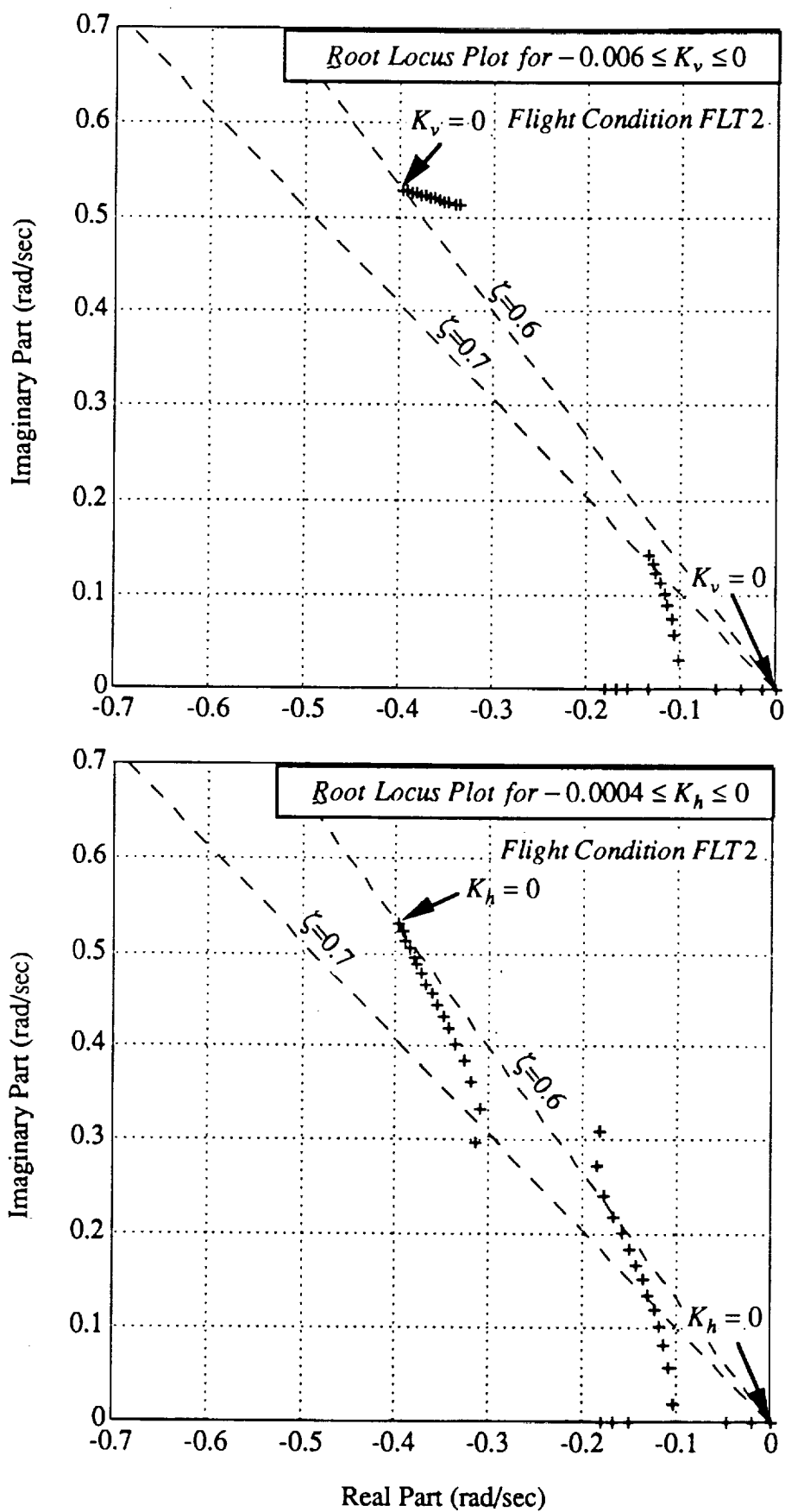
Figure 6.3: Root-Locus Plots versus Design Gains K_v and K_h (FLT2)
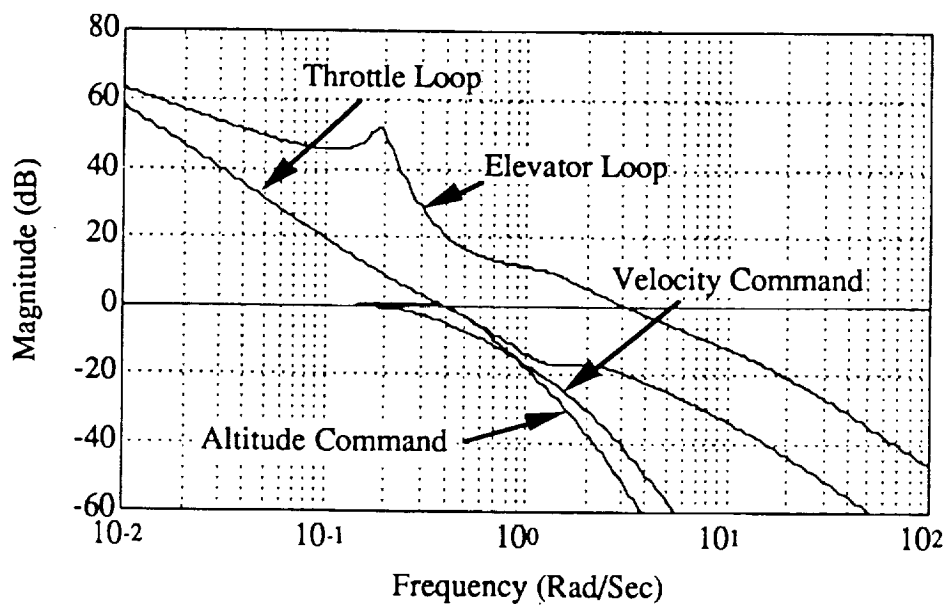
Figure 6.4: Loop Frequency Responses of Optimal Outer-Loop Design (FLT1)
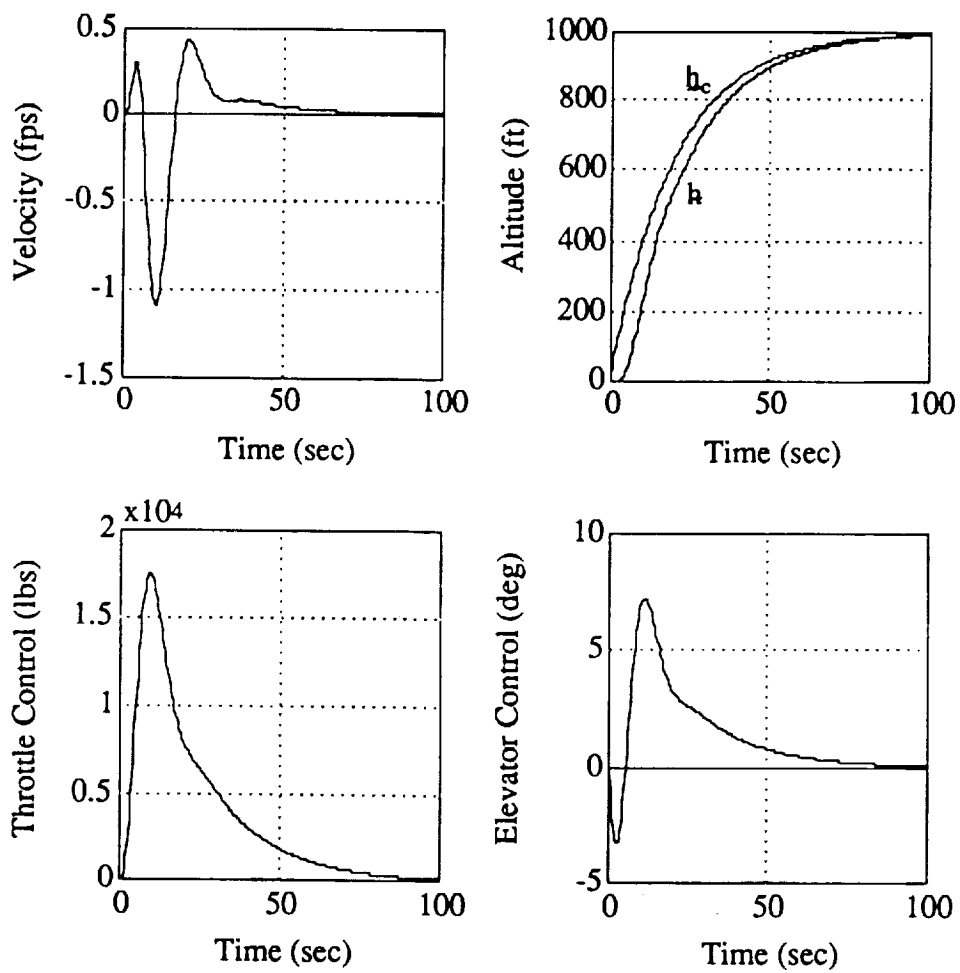
Figure 6.5: h_c Command Responses of Optimal Outer-Loop Design (FLT1)
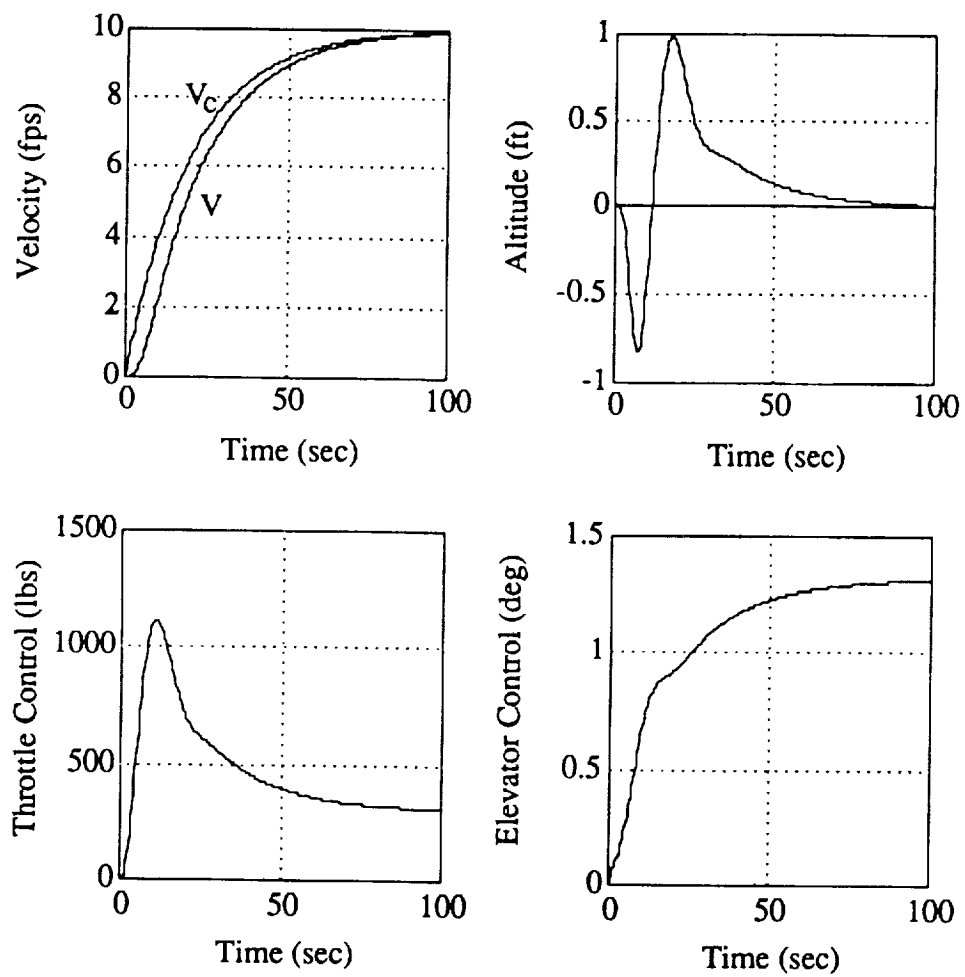
Figure 6.6: V_c Command Responses of Optimal Outer-Loop Design (FLT1)
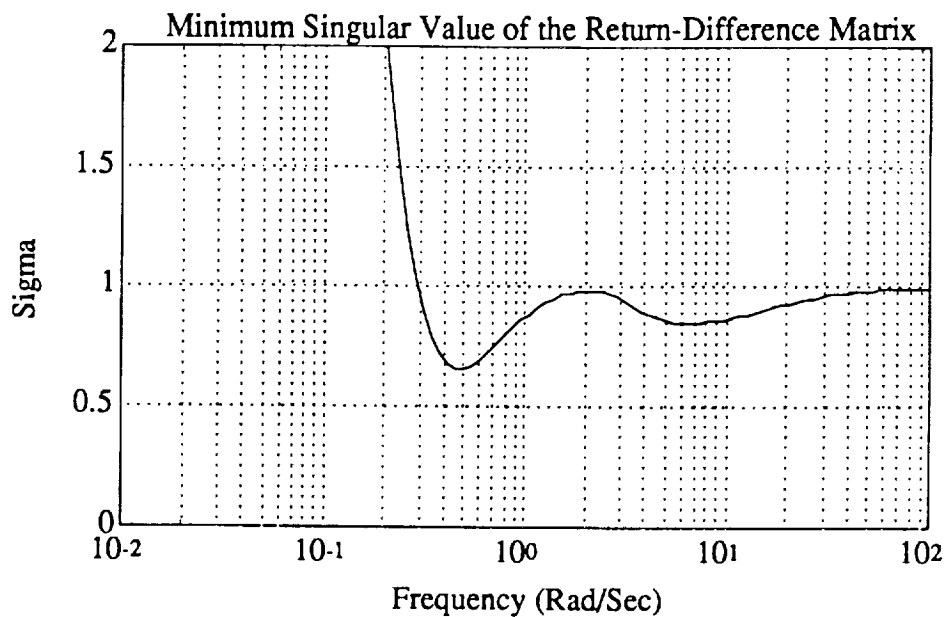
Figure 6.7: Robustness at the Control Paths of Optimal Outer-Loop Design (FLT1)
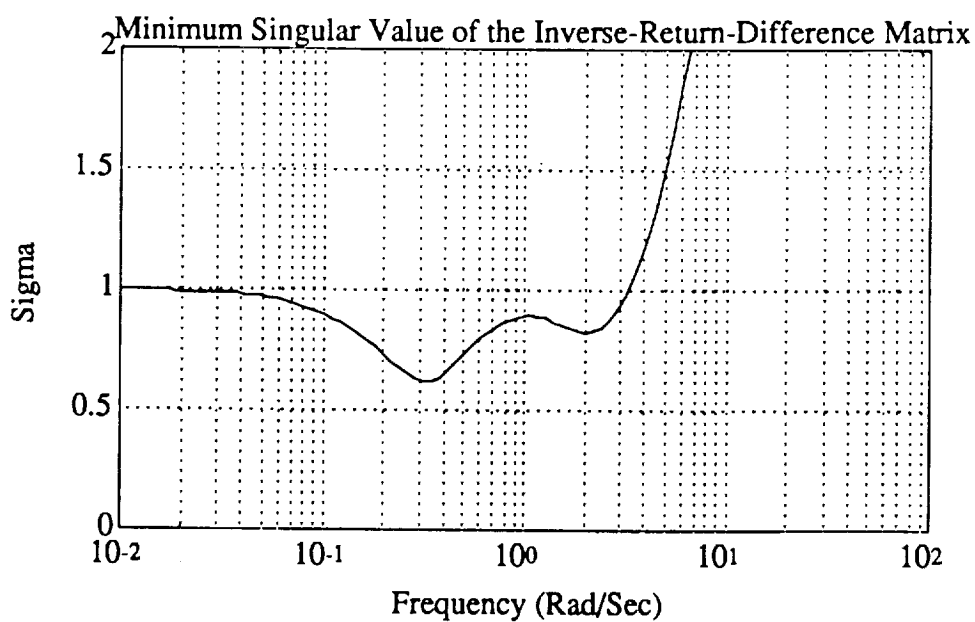
Figure 6.8: Robustness at the Control Paths of Optimal Outer-Loop Design (FLT1)
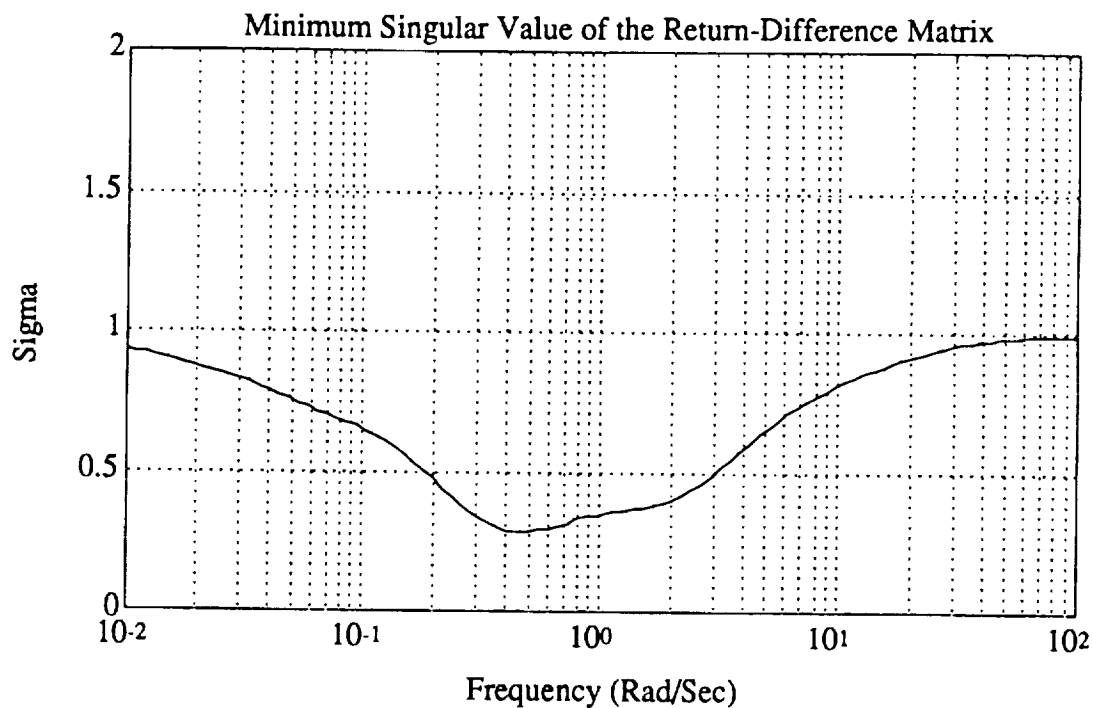
Figure 6.9: Robustness at the Sensor Paths of Optimal Outer-Loop Design (FLT1)
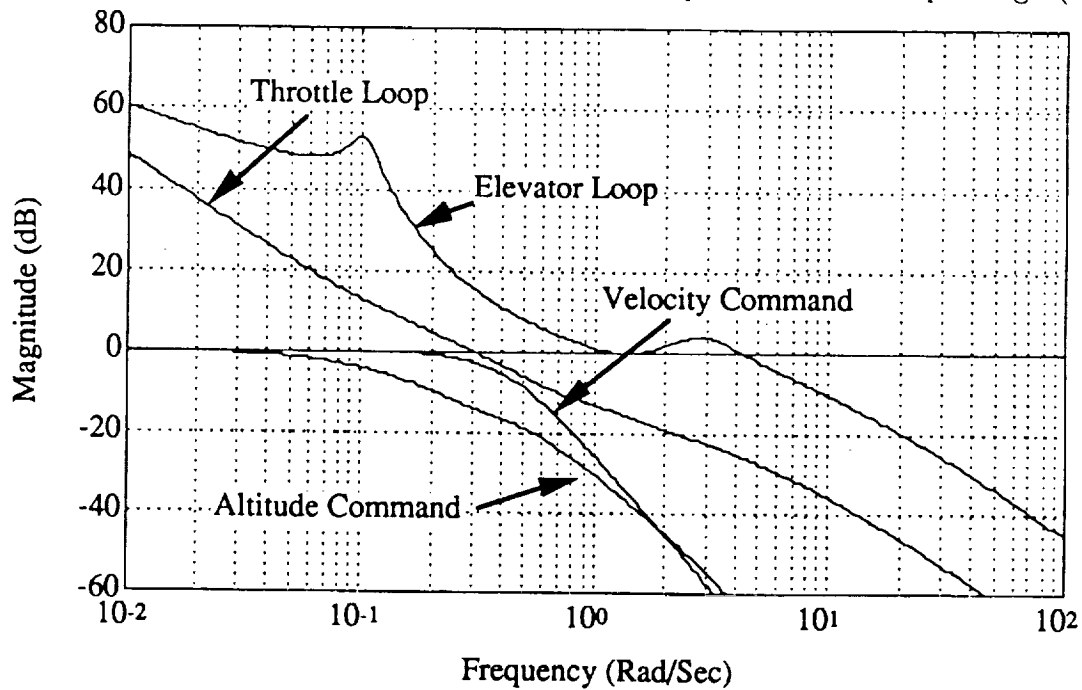
Figure 6.10: Loop Frequency Responses of Optimal Outer-Loop Design (FLT2)
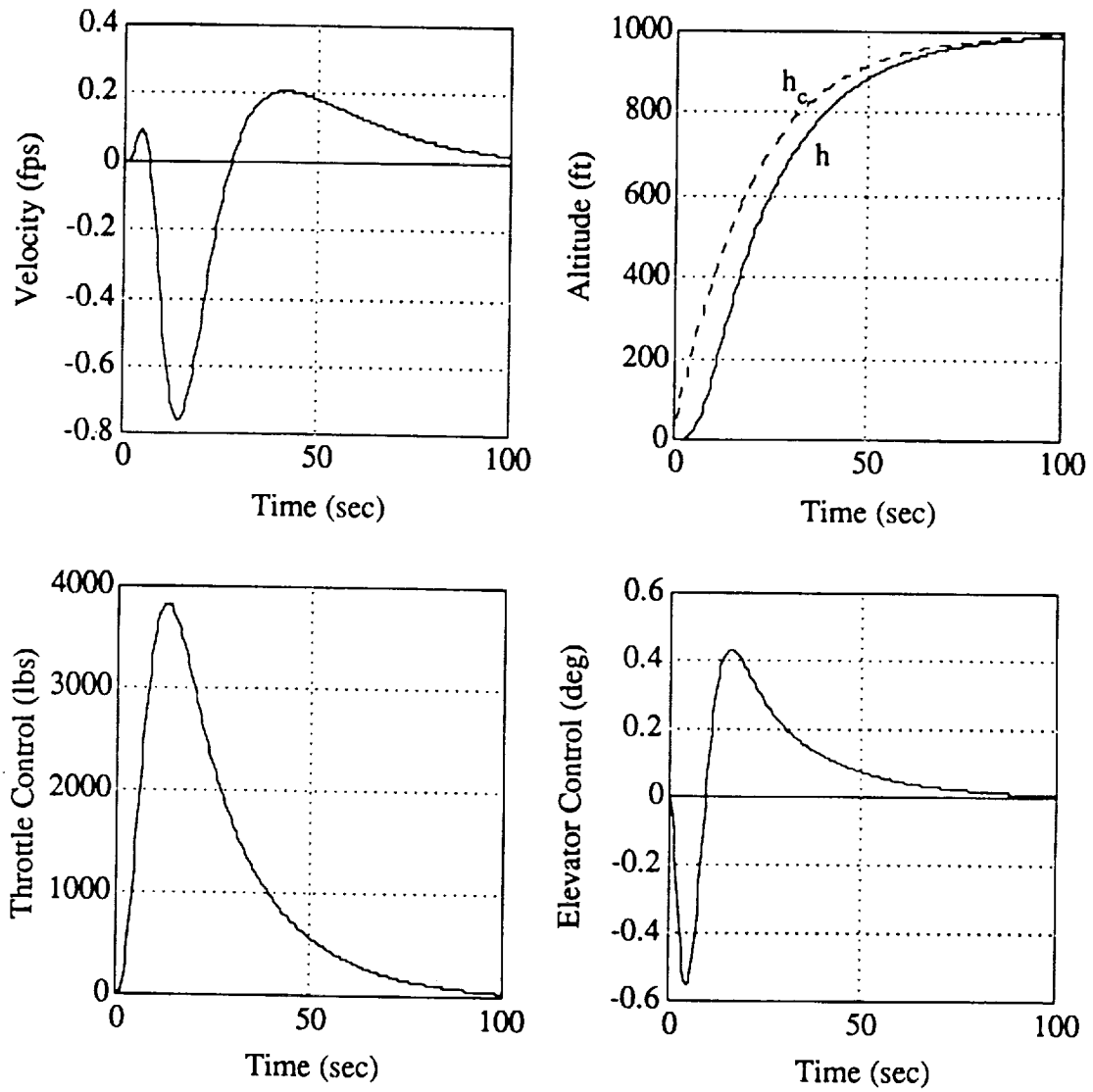
Figure 6.11: h_c Command Responses of Optimal Outer-Loop Design (FLT2)
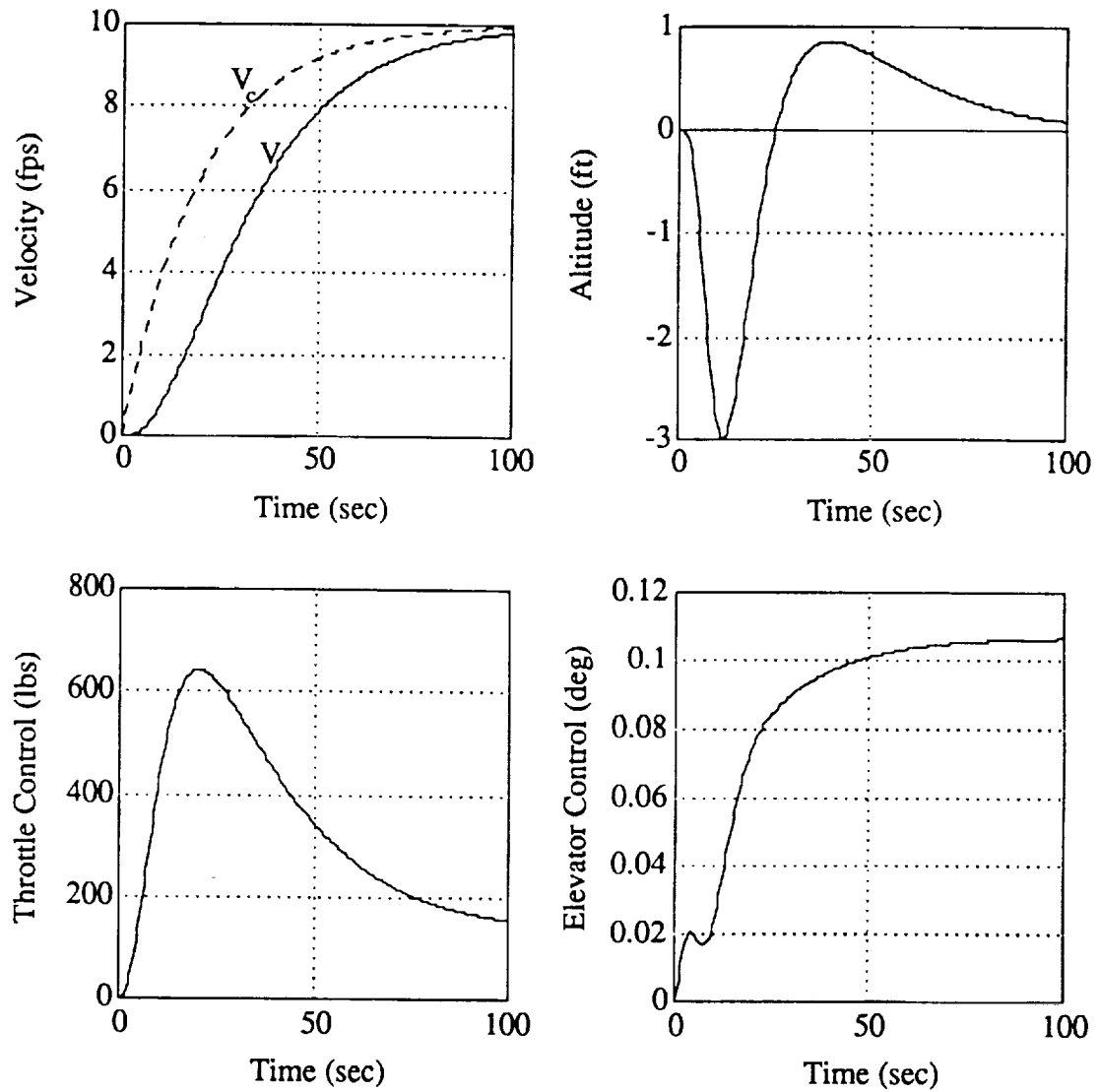
Figure 6.12: V_c Command Responses of Optimal Outer-Loop Design (FLT2)
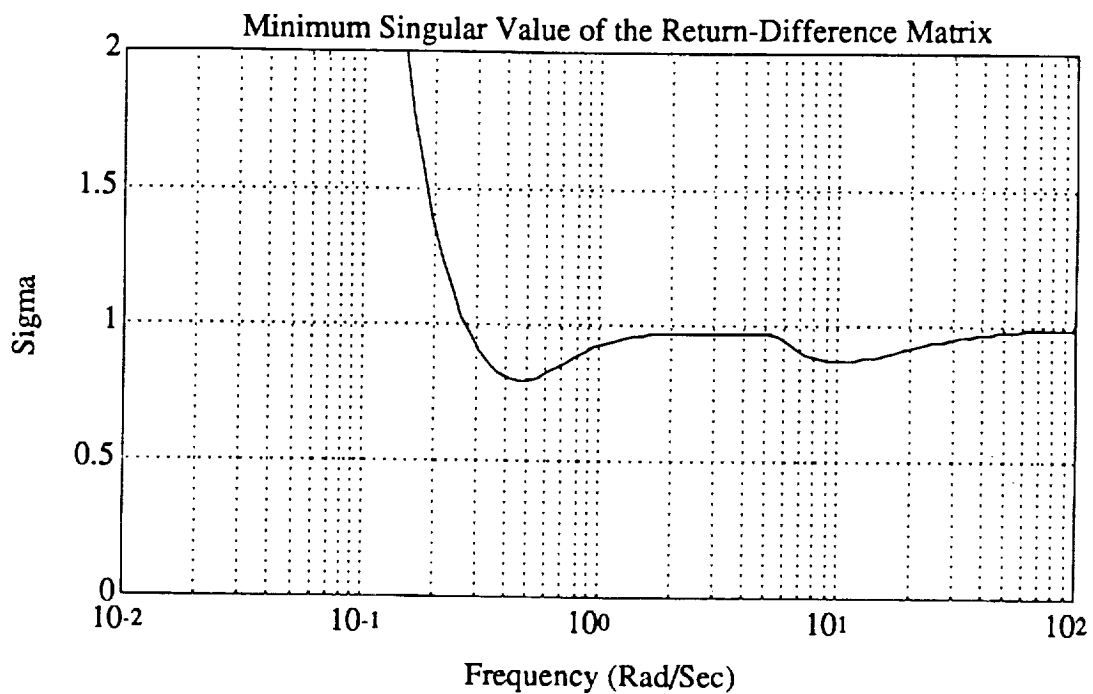
Figure 6.13: Robustness at the Control Paths of Optimal Outer-Loop Design (FLT2)
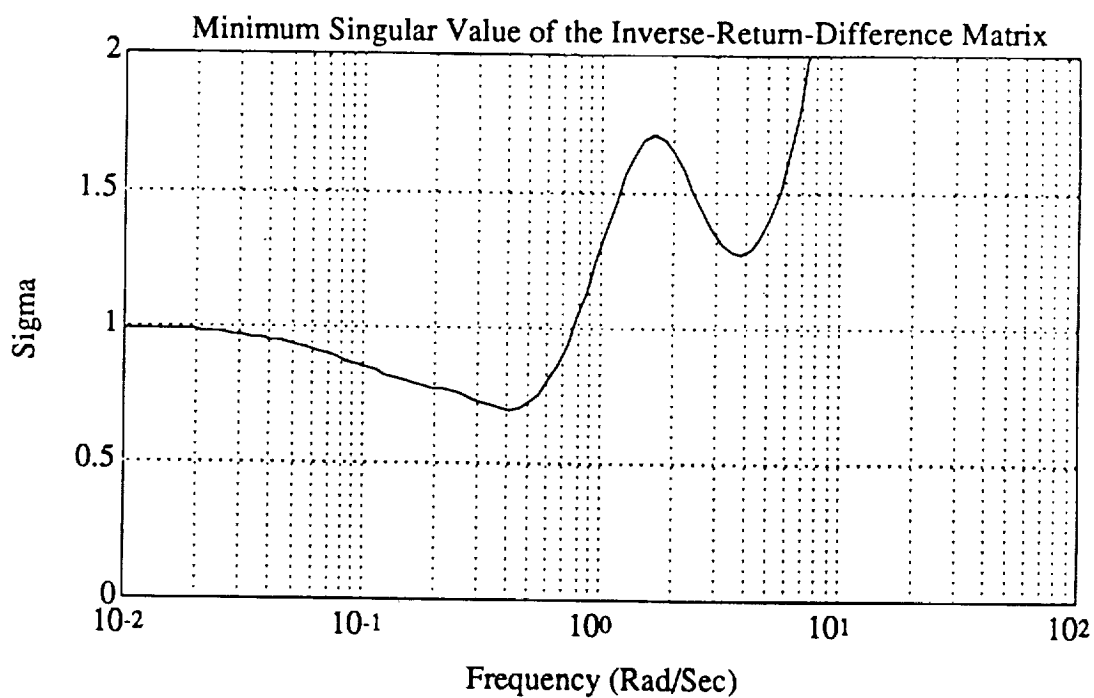
Figure 6.14: Robustness at the Control Paths of Optimal Outer-Loop Design (FLT2)
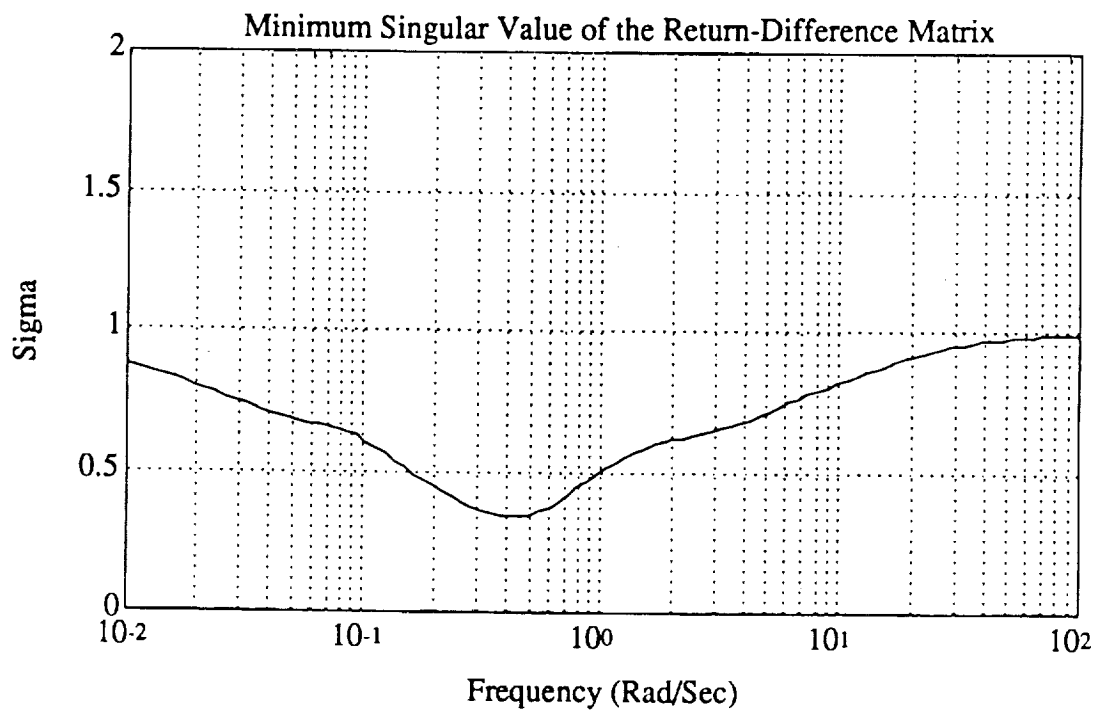
Figure 6.15: Robustness at the Sensor Paths of Optimal Outer-Loop Design (FLT2)

Chapter 7

SIMULTANEOUS DESIGN OF TECS INNER AND OUTER LOOPS

In chapter 5 we have described a design procedure for the synthesis of a TECS controller at two flight conditions FLT1 and FLT2. In these inner-loop designs, controller design parameters were determined so that the closed-loop systems satisfy the desired stability, bandwidth and turbulence requirements. In chapter 6, an airspeed and altitude-hold autopilot design was considered using the existing optimized TECS inner-loop design parameters. In this chapter, we re-examine the autopilot design from the point of view of improving its performance beyond that achieved by the outer-loop design of chapter 6.

Some of the areas that one can improve by re-designing the TECS inner loop are:

- Closed-loop damping of system eigenvalues,

- Closed-loop rms responses to turbulence,

- Control activities to commands,

- Design robustness.

The control design structure consists of the TECS control-laws augmented with, in the outer loop, feedbacks of velocity and altitude errors as shown in figure 6.1. Note that we adopt the design philosophy that errors in airspeed will be fedback to the acceleration command $\dot{V}_c$ through a feedback gain K_v and altitude errors are corrected through feedback signals to the flight-path command γ_c via the gain K_h. A state-space representation of this controller is given below:

$$\begin{pmatrix} \dot{x}_{IE} \\ \dot{x}_{IL} \end{pmatrix} = \begin{bmatrix} 0 & 0 \\ 0 & 0 \end{bmatrix} \begin{pmatrix} x_{IE} \\ x_{IL} \end{pmatrix}$$

$$+ \begin{bmatrix} -1 & -1/g & 0 & 0 & K_v & K_h & 1 & 1/g \\ 1 & -1/g & 0 & 0 & K_v & -K_h & -1 & 1/g \end{bmatrix} \begin{pmatrix} \gamma \\ \dot{V} \\ q \\ \theta \\ \Delta V \\ \Delta h \\ \gamma_c \\ \dot{V}_c \end{pmatrix} \tag{7.1}$$

$$\begin{pmatrix} \delta_{thc} \\ \delta_{ec} \end{pmatrix} = \begin{bmatrix} K_{GW} K_{TI} & 0 \\ 0 & K_{CAS} K_{EI} \end{bmatrix} \begin{pmatrix} x_{IE} \\ x_{IL} \end{pmatrix}$$

$$+ \begin{bmatrix} -K_{GW} K_{TP} & -K_{GW} K_{TP}/g & 0 & 0 & 0 & 0 & 0 & 0 \\ K_{CAS} K_{EP} & -K_{CAS} K_{EP}/g & K_{CAS} K_q & K_{CAS} K_\theta & 0 & 0 & 0 & 0 \end{bmatrix} \begin{pmatrix} \gamma \\ \dot{V} \\ q \\ \theta \\ \Delta V \\ \Delta h \\ \gamma_c \\ \dot{V}_c \end{pmatrix}$$

$$\tag{7.2}$$

where $\Delta V = V - V_c$ is the velocity error in fps and $\Delta h = h - h_c$ is the altitude error in ft. Design parameters in the simultaneous inner and outer loop design are the proportional and integral gains K_{TP}, K_{TI}, K_{EP} and K_{EI}, the pitch damper gains K_q and K_θ, the velocity-error gain K_v and the altitude-error gain K_h. For each flight condition we will determine a new set of feedback gains, hence without loss of generality we use the same gain schedule values for K_{GW} and K_{CAS} in the control-law synthesis. In fact, their contribution to the overall feedback gains are accounted for by the other feedback gains.

Following the design procedure described in chapter 4, the objective function for the airspeed and altitude-hold design consists of the sum of *three* performance indices $J_1^k (k = 1, 2, 3)$,

$$J_1 = \sum_{k=1}^{3} J_1^k \tag{7.3}$$

C.2

The first performance index $J_1^{(1)}$ is formulated to address design requirements in airspeed and altitude command tracking performance. It is given by

$$J_1^{(1)} = \lim_{t_f \to \infty} \frac{1}{2} \int_0^{t_f} E[Q_1(V(t) - V_c(t))^2 + Q_2(h(t) - h_c(t))^2]dt \qquad (7.4)$$

This performance index is evaluated to parameterized random filtered step commands in V_c and h_c with $V_c(t) = V_{co}(1 - e^{-at})\mu(t)$ and $h_c(t) = h_{co}(1 - e^{-at})\mu(t)$ where $\mu(t)$ is the unit-step function. The parameter a determines the bandwidth of both the airspeed and the altitude commands. In this design case, we use $a = 1.2rad/sec$, the same value as the flight-path and velocity command bandwidths. The variables V_{co} and h_{co} are random parameters with zero means and covariances $E[V_{co}^2] = \sigma_{V_c}^2 = 1.0(fps)^2$ and $E[h_{co}^2] = \sigma_{h_c}^2 = 1.0(ft)^2$.

Note that this autopilot design formulation includes feedback of velocity error, hence making the system type 1 in the velocity variable V. In steady-state the aircraft velocity $V(t)$ will settle to the command value $V_c(t)$ if the feedback gain K_v is nonzero and stabilizing. Similarly, the altitude variable introduce an additional integrator in the altitude loop hence making it also a type 1 system. The altitude response will therefore settle to the commanded value if the system has a nonzero stabilizing feedback gain K_h. Thus the integrand of the performance index $J_1^{(1)}$ in equation (7.4) vanishes in the limit as $t_f \to \infty$.

The second performance index $J_1^{(2)}$ is set up to perform trade-off in the control bandwidth of the throttle loop. It is defined as

$$J_1^{(2)} = \lim_{t_f \to \infty} \frac{1}{2} E[R_1 \delta_{thc}^2(t_f)] \qquad (7.5)$$

The performance index $J_1^{(2)}$ is evaluated to a high-pass noise input in the thrust command loop. The noise input is generated from the response of a first-order high-pass filter to white-noise with zero mean $E[\delta_{thw}(t)] = 0$ and covariance $E[\delta_{thw}(t + \tau)\delta_{thw}(t)] = \sigma_{thw}^2\delta(\tau)$. The quantity $\delta_{thc}(t)$ is the thrust feedback control as shown in figure 4.1. Cut-off frequency of the high-pass filter is set approximately equal to the desired broken-loop throttle control bandwidth (i.e. $\omega_{\delta_{thw}} = 0.2$ rad/sec). Frequency-shaping of the disturbance input to the thrust command ensures that only control responses at high frequencies are penalized in $J_1^{(2)}$.

Similarly, the performance index $J_1^{(3)}$ is used to perform trade-off in the control bandwidth of the elevator loop. It is given by

$$J_1^{(3)} = \lim_{t_f \to \infty} \frac{1}{2} E[R_2 \delta_{ec}^2(t_f)] \tag{7.6}$$

In this case, $J_1^{(3)}$ is evaluated to a high-pass noise input in the elevator command loop. Again the noise input is obtained from the response of a first-order high-pass filter to white-noise with zero mean $E[\delta_{ew}(t)] = 0$ and covariance $E[\delta_{ew}(t + \tau)\delta_{ew}(t)] = \sigma_{ew}^2 \delta(\tau)$. The quantity $\delta_{ec}(t)$ is the elevator feedback control. Cut-off frequency of the high-pass filter is approximately equal to the desired broken-loop elevator control bandwidth (i.e. $\omega_{\delta_{ew}} = 2.0$ rad/sec at flight condition FLT1 and $\omega_{\delta_{ew}} = 0.1$ rad/sec at flight condition FLT2). The lower bandwidth selected at the cruise condition FLT2 ensures that the elevator control bandwidth is of the same size as previous inner-loop design.

Other design considerations besides those depicted in the quadratic performance indices $J_1^{(1)}$, $J_1^{(2)}$, and $J_1^{(3)}$ are defined as before with the use of direct constraints. For example, desired closed-loop damping is achieved using the eigenvalue constraint defined in equation (C.41). Nonlinear damping constraints provide a direct means to achieve satisfactory damping of aircraft rigid-body modes. And covariance responses of selected outputs to clear air turbulence of Dryden spectra with RMS intensities from the 99% probability level (figure 4.2) can be bounded using the covariance inequality constraint in equation (3.11). Nonlinear covariance constraints on control outputs ensure that the resulting optimal design has reasonable control activities to turbulence.

In this design case, selection of initial guess for the design parameters and the penalty weighting matrices is facilitated by the results obtained in chapter 5 for the TECS inner-loop designs. All design gains were initially selected to be those determined in chapters 5 and 6 since these solutions have shown to provide reasonable stabilizing designs. Weighting matrices are also initially chosen to be those used in the previous design cases. Starting from these, one can iterate until a satisfactory autopilot design is attained.

7.1 Simultaneous Design of TECS Inner and Outer Loops at Flight Condition FLT1

For the landing approach condition FLT1, the following design objectives were used:

- The performance indices $J_1^i (i = 1, 3)$ described in equations (7.4), (7.5) and (7.6) are given below.

  (a) Command frequency response bandwidths and command tracking performance:

$$J_1^{(1)} = \lim_{t_f \to \infty} \frac{1}{2} \int_0^{t_f} E[10(V(t) - V_c(t))^2 + (h(t) - h_c(t))^2] dt \qquad (7.7)$$

This performance index is evaluated to parameterized random filtered step commands in V_c and h_c with $V_c(t) = V_{co}(1 - e^{-at})\mu(t)$ and $h_c(t) = h_{co}(1 - e^{-at})\mu(t)$ where $\mu(t)$ is the unit-step function. The parameter a determines the bandwidth of both the airspeed and the altitude commands. In this design case, we use $a = 1.2 rad/sec$, the same value as the flight-path and velocity command bandwidths. The variables V_{co} and h_{co} are random parameters with zero means and covariances $E[V_{co}^2] = \sigma_{V_c}^2 = 1.0(fps)^2$ and $E[h_{co}^2] = \sigma_{h_c}^2 = 1.0(ft)^2$.

(b) Broken-loop crossover frequency in the throttle control loop:

$$J_1^{(2)} = \lim_{t_f \to \infty} \frac{1}{2} E[10\delta_{thc}^2(t_f)] \qquad (7.8)$$

The performance index $J_1^{(2)}$ is evaluated to a high-pass noise input in the thrust command loop. The noise input is generated from the response of a first-order high-pass filter to white-noise with zero mean $E[\delta_{thw}(t)] = 0$ and covariance $E[\delta_{thw}(t+\tau)\delta_{thw}(t)] = \sigma_{thw}^2 \delta(\tau)$. In this design, we choose $\sigma_{thw} = 1$. The quantity $\delta_{thc}(t)$ is the thrust feedback control as shown in figure 4.1 . Cut-off frequency of the high-pass filter is set approximately equal to the desired broken-loop throttle control bandwidth (i.e. $\omega_{\delta_{thw}} = 0.2$ rad/sec).

(c) Broken-loop crossover frequency in the elevator control loop:

$$J_1^{(3)} = \lim_{t_f \to \infty} \frac{1}{2} E[3\delta_{ec}^2(t_f)] \qquad (7.9)$$

The performance index $J_1^{(3)}$ is evaluated to a high-pass noise input in the elevator command loop. The noise input is generated from the response of a first-order

high-pass filter to white-noise with zero mean $E[\delta_{ew}(t)] = 0$ and covariance $E[\delta_{ew}(t+\tau)\delta_{ew}(t)] = \sigma_{ew}^2 \delta(\tau)$. In this design, we choose $\sigma_{ew} = 0.16$. The quantity $\delta_{ec}(t)$ is the elevator feedback control as shown in figure 4.1 . Cut-off frequency of the high-pass filter is set approximately equal to the desired broken-loop elevator control bandwidth (i.e. $\omega_{\delta_{ew}} = 2.0$ rad/sec).

- Stability of the closed-loop eigenvalues:
  (a) Real part of the eigenvalues must be less than zero,

$$\sigma_i \leq 0 \ (i = 1, n) \tag{7.10}$$

  (b) Damping ratio of the eigenvalues must be greater than 0.7, i.e

$$\zeta_i \geq 0.7 \ (i = 1, n) \tag{7.11}$$

- Mean square responses of control activities to clear air Dryden turbulence of $\sigma_u = 6.6 fps$ and $\sigma_w = 6.3 fps$,

$$E[\delta_{thc}^2] \leq 7.56 \times 10^{-4}(lbst/lbsw)^2 \tag{7.12}$$

$$E[\delta_{ec}^2] \leq 6.735 \times 10^{-4}(rad)^2 \tag{7.13}$$

The resulting set of optimal feedback gains is shown in table 7.1. Overall these gains differ significantly from those where the inner and outer loops are designed separately. Improved performance and damping are achieved with higher values of K_{TP}, K_q, K_θ and K_v. Table 7.2 gives the damping ratio and natural frequency of the closed-loop system eigenvalues. A minimum damping of 0.7 is achieved through the use of nonlinear constraints; this is an improvement over the minimum damping of 0.60 in the optimal outer-loop design in chapter 6.

Figures 7.1 shows the command and broken-loop control frequency responses of the optimized design. Command and control-loop bandwidths for these designs are summarized in table 7.3. Note that the design has slightly higher command bandwidth in the velocity variable than the outer-loop design in chapter 6, while the altitude command bandwidth is significantly reduced. This is primarily due to the fact that

we have limited the control activities to the values defined by the classical TECS design described in chapter 5 and we are imposing a higher damping requirement. Control-loop bandwidths are similar in the two designs.

Figures 7.2 and 7.3 show time responses of the closed-loop systems to a step command in altitude of $1000ft$ and in airspeed of $10fps$ respectively. Control activities are less than half of those shown in table 6.5 for the previous outer-loop design. Table 7.4 summarizes the closed-loop rms responses to Dryden clear air turbulence at the 99% probability level of intensities. Results clearly illustrate the effective usage of direct bounds on the respective output covariances. By imposing inequality constraints on the control covariances, one is guaranteed at the outset that the optimal design, when converged, will have the same or lower control activities than the classical design. Furthermore, covariance responses of other aircraft variables are lower or equal to those of the classical design shown in table 5.4.

Table 7.5 summarizes values of single-loop stability margins. Single-loop stability margins are found to be satisfactory and improved over those in table 6.5 of the previously optimized outer-loop design.

Figures 7.4–7.6 show plots of minimum singular values of the return-difference and the inverse-return-difference transfer matrices respectively at both the control and sensor paths. In these plots, diagonal scaling on the transfer function matrices has been used to reduce conservatism and thereby improve estimates of actual multiloop stability margins. Table 7.6 gives guaranteed multivariable stability margins in both the control actuator and sensor paths according to equations (D.8) and (D.14) of Appendix D. Again these results are better than those in table 6.6 for the optimized outer-loop design of chapter 6.

7.2 Simultaneous Design of TECS Inner and Outer Loops at Flight Condition FLT2

Instead of performing a simple gain schedule design based on the results obtained in the previous section 7.1 for the landing approach condition, we choose to re-design all the TECS inner and outer-loop gains at the cruise condition FLT2. The objective is to see whether one can improve the design performance beyond those achieved in chapter 5 and 6 combined. Another set of design objectives are established for the cruise condition similar in form to that given in equations (7.7)-(7.13). They are as

follows,

- The performance indices $J_1^i(i = 1, 3)$ described in equations (7.4), (7.5) and (7.6) are given below.

(a) Command frequency response bandwidths and command tracking performance:

$$J_1^{(1)} = \lim_{t_f \to \infty} \frac{1}{2} \int_0^{t_f} E[5(V(t) - V_c(t))^2 + 2(h(t) - h_c(t))^2]dt \qquad (7.14)$$

This performance index is evaluated to parameterized random filtered step commands in V_c and h_c with $V_c(t) = V_{co}(1 - e^{-at})\mu(t)$ and $h_c(t) = h_{co}(1 - e^{-at})\mu(t)$ where $\mu(t)$ is the unit-step function. The parameter a determines the bandwidth of both the airspeed and the altitude commands. In this design case, we use $a = 1.2rad/sec$, the same value as the flight-path and velocity command bandwidths. The variables V_{co} and h_{co} are random parameters with zero means and covariances $E[V_{co}^2] = \sigma_{V_c}^2 = 1.0(fps)^2$ and $E[h_{co}^2] = \sigma_{h_c}^2 = 1.0(ft)^2$.

(b) Broken-loop crossover frequency in the throttle control loop:

$$J_1^{(2)} = \lim_{t_f \to \infty} \frac{1}{2} E[0.03\delta_{thc}^2(t_f)] \qquad (7.15)$$

The performance index $J_1^{(2)}$ is evaluated to a high-pass noise input in the thrust command loop. The noise input is generated from the response of a first-order high-pass filter to white-noise with zero mean $E[\delta_{thw}(t)] = 0$ and covariance $E[\delta_{thw}(t+\tau)\delta_{thw}(t)] = \sigma_{thw}^2\delta(\tau)$. In this design, we choose $\sigma_{thw} = 1$. The quantity $\delta_{thc}(t)$ is the thrust feedback control as shown in figure 4.1 . Cut-off frequency of the high-pass filter is set approximately equal to the desired broken-loop throttle control bandwidth (i.e. $\omega_{\delta_{thw}} = 0.2$ rad/sec).

(c) Broken-loop crossover frequency in the elevator control loop:

$$J_1^{(3)} = \lim_{t_f \to \infty} \frac{1}{2} E[100\delta_{ec}^2(t_f)] \qquad (7.16)$$

The performance index $J_1^{(3)}$ is evaluated to a high-pass noise input in the elevator command loop. The noise input is generated from the response of a first-order high-pass filter to white-noise with zero mean $E[\delta_{ew}(t)] = 0$ and covariance

$E[\delta_{ew}(t+\tau)\delta_{ew}(t)] = \sigma_{ew}^2 \delta(\tau)$. In this design, we choose $\sigma_{ew} = 1.0$. The quantity $\delta_{ec}(t)$ is the elevator feedback control as shown in figure 4.1 . Cut-off frequency of the high-pass filter is set approximately equal to the desired broken-loop elevator control bandwidth (i.e. $\omega_{\delta_{ew}} = 0.1$ rad/sec).

- Stability of the closed-loop eigenvalues:
  (a) Real part of the eigenvalues must be less than zero,

$$\sigma_i \leq 0 \ (i = 1, n) \tag{7.17}$$

(b) Damping ratio of the eigenvalues must be greater than 0.65, i.e

$$\zeta_i \geq 0.65 \ (i = 1, n) \tag{7.18}$$

Note that no feasible solutions can be found that will satisfy damping require-ment exceeding 0.65 and at the same time maintaining the covariance responses achieved under the classical design (Table 5.10).

- Mean square responses of control activities to clear air Dryden turbulence of $\sigma_u = 4.7 fps$ and $\sigma_w = 4.7 fps$,
  We are restricting our design to provide the same levels of covariance responses as the classical design shown in table 5.10.

$$E[\delta_{thc}^2] \leq 0.18037 \times 10^{-4} (lbst/lbsw)^2 \tag{7.19}$$

$$E[\delta_{ec}^2] \leq 0.17581 \times 10^{-2} (rad)^2 \tag{7.20}$$

$$E[V^2] \leq 0.0424 (fps)^2 \tag{7.21}$$

$$E[n_{zcg}^2] \leq 0.648 \times 10^{-2} (g)^2 \tag{7.22}$$

The set of optimized feedback gains is shown in table 7.7. These gains differ signif-icantly from those shown in table 6.7 where the inner and outer loops are designed separately. Table 7.8 gives the damping ratio and natural frequency of the closed-loop system eigenvalues. A minimum damping of 0.65 is achieved through the use of

nonlinear constraints; this is an improvement over the minimum damping of 0.60 in the optimal outer-loop design in chapter 6.

Figures 7.7 shows the command and broken-loop control frequency responses of the optimized design. Command and control-loop bandwidths for these designs are summarized in table 7.9. Note that the design has equal bandwidth in both the airspeed and altitude paths. The command bandwidth in the velocity variable is slightly less than the one of the outer-loop design in chapter 6, while the altitude command bandwidth is improved. Control-loop bandwidths are similar in the two designs.

Figures 7.8 and 7.9 show time responses of the closed-loop systems to a step command in altitude of $1000 ft$ and in airspeed of $10 fps$ respectively. Both command responses have almost the same time constant confirming the results of table 7.9.

Table 7.10 summarizes the closed-loop rms responses to Dryden clear air turbulence at the 99% probability level of intensities. Results clearly illustrate the effective usage of direct bounds on the respective output covariances. By imposing inequality constraints on the control and output covariances, one is guaranteed at the outset that the optimal design, when converged, will have the same or lower control and output covariances than those of the classical design in table 5.4.

Table 7.11 summarizes values of single-loop stability margins. Single-loop stability margins are found to be satisfactory and similar to those in table 6.11 of the previously optimized outer-loop design.

Figures 7.10–7.12 show plots of minimum singular values of the return-difference and the inverse-return-difference transfer matrices respectively at both the control and sensor paths. In these plots, diagonal scaling on the transfer function matrices has been used to reduce conservatism and thereby improve estimates of actual multiloop stability margins. Table 7.12 gives guaranteed multivariable stability margins in both the control actuator and sensor paths according to equations (D.8) and (D.14) of Appendix D. Again these results are comparable to those in table 6.12 for the optimized outer-loop design of chapter 6.

From the above results, one can deduce that to maximize tracking performance along with other requirements such as closed-loop damping, covariance responses to turbulence in an autopilot design problem, it is often necessary to re-examine the inner-loop design gains in conjunction with the outer-loop gains. We have demon-

strate in this chapter the usage of constrained nonlinear optimization in the synthesis of an airspeed and altitude-hold autopilot. Here the inner and outer-loop gains are optimized simultaneously to yield an overall improved design over those presented in chapters 5 and 6.

Table 7.1: Optimal Inner- and Outer-Loop Feedback Gains (FLT1)

Parameter	SANDY
K_{TP}	0.56168
K_{EP}	3.2326
K_{TI}	0.33981
K_{EI}	2.2854
K_q	3.2620
K_θ	5.0000
K_V	-0.010517
K_h	-2.3882×10^{-4}
K_{CAS}	0.9322
K_{GW}	80,000

Table 7.2: Closed-Loop System Poles (FLT1)

Design	SANDY	
Mode	ζ	ω_n (rad/sec)
Phugoid mode	0.8	0.58
Short period	0.74	3.13
Altitude Mode	1	0.065
Integral Speed Mode	1	0.125

Table 7.3: Command and Broken-Loop Control Bandwidths (FLT1)

Command/Control Path	SANDY
	Bandwidths (rad/sec)
h_c	0.06
V_c	0.42
δ_{ec}	3.67
δ_{thc}	0.40

Table 7.4: Closed-Loop RMS Responses to Turbulence (FLT1)

$(\sigma_u = 6.6 \text{ fps}, \sigma_w = 6.3 \text{ fps})$

Variable	SANDY
γ (deg)	0.9538
V (fps)	0.4755
h (ft)	13.1
n_{zcg} (g)	0.07585
δ_{th} (lbst/lbsw)	0.02718
δ_e (deg)	1.2982

Table 7.5: Single-Loop Type Stability Margins (FLT1)

Design	SANDY	
Margins	Gain Margin (dB)	Phase Margin (deg)
Actuator Paths	$(-35, +\infty)$	-57
Sensor Paths	$(-19, +14.5)$	$(-55, +70)$

Table 7.6: Guaranteed Multivariable Stability Margins (FLT1)

Design	SANDY	
Margins	Gain Margin (dB)	Phase Margin (deg)
Actuator Paths	$(-14, +5.1)$ $(-5.2, +14.5)$	± 47.9
Sensor Paths	$(-2.7, +3.95)$	± 21

Table 7.7: Optimal Inner- and Outer-Loop Feedback Gains (FLT2)

Parameter	SANDY
K_{TP}	0.3965
K_{EP}	6.549
K_{TI}	0.27233
K_{EI}	1.5469
K_q	5.3573
K_θ	-0.09335
K_V	-3.593×10^{-3}
K_h	-1.2038×10^{-4}
K_{CAS}	0.07006
K_{GW}	80,000

Table 7.8: Closed-Loop System Poles (FLT2)

Design	SANDY	
Mode	ζ	ω_n (rad/sec)
Phugoid mode	0.65	0.28
Short period	0.65	3.27
Altitude Mode	1	0.165
Integral Speed Mode	0.65	0.16

Table 7.9: Command and Broken-Loop Control Bandwidths (FLT2)

Command/Control Path	SANDY
	Bandwidths (rad/sec)
h_c	0.20
V_c	0.20
δ_{ec}	4.0
δ_{thc}	0.27

Table 7.10: Closed-Loop RMS Responses to Turbulence (FLT2)

$(\sigma_u = 4.7 \text{ fps}, \sigma_w = 4.7 \text{ fps})$

Variable	SANDY
γ (deg)	0.1562
V (fps)	0.2059
h (ft)	5.5316
n_{zcg} (g)	0.08050
δ_{th} (lbst/lbsw)	0.003878
δ_e (deg)	0.1388

Table 7.11: Single-Loop Type Stability Margins (FLT2)

Design	SANDY	
Margins	Gain Margin (dB)	Phase Margin (deg)
Actuator Paths	$(-17, +\infty)$	-68
Sensor Paths	$(-8.6, +12.7)$	$(-50, +73)$

Table 7.12: Guaranteed Multivariable Stability Margins (FLT2)

Design	SANDY	
Margins	Gain Margin (dB)	Phase Margin (deg)
Actuator Paths	$(-11, +4.7)$ $(-5.7, +22)$	± 55
Sensor Paths	$(-2.9, +4.42)$	± 23
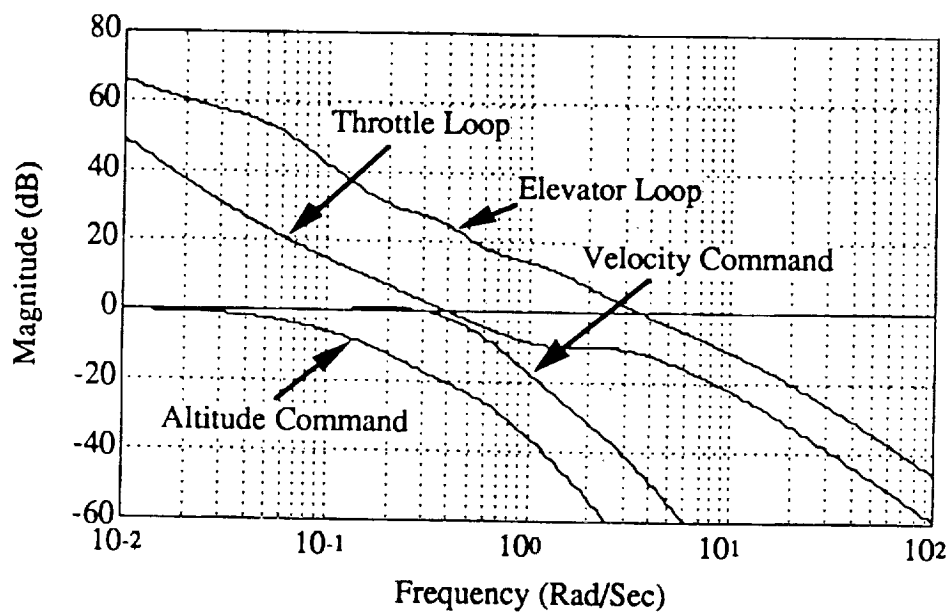
Figure 7.1: Loop Frequency Responses of Optimal Inner and Outer-Loop Design (FLT1)
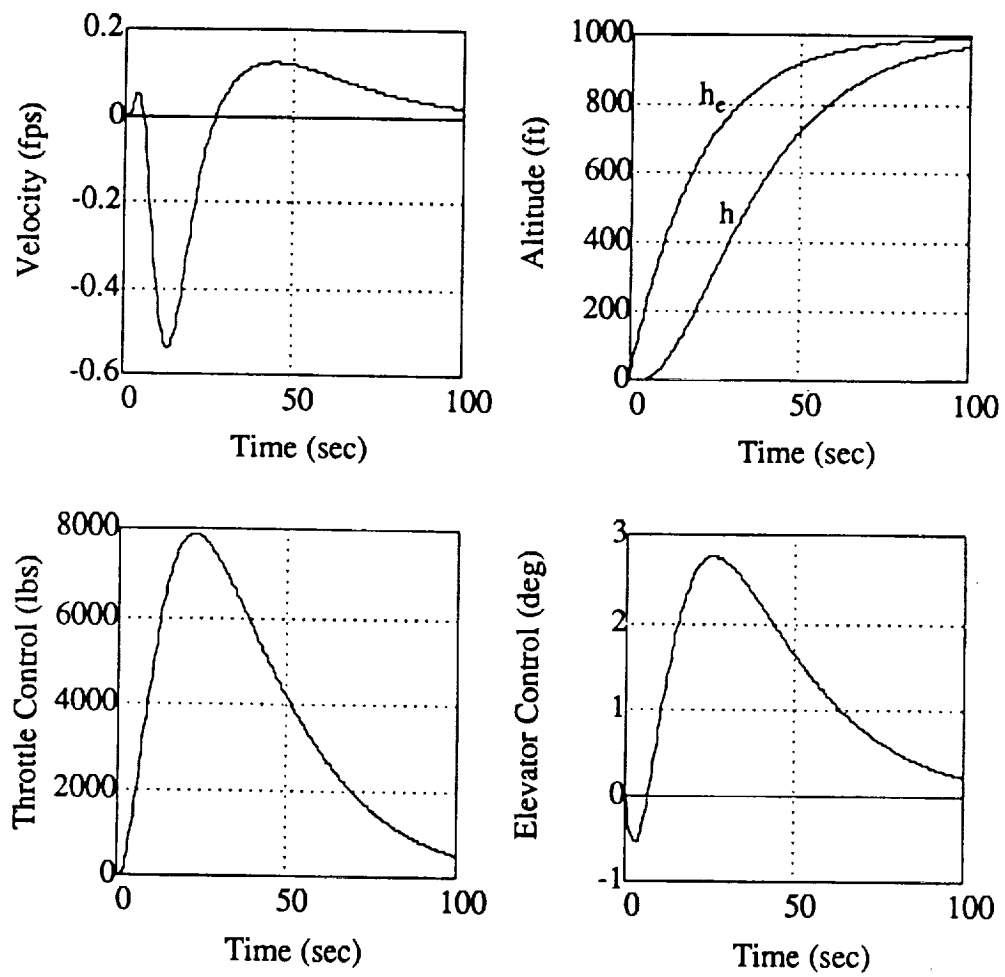
Figure 7.2: h_c Command Responses of Optimal Inner and Outer-Loop Design (FLT1)
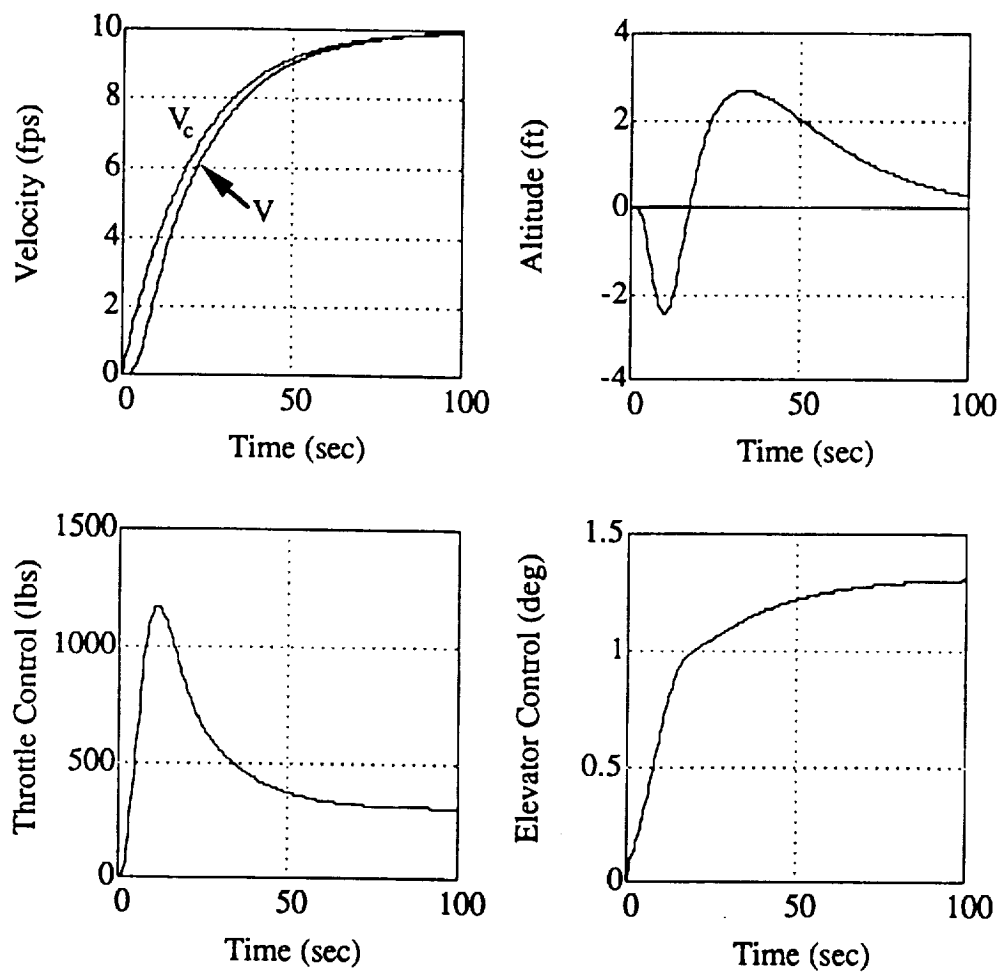
Figure 7.3: V_c Command Responses of Optimal Inner and Outer-Loop Design (FLT1)
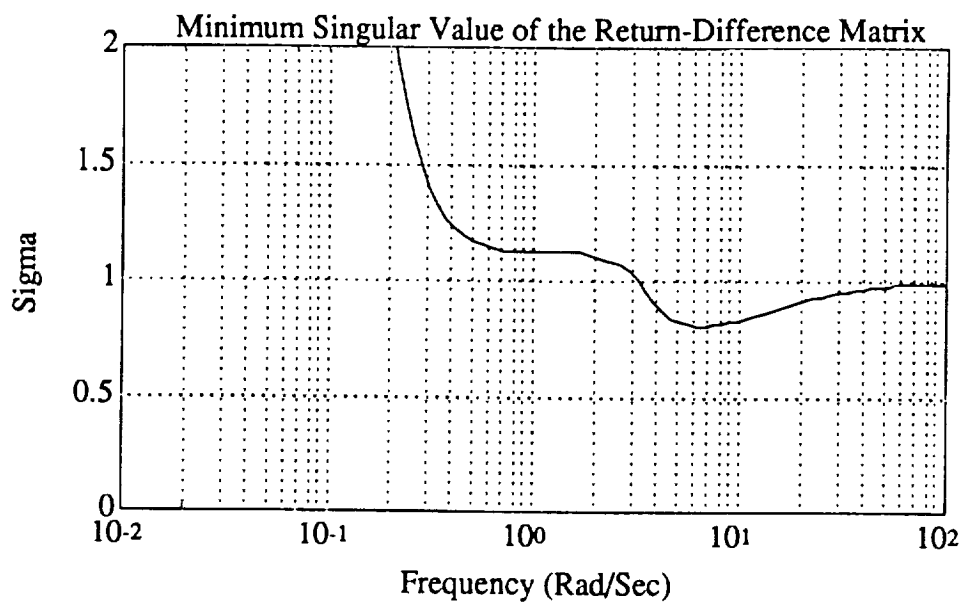
Figure 7.4: Robustness at the Control Paths of Optimal Inner and Outer-Loop Design (FLT1)
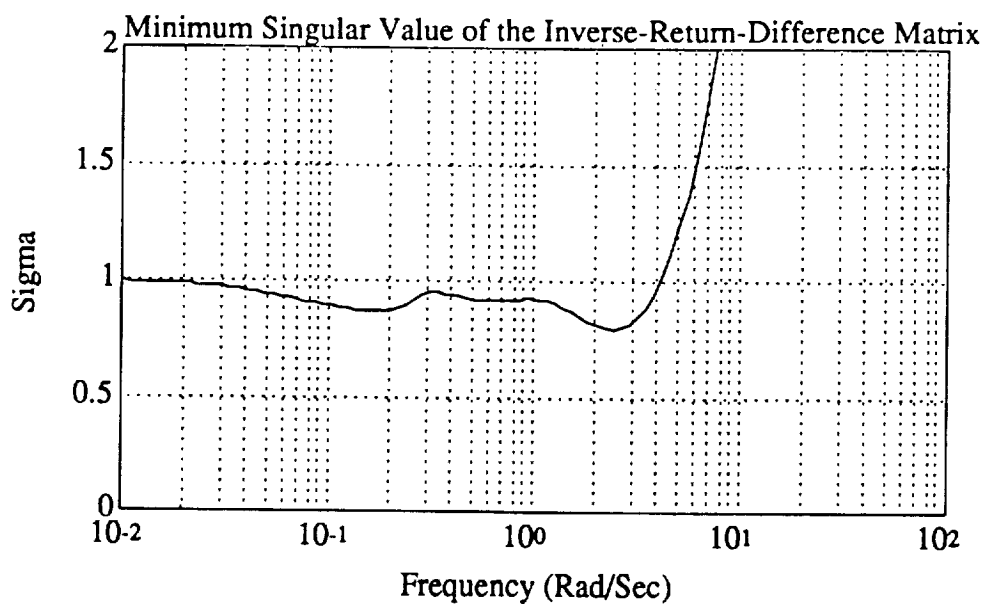
Figure 7.5: Robustness at the Control Paths of Optimal Inner and Outer-Loop Design (FLT1)
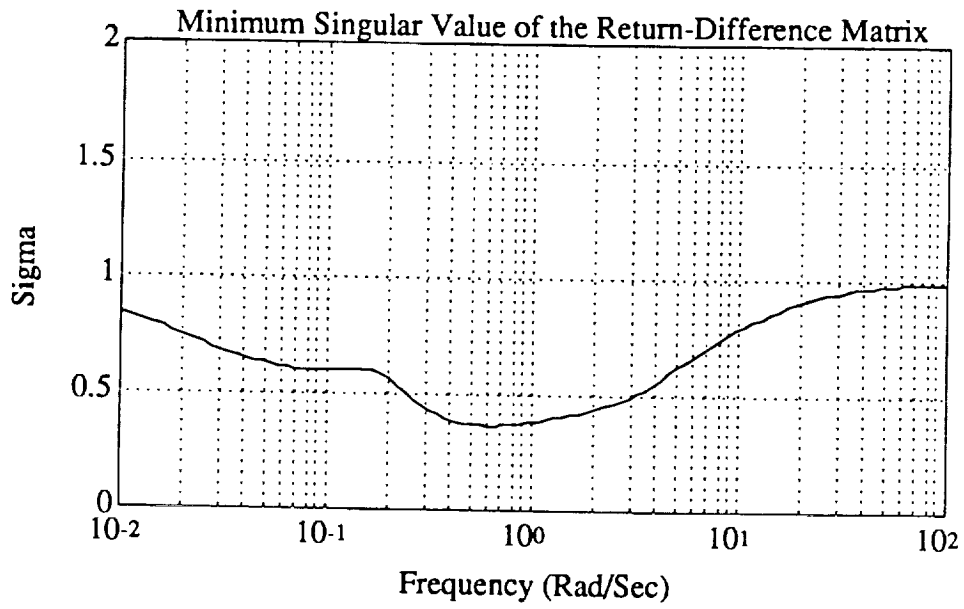
Figure 7.6: Robustness at the Sensor Paths of Optimal Inner and Outer-Loop Design (FLT1)
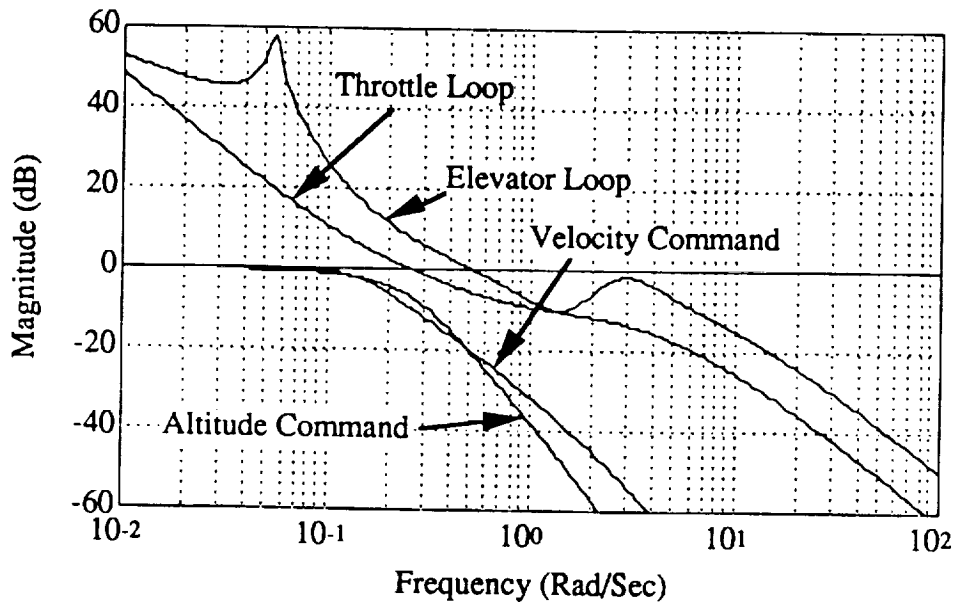
Figure 7.7: Loop Frequency Responses of Optimal Inner and Outer-Loop Design (FLT2)
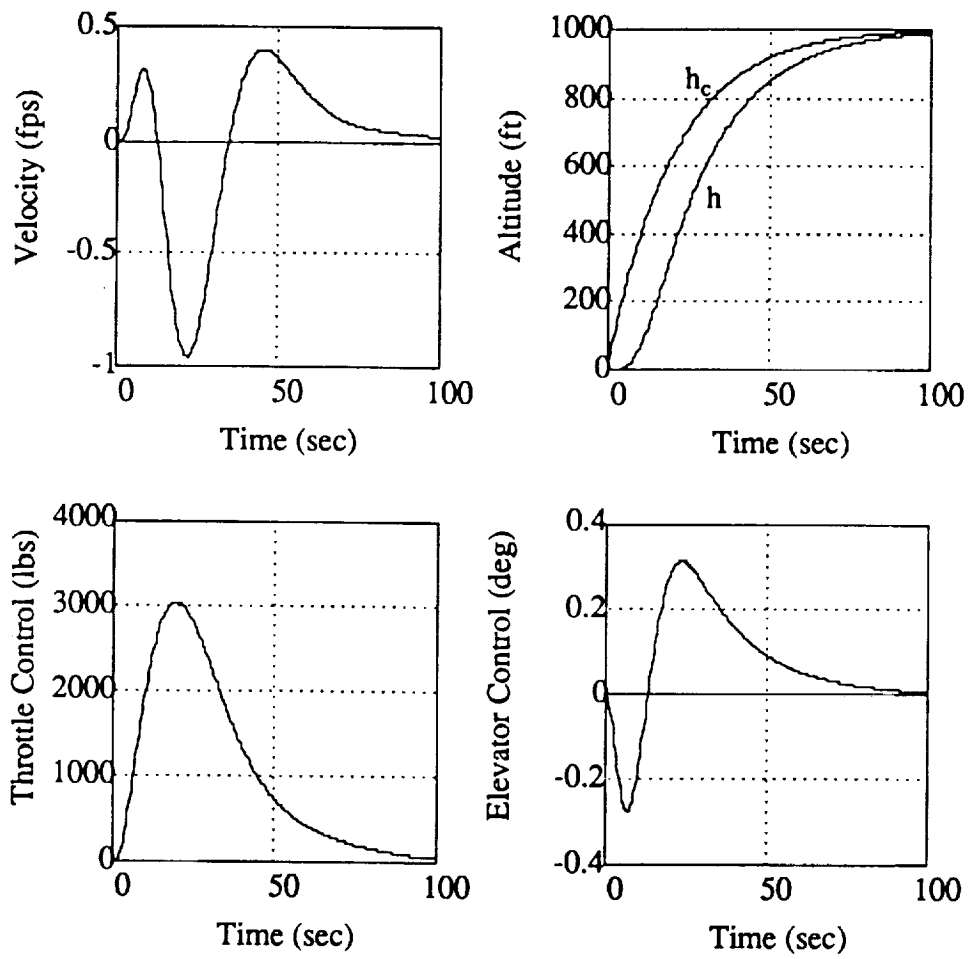
Figure 7.8: h_c Command Responses of Optimal Inner and Outer-Loop Design (FLT2)
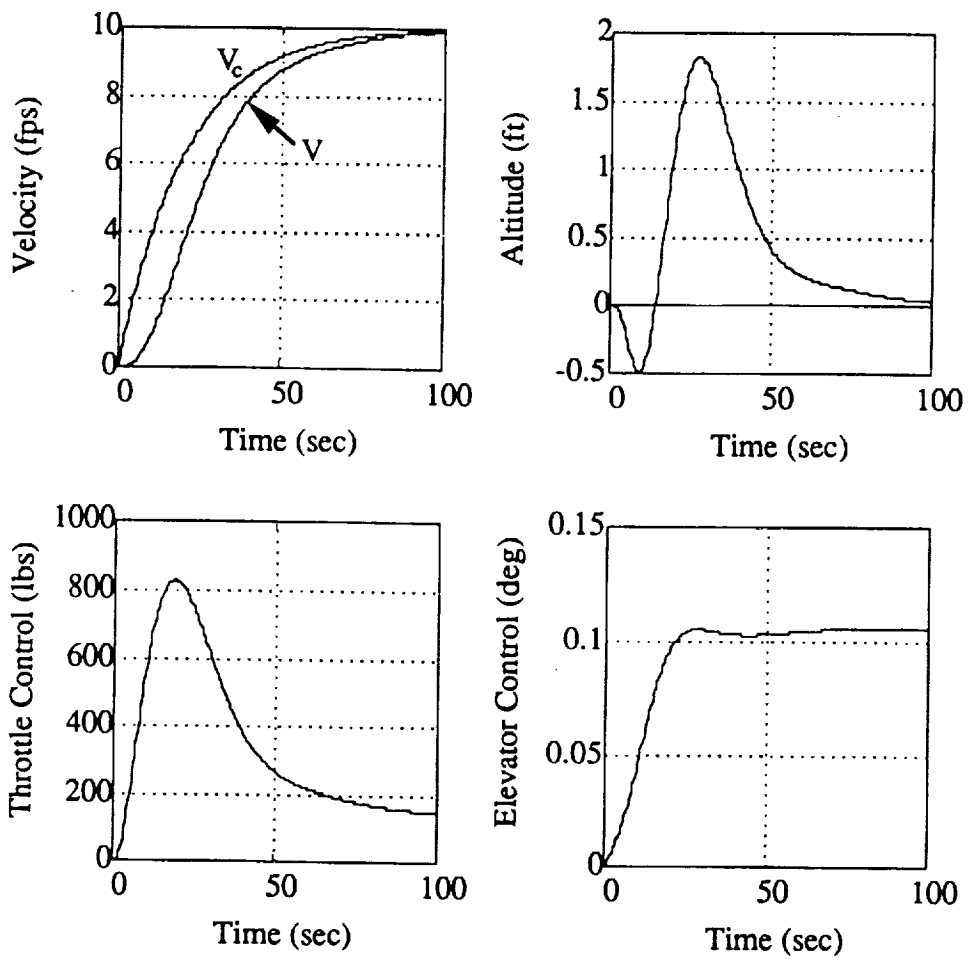
Figure 7.9: V_c Command Responses of Optimal Inner and Outer-Loop Design (FLT2)
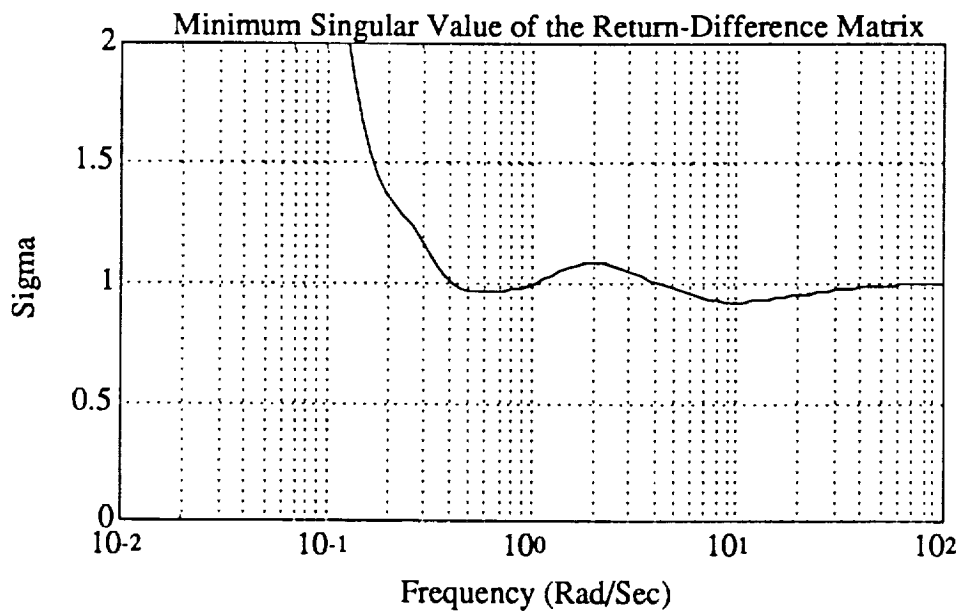
Figure 7.10: Robustness at the Control Paths of Optimal Inner and Outer-Loop Design (FLT2)
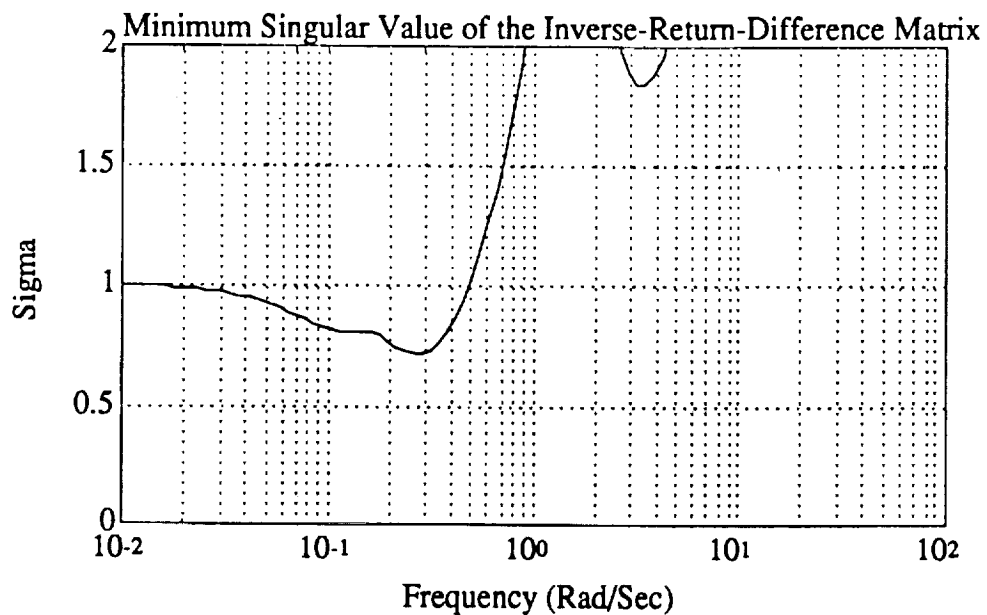
Figure 7.11: Robustness at the Control Paths of Optimal Inner and Outer-Loop Design (FLT2)
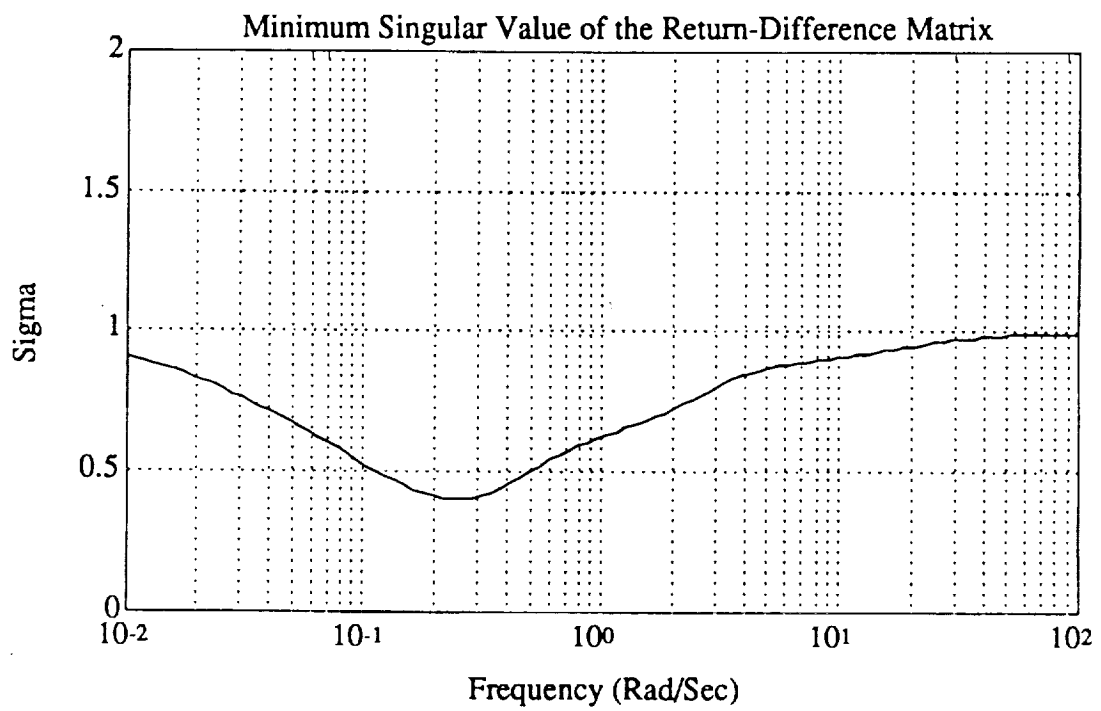
Figure 7.12: Robustness at the Sensor Paths of Optimal Inner and Outer-Loop Design (FLT2)

Chapter 8

CONCLUSIONS AND RECOMMENDATIONS

8.1 Conclusions

Traditionally, classical methods for control system design via successive single loop closure using root locus or Bode diagrams have been applied to the synthesis of feedback controllers for multiloop systems. Such designs often lack performance and robustness to uncertainties in the plant model. Automatic flight control systems (AFCS) on commercial aircraft are a prime example. Current AFCS design based on the single loop approach is evident in the architecture of the autothrottle and autopilot control systems. The autopilot is designed to regulate altitude through feedback to the elevator control surfaces while the autothrottle separately controls speed through feedback to the engines.

The basic problem with classical design procedures is that they usually overlook the multiloop aspects of the system dynamics, neglecting significant cross-coupling among different feedback control systems. In the case of the AFCS, flight path and speed errors are produced by both the throttle and elevator controls such that closure of both the autothrottle and autopilot control loops may be destabilizing. Furthermore, classical design procedures applied to multiloop controllers yield little insight into the problem of design tradeoff between performance and robustness to modeling uncertainties. Obtaining a satisfactory design with classical procedures is far from straightforward, and can be quite time consuming if previous design experiences are lacking. What is needed is a multivariable design procedure that directly incorporates design objectives in terms of closed-loop stability, performance, and robustness into the design tradeoff.

Development in multivariable design techniques have concentrated on improving controller performance and robustness to modeling uncertainties. Modern control design methods such as LQG, H^∞, and μ-synthesis allow designers to synthesize controllers that meet different measures of performance and robustness. Controller

designs obtained with modern techniques are usually of high order (i.e. the order of the controller is greater than or equal to the order of the plant model). Consequently, controller model reduction must be considered for practical implementation. Furthermore, design tradeoff between many real design goals (i.e. damping of system poles, disturbance rejection, command tracking, etc.), while easier than with classical procedures, is still far from simple.

In this study, the design method SANDY for robust controller design described in reference 6 is successfully applied to the design of an integrated autothrottle/autopilot control system. A complete design procedure encompassing key concerns such as closed-loop stability, control and command bandwidths, limited control activities to disturbance and command tracking performance has been developed for the synthesis of an integrated autothrottle/autopilot design based on the TECS concept. The usefulness of the procedure has been extensively demonstrated in actual design of an airspeed and altitude-hold system for a TSRV vehicle at two typical flight conditions. It should be noted that the constrained parameter optimization method implemented in the computer software SANDY has found wide application in aircraft flight controls and control of flexible mechanical systems, and provides a systematic approach for incorporating many real design objectives into the design tradeoff. Design goals such as damping of system modes, disturbance rejection, and command tracking are directly included into the design procedure. Direct tradeoffs are found to be systematic, and satisfactory designs are obtained with few iterations.

The philosophy of total energy control (TECS) enables us to define a multiloop AFCS feedback control structure. Previous TECS designs use classical methods for obtaining the controller feedback gains and gain schedule. Results in this research demonstrate the application of the SANDY design algorithm to a practical flight control problem; design of an integrated autothrottle/autopilot control system. The procedure allows designers to address a number of objectives such as stability, disturbance rejection and command tracking. Robustness to plant modeling uncertainties are maintained in the optimal design as compared with previous designs.

Contributions of this research are in the following areas:

- Formulation of performance indices for trade-offs in command and control bandwidths.

- Innovative formulation of the nonlinear constraints for the closed-loop system eigenvalues.

- Definition of a design variable $V_c^*(t)$ in terms of linear combinations of flight-path angle and velocity commands, and appropriate constraints on the design parameters to synthesize different levels of decoupling between the flight path command and velocity errors. This approach has a broad implication in the area of output decoupling control where cross-coupling between command paths can be systematically formulated.

- Development of systematic design procedure for the TECS control laws with clearly defined design trade-offs using multiple performance indices, direct bound constraints, constraints on closed-loop stability and gain schedule across different flight condition.

- Development of an integrated "inner loop" and "outer loop" design procedure for the TECS control-laws.

8.2   Recommendations for Future Research

Areas for future investigation include,

- Examination of sensor implementation issues such as filtering of signals and estimation.

- Extension of design procedures to directly include robustness measures into the design tradeoff.

- Application of the design procedure to flexible-body aircraft with low structural damping.

In this study, we have chosen to ignore the issue of sensor implementation for feedback of acceleration, flight path angle, and pitch damping variables. In practice, filtering of sensor signals is usually required. In fact, present TECS designs have included complementary filters for estimation of certain feedback quantities. The

design procedure developed in this investigation may be used to simultaneously design the feedback controller and the associated filter/estimator for the feedback sensors. Dynamic models of sensor signal conditioning can be incorporated into the synthesis model. The sensor filter/estimator parameters are then optimized along with gain parameters in the feedback controller.

The design procedure outlined in this research allows for the direct tradeoff between controller design goals of stability, performance, and robustness to modeling uncertainties. However, application of methods for incorporating robustness measures into the controller design procedure have not been extensively investigated. These techniques consist of including additional plant models for off-nominal conditions into the design procedure, and specification of H^∞ bounds on outputs of selected system transfer matrices for unstructured plant uncertainties.

A useful extension of this research would be to investigate the design tradeoff with robustness to modeling uncertainties. Available techniques for analysis of structured singular values could be used in defining "worst-case" design conditions for inclusion as off-nominal plant models into the design procedure, as discussed in section 4.3. Furthermore, methods for improving multivariable stability margins through H^∞ bounds on selected system transfer matrices could be explored.

The design procedure developed in this research is well suited to the synthesis of controllers for flexible mechanical systems. An interesting application of this procedure would be to the design of an AFCS for a highly flexible aircraft, such as for modal suppression, gust alleviation, and ride quality control. Nonlinear inequality constraints for damping of system eigenvalues would be useful for ensuring minimal damping in the flexible-body modes. Numerical algorithms need to be extended to handle systems with repeated eigenvalues that are not diagonalizable.

BIBLIOGRAPHY

[1] G. Stein and M. Athans. The LQG/LTR Procedure for Multivariable Feedback Control Design. *IEEE Transactions on Automatic Control*, Vol.AC-32, No.2, Feb. 1987.

[2] J. C. Doyle and K. Glover. State-Space Formulae for All Stabilizing Controllers that Satisfy an H^∞–Norm Bound and Relation to Risk Sensitivity. *Systems and Control Letters*, 11, November 1988, North Holland, pp. 167-172.

[3] J. C. Doyle. Analysis of Feedback Systems with Structured Uncertainties. *IEE Proceedings*, November 1982.

[4] W. S. Levine, T. L. Johnson and M. Athans. Optimal Limited State Variable Feedback Controllers for Linear Systems. *IEEE Transactions on Automatic Controls*, Vol. AC-16, No. 6, December 1971.

[5] N. Halyo and J. R. Broussard. *Algorithms for the Output Feedback, Multiple Model and Decentralized Control Problems*. NASA CP-2296, October 1983.

[6] U. Ly. *A Design Algorithm for Robust Low-Order Controllers*. PhD thesis, Stanford University, Department of Aeronautics and Astronautics, November 1982.

[7] U. Ly. H^2 and H^∞-Design Tools for Linear Time-Invariant Systems. *Third Annual Conference on Aerospace Computational Control*, Oxnard, California, August 1989.

[8] P. E. Gill, W. Murray, M. A. Saunders, and M. H. Wright. *User's Guide for NPSOL (Version 4.0): A Fortran Package for Nonlinear Programming*. Technical Report SOL 86-2, Stanford University, January 1986.

[9] A. A. Lambregts. *Integrated System Design for Flight and Propulsion Control using Total Energy Principles.* Technical Report AIAA 83-2561, American Institute of Aeronautics and Astronautics, October 1983.

[10] A. A. Lambregts. *Operational Aspects of the Integrated Vertical Flight Path and Speed Control System.* Technical Report SAE 831420, Aerospace Congress & Exposition, Long Beach, California, August 1983.

[11] A. A. Lambregts. Vertical Flight Path and Speed Control Autopilot Design using Total Energy Principles. *AIAA Guidance and Control Conference Proceedings,* August 1983. AIAA 83-2239-CP.

[12] K. R. Bruce. *Integrated Autopilot/Autothrottle Based on a Total Energy Control Concept: Design and Evaluation of Additional Autopilot Modes.* Technical Report NASA TCV Contract NAS1-16300, Boeing Commercial Airplane Company, August 1987.

[13] K. R. Bruce. *Integrated Autopilot/Autothrottle for the NASA TSRV B-737 Aircraft: Design and Verification by Nonlinear Simulation.* Technical Report NASA CR 4217, NASA Langley Research Center, February 1989.

[14] K. R. Bruce, J. R. Kelly, and L. H. Person. *NASA B737 Flight Test Results of the Total Energy Control System.* Technical Report AIAA 86-2143-CP, AIAA Guidance, Navigation and Control Conference, August 1986.

[15] A. P. Vinkler, L. J. Wood, U. Ly, and R. H. Cannon. Minimum Expected Cost Control of Linear Systems with Uncertain Parameters – Application to Remotely Piloted Vehicle Flight Control Systems. *AIAA Guidance and Control Conference,* Boulder, Colorado, August 1979.

[16] U. Ly. Optimal Low-Order Flight Critical Pitch Augmentation Control-Law for a Transport Airplane. *Proceedings of the AIAA Guidance and Control Conference,* August 1984, pp.743-757.

[17] R. D. Jones, J. Bossi and U. Ly. Multivariable Regulator Design for Robustness and Performance: A Realistic Example. *Proceedings of the American Control Conference*, Seattle, Washington, June 1986, pp. 285-288.

[18] D. E. Rosenthal. *Experiments in Control of Flexible Structures with Uncertain Parameters*. Technical Report SUDAAR 542, Stanford University, March 1984.

[19] K. K. Byun. Robust Control Synthesis for Uncertain Dynamical Systems. *AIAA Guidance and Control Conference*, pp. 792-801, August 1989.

[20] U. Ly. Robustness Analysis of a Multiloop Flight Control System. *AIAA Guidance and Control Conference*, pp. 155-165, Gatlinburg, Tennessee, August 1983.

[21] U. Ly and R. H. Cannon. A Direct Method for Designing Robust Optimal Control Systems. *AIAA Guidance and Control Conference*, pp. 440-448, Palo Alto, California, August 1978.

[22] E. E. Osborne. On Pre-Conditioning of Matrices. *Journal of the Association for Computing Machinery*, pp. 338-345, Los Angeles, California, March 1960.

[23] D. R. Schaeffer, D. Gangsaas, and M. Barr. *Wind Models for Flight Simulator Certification of Landing and Approach Guidance and Control Simulator*. Technical Report NASA TP 2412, May 1985.

[24] J. R. Kelly, L. H. Person, and K. R. Bruce. *Flight Testing TECS - The Total Energy Control System*. Technical Report SAE 861803, SAE Aerospace Technology Conference, October 1986.

[25] C. M. Thompson, E. E. Coleman, and J. D. Blight. *Integral LQG Controller Design for a Fighter Aircraft*. Technical Report 87-2452, AIAA Guidance and Control Conference, August 1987.

Appendix A

EVALUATION OF A QUADRATIC PERFORMANCE INDEX TO RANDOM INITIAL CONDITIONS AND IMPULSE INPUTS

The finite-time performance index in equation (3.6) evaluated to random initial conditions or impulse inputs can be evaluated as in equation (3.7) for white-noise inputs when certain conditions are met. This equivalence is established in the following sections.

A.1 Random Initial Conditions

The closed-loop system associated with each plant condition has the following form

$$\dot{x}'(t) = A'x'(t) \tag{A.1}$$

$$y_p(t) = C'_p x'(t) \tag{A.2}$$

$$x'(0) = x'_o \tag{A.3}$$

where the initial conditions $x'(0)$ are gaussian random variables with zero mean $E[x'_o] = 0$ and covariance $E[x'_o x'^T_o] = X'_o$. The feedback control inputs can also be expressed in terms of the states of the closed-loop system as

$$u_p(t) = y_c(t) = C'_c x'(t) \tag{A.4}$$

The performance index evaluated to random initial conditions is

$$J_1(t_f) = \frac{1}{2} \int_0^{t_f} e^{2\alpha t} E[y_p^T(t) Q y_p(t) + u_p^T(t) R u_p(t)] dt \tag{A.5}$$

Using equations (A.2) and (A.4), the performance index $J_1(t_f)$ becomes

$$J_1(t_f) = \frac{1}{2} tr \left\{ (C_p'^T Q C'_p + C_c'^T R C'_c) \int_0^{t_f} e^{2\alpha t} E[x'(t) x'^T(t)] dt \right\} \tag{A.6}$$

Solution of the closed-loop system responses to initial conditions is simply

$$x'(t) = e^{A't}x'_o \qquad (A.7)$$

Combining equations (A.6) and (A.7) yields

$$J_1(t_f) = \frac{1}{2}tr\left\{ \int_0^{t_f} e^{(A'+\alpha I)^T t}(C_p'^T Q C_p' + C_c'^T R C_c')e^{(A'+\alpha I)t}dt \ X'_o \right\} \qquad (A.8)$$

The feedback controller must provide an asymptotically stable closed-loop system so that the limit in equation (A.8) exists and is finite.

A.2   White-Noise Inputs

For random white-noise inputs, we consider the following closed-loop system

$$\dot{x}'(t) \quad = \quad A'x'(t) + \Gamma'w(t) \qquad (A.9)$$

$$y_p(t) \quad = \quad C_p'x'(t) \qquad (A.10)$$

$$x'(0) \quad = \quad 0 \qquad (A.11)$$

where the disturbance inputs $w(t)$ are gaussian random processes with zero mean $E[w(t)] = 0$ and covariance $E[w(t)w(\tau)^T] = W_o\delta(t-\tau)$. The feedback control inputs can be written as

$$u_p(t) = y_c(t) = C_c'x'(t) \qquad (A.12)$$

The finite-time performance index to random disturbance inputs is

$$J_2(t_f) = \frac{1}{2}E_\alpha[y_p^T(t_f)Qy_p(t_f) + u_p^T(t_f)Ru_p(t_f)] \qquad (A.13)$$

where $E_\alpha[\cdot]$ is the expectation operator for a closed-loop system destabilized by a factor α.

Substituting equations (A.10) and (A.12) into the expression for $J_2(t_f)$, we obtain after some manipulations

$$J_2(t_f) = \frac{1}{2}tr\left\{ (C_p'^T Q C_p' + C_c'^T R C_c')E_\alpha[x'(t_f)x'^T(t_f)] \right\} \qquad (A.14)$$

where the time response $x'(t)$ is given by

$$x'(t) = \int_0^t e^{(A'+\alpha I)(t-\tau)} \Gamma' w(\tau) d\tau \tag{A.15}$$

The performance index $J_2(t_f)$ becomes

$$J_2(t_f) = \frac{1}{2} tr\{(C_p'^T Q C_p' + C_c'^T R C_c') \tag{A.16}$$
$$\int_0^{t_f} \int_0^{t_f} e^{(A'+\alpha I)(t_f-\tau)} \Gamma' E[w(\tau)w^T(s)] \Gamma'^T e^{(A'+\alpha I)^T(t_f-s)} d\tau ds\}$$

Recalling that $E[w(\tau)w(s)^T] = W_o\delta(\tau-s)$, and with some rearranging $J_2(t_f)$ becomes

$$J_2(t_f) = \frac{1}{2} tr\{\int_0^{t_f} e^{(A'+\alpha I)^T(t_f-\tau)} \tag{A.17}$$
$$(C_p'^T Q C_p' + C_c'^T R C_c') e^{(A'+\alpha I)(t_f-\tau)} d\tau \Gamma' W_o \Gamma'^T\}$$

If we perform a change of variable $t = t_f - \tau$, then

$$J_2(t_f) = \frac{1}{2} Trace\{\int_0^{t_f} e^{(A'+\alpha I)^T t} \tag{A.18}$$
$$(C_p'^T Q C_p' + C_c'^T R C_c') e^{(A'+\alpha I)t} dt \Gamma' W_o \Gamma'^T\}$$

Therefore it can be seen from equations (A.8) and (A.18) that if

$$\Gamma' W_o \Gamma'^T = X_o' \tag{A.19}$$

then $J_1(t_f) = J_2(t_f)$. With this equivalence established, the problem associated with random initial conditions can be formulated as the one corresponding to random white-noise inputs.

A.3 Parameterized Random Impulse Inputs

For random impulse inputs, the closed-loop system has the following form

$$\dot{x}'(t) = A'x'(t) + B'w(t) \tag{A.20}$$
$$y_p(t) = C_p'x'(t) \tag{A.21}$$
$$x'(0) = 0 \tag{A.22}$$

where the inputs $w(t)$ are parameterized random impulses $w(t) = y_{cmd}\delta(t)$ with amplitude vector y_{cmd} being random with zero mean $E[y_{cmd}] = 0$ and covariance $E[y_{cmd}y_{cmd}^T] = Y_{cmd}$. The feedback control inputs can be written as

$$u_p(t) = y_c(t) = C_c' x'(t) \tag{A.23}$$

The finite-time performance index to random impulse inputs is

$$J_3(t_f) = \frac{1}{2}\int_0^{t_f} e^{2\alpha t} E[y_p^T(t)Qy_p(t) + u_p^T(t)Ru_p(t)]dt \tag{A.24}$$

Substituting equations (A.21) and (A.23) into the expression for $J_3(t_f)$, we obtain after some manipulations

$$J_3(t_f) = \frac{1}{2}tr\left\{(C_p'^T QC_p' + C_c'^T RC_c')\int_0^{t_f} e^{2\alpha t} E[x'(t)x'^T(t)]dt\right\} \tag{A.25}$$

where the time response $x'(t)$ is given by the time-convolution integral as

$$x'(t) = \int_0^t e^{(A'+\alpha I)(t-\tau)}B'w(\tau)d\tau \tag{A.26}$$

and since $w(\tau) = y_{cmd}\delta(\tau)$, we have

$$x'(t) = e^{(A'+\alpha I)t}B'y_{cmd} \tag{A.27}$$

The performance index $J_3(t_f)$ becomes

$$J_3(t_f) = \frac{1}{2}tr\{\int_0^{t_f} e^{(A'+\alpha I)^T t} \tag{A.28}$$
$$(C_p'^T QC_p' + C_c'^T RC_c')e^{(A'+\alpha I)t}dt E[B'y_{cmd}y_{cmd}^T B'^T]\}$$

Recalling that $E[y_{cmd}y_{cmd}^T] = Y_{cmd}$, we have

$$J_3(t_f) = \frac{1}{2}tr\left\{\int_0^{t_f} e^{(A'+\alpha I)^T t}(C_p'^T QC_p' + C_c'^T RC_c')e^{(A'+\alpha I)t}dt B'Y_{cmd}B'^T\right\} \tag{A.29}$$

It can be seen from equations (A.18) and (A.29) that if

$$\Gamma' W_o \Gamma'^T = B'Y_{cmd}B'^T \tag{A.30}$$

then we have $J_3(t_f) = J_2(t_f)$. Thus, the problem associated with parameterized random impulse inputs can also be formulated as one corresponding to white-noise inputs if we use the equivalence relation of (A.30).

Appendix B

CONTROLLER DESIGN FOR COMMAND TRACKING AND DISTURBANCE REJECTION

Two common classes of control designs to external inputs are: command tracking or model-following and disturbance rejection. Control-law synthesis for these design problems can be formulated in terms of the minimization of a quadratic performance index of the form

$$J = \lim_{t_f \to \infty} \int_0^{t_f} E[y_\epsilon^T(t)Qy_\epsilon(t) + u_\epsilon^T(t)Ru_\epsilon(t)]dt \tag{B.1}$$

The quadratic performance index J contains penalties on transient responses of the closed-loop system to random commands and/or disturbances. For command tracking, the variables $y_\epsilon(t)$ and $u_\epsilon(t)$ in equation (B.1) are the tracking errors defined by

$$y_\epsilon(t) = y_p(t) - y_m(t) \tag{B.2}$$

$$u_\epsilon(t) = u_p(t) - u_{cmd}(t) \tag{B.3}$$

where $y_m(t)$ are the outputs of a command generator model and $u_{cmd}(t)$ are the control inputs that produce zero tracking errors in $y_\epsilon(t)$ at steady state. In order to ensure that the performance index in equation (B.1) be bounded, *all* the penalized variables in $y_\epsilon(t)$ and $u_\epsilon(t)$ corresponding to the nonzero weighting matrices Q and R must converge asymptotically to zero as $t \to \infty$. For example, in the case of output commands $y_m(t)$ having nonzero constant steady-state values (i.e $y_m(t) = y_{cmd_0}\mu(t)$ where $\mu(t)$ is the unit-step), it can be shown through the set point calculations (section B.3) that the required controls $u_{cmd}(t)$ at steady state are linear functions of y_{cmd_0}.

For the problem of disturbance rejection, the tracking errors $y_\epsilon(t)$ and $u_\epsilon(t)$ in equation (B.1) are defined as

$$y_\epsilon(t) = y_p(t) - y_{p_{ss}}(t) \tag{B.4}$$

$$u_\epsilon(t) \;=\; u_p(t) - u_{p_{**}}(t) \tag{B.5}$$

where $y_{p_{**}}(t)$ are the desired output responses while $u_{p_{**}}(t)$ are the necessary control inputs to maintain the desired outputs $y_{p_{**}}(t)$ in the presence of disturbances $w(t)$. The relationships between $u_{p_{**}}(t)$, $y_{p_{**}}(t)$ and the disturbances $w(t)$ are derived in section B.4.

Command outputs $y_m(t)$ and disturbance outputs $w(t)$ in the form of impulses, steps, ramps or a combination of these can be derived from linear time-invariant models with appropriately choosen initial conditions and impulse inputs. Details are given in sections B.1 and B.2.

B.1 Models for Parameterized Random Commands

Commands $y_m(t)$ in the form of impulses, steps or ramps can be generated using a linear time-invariant model of the form,

$$\dot{x}_m(t) \;=\; A_m x_m(t) + B_m y_{cmd}(t) \tag{B.6}$$

$$y_m(t) \;=\; C_m x_m(t) + D_m y_{cmd}(t) \tag{B.7}$$

with $x_m(0) = x_{m_0}$ and $y_{cmd}(t) = y_{cmd_0}\delta(t)$. The quantities x_{m_0}, y_{cmd_0} along with the state matrices A_m, B_m, C_m and D_m define the desired outputs $y_m(t)$.

For example, a command vector of impulses can be created using

$$y_m(t) = y_{cmd_0}\delta(t) \tag{B.8}$$

where the state vector $x_m(t)$ is of zero dimension and the matrix $D_m = I$. The impulse magnitude y_{cmd_0} is a vector of gaussian random parameters with zero mean $E[y_{cmd_0}] = 0$ and covariance $E[y_{cmd_0}y_{cmd_0}^T] = Y_{cmd_0}$.

On the other hand, a vector of step commands can be obtained from

$$\dot{x}_m(t) \;=\; (0)x_m(t) + y_{cmd_0}\delta(t) \tag{B.9}$$

$$y_m(t) \;=\; x_m(t) \tag{B.10}$$

$$x_m(0) \;=\; 0 \tag{B.11}$$

yielding a step command vector $y_m(t) = y_{cmd_0}\mu(t)$ where $\mu(t)$ is a unit-step function and y_{cmd_0} is a vector of gaussian random parameters with zero mean $E[y_{cmd_0}] = 0$ and covariance $E[y_{cmd_0}y_{cmd_0}^T] = Y_{cmd_0}$.

An alternate formulation for the vector of step commands is

$$\dot{x}_m(t) = (0)x_m(t) \tag{B.12}$$

$$y_m(t) = x_m(t) \tag{B.13}$$

$$x_m(0) = x_{m_0} \tag{B.14}$$

In this case, the resulting step command is $y_m(t) = x_{m_0}\mu(t)$ where x_{m_0} is a vector of gaussian random parameters with zero mean $E[x_{m_0}] = 0$ and covariance $E[x_{m_0}x_{m_0}^T] = X_{m_0}$.

Filtering of command outputs can be done by introducing additional dynamics into the command generator model described in equations (B.6)-(B.7). The choice of the state matrices A_m, B_m, C_m and D_m will completely define the command signals $y_m(t)$. For example, if the system matrix A_m has a pair of eigenvalues at $\lambda = \pm j\omega_0$ (i.e on the imaginary axis), then the outputs $y_m(t)$ will have components of sinusoidal functions of frequency ω_0. Figures (B.1) and (B.2) show time responses of a stable first-order filter to a scalar impulse command and a step command respectively.

B.2   Models for Parameterized Random Disturbances

In a similar manner, external random disturbances $w(t)$ in the form impulses, steps and ramps can be generated using a linear time-invariant model of the form,

$$\dot{x}_d(t) = A_d x_d(t) + B_d w_d(t) \tag{B.15}$$

$$w(t) = C_d x_d(t) + D_d w_d(t) \tag{B.16}$$

with $x_d(0) = x_{d_0}$ and $w_d(t) = w_0\delta(t)$. The quantities x_{d_0}, w_0 along with the state matrices A_d, B_d, C_d and D_d are parameters that define the disturbances $w(t)$.

For example, a disturbance vector of impulses can be created using

$$w(t) = w_0\delta(t) \tag{B.17}$$

where the state vector $x_d(t)$ is of zero dimension and the matrix $D_d = I$. The amplitude w_0 is a vector of gaussian random parameters with zero mean $E[w_0] = 0$ and covariance $E[w_0 w_0^T] = W_0$.

On the other hand, a vector of constant disturbances can be obtained from

$$\dot{x}_d(t) = (0)x_d(t) + w_0 \delta(t) \tag{B.18}$$

$$w(t) = x_d(t) \tag{B.19}$$

$$x_d(0) = 0 \tag{B.20}$$

yielding a disturbance vector $w(t) = w_0 \mu(t)$ where w_0 is a vector of gaussian random parameters with zero mean $E[w_0] = 0$ and covariance $E[w_0 w_0^T] = W_0$.

Note that an alternate formulation for the vector of constant disturbances can be done using random initial conditions as described below,

$$\dot{x}_d(t) = (0)x_d(t) \tag{B.21}$$

$$w(t) = x_d(t) \tag{B.22}$$

$$x_d(0) = x_{d_0} \tag{B.23}$$

In this case, the resulting step disturbance vector is $w(t) = x_{d_0} \mu(t)$ where x_{d_0} is a vector of gaussian random parameters with zero mean $E[x_{d_0}] = 0$ and covariance $E[x_{d_0} x_{d_0}^T] = X_{d_0}$.

Other parameterized random disturbance functions can be produced, similarly to the command generator models of section B.1, by introducing additional linear filters into the disturbance model of equations (B.15)-(B.16).

Random stochastic processes can also be modeled using equations (B.15)-(B.16) where, in this case, the disturbance inputs $w_d(t)$ are white-noises with zero mean $E[w_d(t)] = 0$ and covariance $E[w_d(t) w_d^T(\tau)] = W_0 \delta(t - \tau)$. Outputs $w(t)$ of the disturbance model are depicted as colored noises having power spectral characteristics defined by the disturbance state matrices A_d, B_d, C_d and D_d.

B.3 Steady-State Responses to Command Inputs

Command tracking and model-following designs involve the formulation of a performance index that contains tracking errors $y_\epsilon(t) = y_p(t) - y_m(t)$ and control feedback

errors $u_\epsilon(t) = u_p(t) - u_{cmd}(t)$ as depicted in equation (B.1). These error variables can always be written as outputs of a closed-loop system. The quantities $y_m(t)$ are commanded outputs while $u_{cmd}(t)$ are the control inputs used to maintain zero steady-state tracking errors in $y_\epsilon(t)$. We would like to establish the necessary relationships between the commanded outputs $y_m(t)$ and the control inputs $u_{cmd}(t)$.

Let's consider a linear time-invariant plant model with control inputs $u_p(t)$ and outputs $y_p(t)$,

$$\dot{x}_p(t) = A_p x_p(t) + B_p u_p(t) \tag{B.24}$$

$$y_p(t) = C_p x_p(t) + D_p u_p(t) \tag{B.25}$$

In the following derivation, we restrict ourselves to the case where the commanded outputs $y_m(t)$ have only *constant* steady-state components; that is, we exclude any commanded outputs that are sinusoidal or grow unbounded with time such as ramp functions. This assumption enables us to treat this problem as one corresponding to the calculation of setpoints. Steady-state system responses are determined by letting $\dot{x}_p(t) = 0$, $u_p(t) \to u_{cmd}(t)$ and $y_p(t) \to y_m(t)$ in the limit as $t \to \infty$. Dimension of $y_p(t)$ (and thus $y_m(t)$) must be equal to the dimension of $u_p(t)$ so that we have

$$\begin{pmatrix} x_p(t) \\ u_p(t) \end{pmatrix}_{ss} = \begin{bmatrix} A_p & B_p \\ C_p & D_p \end{bmatrix}^{-1} \begin{pmatrix} 0 \\ y_p(t) \end{pmatrix}_{ss} \tag{B.26}$$

or

$$\begin{pmatrix} x_{p_{ss}}(t) \\ u_{cmd}(t) \end{pmatrix} = \begin{bmatrix} A_p & B_p \\ C_p & D_p \end{bmatrix}^{-1} \begin{pmatrix} 0 \\ y_m(t) \end{pmatrix} \tag{B.27}$$

where the notation $(\cdot)_{ss}$ denotes the quasi-steady values. We should emphasize that these relationships are *correct* only when the steady-state conditions have been reached. Nonetheless one can use relations in equation (B.27) to express the desired states and control command inputs as a function of the commanded outputs $y_m(t)$ for all time $t \geq 0$. The control command inputs $u_{cmd}(t)$ and the state vector $x_{p_{ss}}(t)$ are therefore functions of time since the commands $y_m(t)$ may be time-varying, and they will settle to constant values as $t \to \infty$. Note that the system matrix formed by the quadruple A_p, B_p, C_p and D_p in equation (B.27) is square and it must also

be invertible for the setpoint calculation. The quantities $y_m(t)$ are outputs of a command generator model and the values $x_{p_{ss}}(t)$ and $u_{cmd}(t)$ are computed according to equation (B.27).

Let's denote the inverse of the system matrix as

$$\begin{bmatrix} A_p & B_p \\ C_p & D_p \end{bmatrix}^{-1} = \begin{bmatrix} K & M \\ L & N \end{bmatrix} \tag{B.28}$$

where the matrix partitions K through N have the same dimensions as their counterparts A_p through D_p on the left-side of the equation. With these definitions, the command inputs $u_{cmd}(t)$ in equation (B.27) can be written explicitly in terms of $y_m(t)$ as $u_{cmd}(t) = N y_m(t)$. The plant synthesis model in equation (B.24) for a command tracking problem is given by,

$$\dot{x}_p(t) = A_p x_p(t) + B_p u_p(t) + (0) y_m(t) \tag{B.29}$$

$$y_\epsilon(t) = C_p x_p(t) + D_p u_p(t) - I y_m(t) \tag{B.30}$$

$$u_\epsilon(t) = (0) x_p(t) + I u_p(t) - N y_m(t) \tag{B.31}$$

where $y_m(t)$ is the command input vector discussed in section B.1. The tracking errors $y_\epsilon(t)$ and $u_\epsilon(t)$ in the performance index of equation (B.1) are now outputs of the plant model in equations (B.29)-(B.31).

To complete the problem formulation, plant model in equations (B.29)-(B.31) must be augmented with a command generation model as described in section B.1 to form the final synthesis model in a command tracking problem.

B.4 Steady-State Responses to External Disturbances

The design problem for disturbance rejection involves the formulation of a performance index as in equation (B.1) that contains tracking errors $y_\epsilon(t) = y_p(t) - y_{p_{ss}}(t)$ and control feedback errors $u_\epsilon(t) = u_p(t) - u_{p_{ss}}(t)$. These error variables can be written as outputs of a closed-loop system. The quantities $y_{p_{ss}}(t)$ are the desired outputs of the closed-loop system in the presence of disturbances. The control inputs $u_{p_{ss}}(t)$ are used to reject the unwanted disturbances in the output responses and thereby

enforce zero tracking errors in $y_\epsilon(t)$ at steady state. We need to establish a set of relations similar to equation (B.27) of the tracking problem for the desired state vector $x_{p_{ss}}(t)$ and control inputs $u_{p_{ss}}(t)$.

Let's consider a linear time-invariant plant model with control inputs $u_p(t)$, disturbance inputs $w(t)$ and outputs $y_p(t)$,

$$\dot{x}_p(t) = A_p x_p(t) + B_p u_p(t) + \Gamma_p w(t) \qquad (B.32)$$

$$y_p(t) = C_p x_p(t) + D_p u_p(t) + \Omega_p w(t) \qquad (B.33)$$

As before, the desired steady-state system responses are determined by letting $\dot{x}_p(t) = 0$, $y_p(t) \to y_{p_{ss}}(t)$, $u_p(t) \to u_{p_{ss}}(t)$ and $w(t) \to w_{ss}(t)$ in the limit as $t \to \infty$. Again, the dimension of $y_p(t)$ must be equal to the dimension of $u_p(t)$ so that we have

$$\begin{pmatrix} x_p(t) \\ u_p(t) \end{pmatrix}_{ss} = \begin{bmatrix} A_p & B_p \\ C_p & D_p \end{bmatrix}^{-1} \begin{pmatrix} -\Gamma_p w(t) \\ y_p(t) - \Omega_p w(t) \end{pmatrix}_{ss} \qquad (B.34)$$

where the notation $(\cdot)_{ss}$ again denotes the quasi-steady values. The control input $u_{p_{ss}}(t)$ and the state vector $x_{p_{ss}}(t)$ are now functions of the external disturbances $w_{ss}(t)$ and the desired outputs $y_{p_{ss}}(t)$. And they may be time-varying.

Note that the system matrix formed by A_p, B_p, C_p and D_p in (B.34) is a square matrix and it must have full rank for its inverse to exist.

We denote the inverse of the system matrix as

$$\begin{bmatrix} A_p & B_p \\ C_p & D_p \end{bmatrix}^{-1} = \begin{bmatrix} K & M \\ L & N \end{bmatrix} \qquad (B.35)$$

where the matrix partitions K through N have the same dimensions as their counterparts A_p through D_p on the left-side of equation (B.35). The plant synthesis model in equation (B.32) for a disturbance rejection problem is given by

$$\dot{x}_p(t) = A_p x_p(t) + B_p u_p(t) + (0) y_{p_{ss}}(t) + \Gamma_p w_{ss}(t) \qquad (B.36)$$

$$y_\epsilon(t) = C_p x_p(t) + D_p u_p(t) - I y_{p_{ss}}(t) + \Omega_p w_{ss}(t) \qquad (B.37)$$

$$u_\epsilon(t) = (0) x_p(t) + I u_p(t) - N y_{p_{ss}}(t) + N \Omega_p w_{ss}(t) \qquad (B.38)$$

The tracking errors $y_\epsilon(t)$ and $u_\epsilon(t)$ in the performance index given in equation (B.1) are now outputs of the plant synthesis model in equations (B.36)-(B.38).

To complete the problem formulation, the plant model in equations (B.36)-(B.38) must be augmented with a disturbance model as described in section B.2 to form the final synthesis model in a disturbance rejection problem.
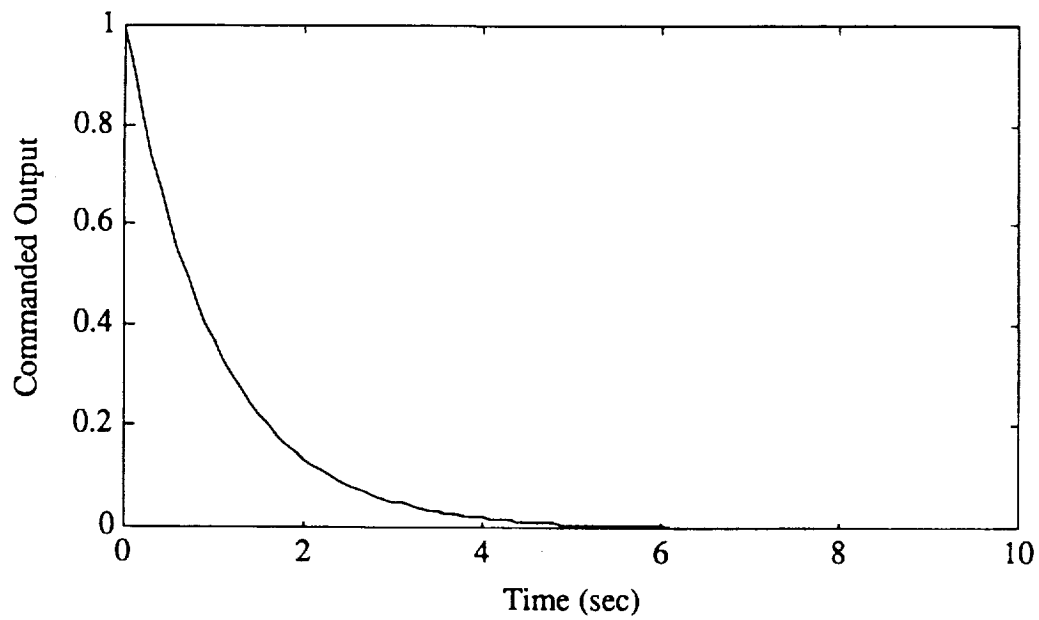
Figure B.1: Response of a First-Order Stable Filter to an Impulse Command
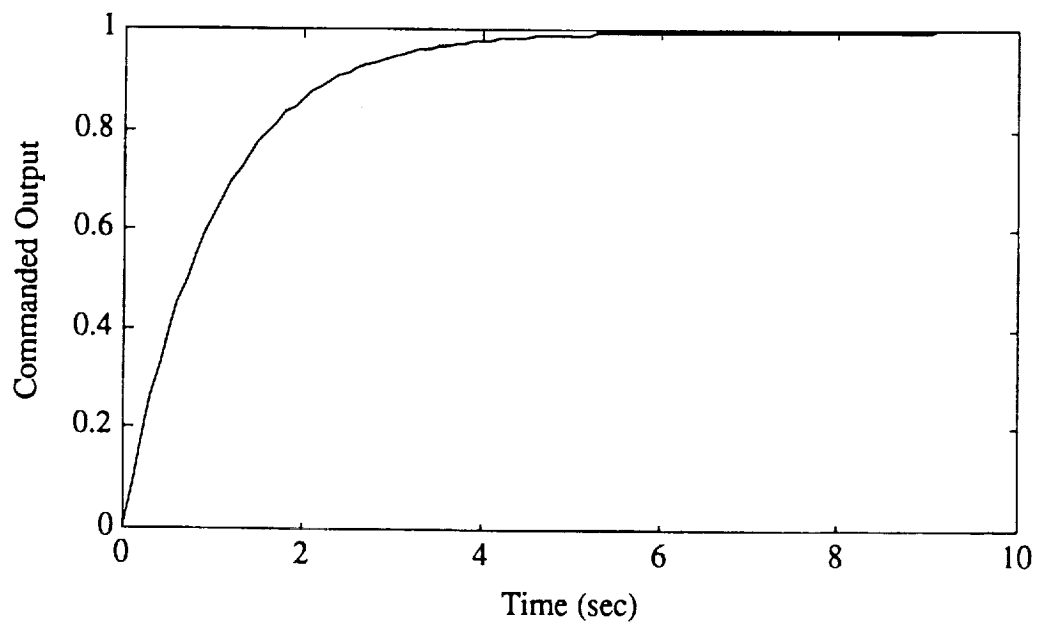
Figure B.2: Response of a First-Order Stable Filter to a Step Command

Appendix C

NONLINEAR CONSTRAINTS ON SYSTEM EIGENVALUES

Design requirements involving damping ratio and frequency of closed-loop eigenvalues are one of many important design criteria that a feedback control system must satisfy. For example, flying qualities in the longitudinal axis are often expressed in terms of desired locations of the short-period and phugoid modes. To achieve the desired characteristics in the closed-loop eigenvalues, one common design procedure based on optimal control would be through the use of output penalty variables in the quadratic performance index. Clearly, a design procedure for closed-loop stability via a performance index is indirect and necessitates numerous trials before arriving at a reasonable set of penalty variables.

The reason behind this difficulty is that there is no one-to-one correspondance between location of closed-loop system eigenvalues and transient responses of output variables to disturbances. A more direct approach for the assignment of closed-loop eigenvalues is with the use of direct constraints. The following sections will describe the formulation of two types of eigenvalue constraints: one type of constraint is on the real parts of the eigenvalues, and the other is on their damping ratio parameters. Other variation or extension from these set-ups can be easily implemented by a simple modification of the proposed schemes; for example, the case involving damping and frequency constraint requirements that are frequency-dependent. The advantage of the proposed formulation of eigenvalue constraints is that the constraint functions in both cases are continuously differentiable with respect to the design parameters in the system matrix. However the above statement holds only for systems that are diagonalizable, i.e having a non-degenerate Jordan structure.

C.1 Constraints on the System Eigenvalues

Consider a linear time-invariant system described by the following state model

$$\dot{x}(t) = Ax(t) \tag{C.1}$$

where $x(t)$ is a state vector of dimension n, and A is a system matrix of dimension $n \times n$. System stability is governed by the eigenvalues of the system matrix A defined by

$$Av_i = \lambda_i v_i, (i = 1, ..., n) \tag{C.2}$$

where λ_i is the ith eigenvalue of the system matrix A and v_i is the corresponding eigenvector. For *practical* purposes and from here on, we assume that the system matrix A is *diagonalizable*, i.e. there exists a nonsingular similarity transformation T constructed from a set of n completely independent eigenvectors $[v_i]_{i=1,...,n}$ such that

$$T^{-1}AT = \Lambda \tag{C.3}$$

$$= diag(\lambda_i)_{i=1,...,n} \tag{C.4}$$

In this appendix, we examine constraint formulation on two basic parameters of an eigenvalue $\lambda_i = \sigma_i + j\omega_i, (i = 1, ..., n)$ where $j = \sqrt{-1}$, namely: (1) its real part σ_i and, (2) its damping ratio ζ_i defined as

$$\zeta_i = \frac{-\sigma_i}{\sqrt{\sigma_i^2 + \omega_i^2}} \tag{C.5}$$

Clearly for stability, one must have at least $\sigma_i < 0$ or $\zeta_i > 0$, $(i = 1, ..., n)$. Usually requirements for closed-loop stability are expressible in terms of desired real parts and damping of system eigenvalues as indicated in figure C.1.

The corresponding constraint inequalities are

$$\sigma_i \leq \sigma_{\max}, (i = 1, ..., n) \tag{C.6}$$

$$\zeta_i \geq \zeta_{\min}, (i = 1, ..., n) \tag{C.7}$$

where $\sigma_{\max}$ and $\zeta_{\min}$ are design specification parameters. Equations (C.6) and (C.7) constitute a set of $2n$ inequality constraints on the system eigenvalues. For convenience and simplicity of implementation, one can employ an equivalent formulation

that yields basically the same results, but would involve only a single inequality constraint. To understand the achieved accuracy level of a constrained eigenvalue under a given tolerance on the inequality constraint, we need to examine, as given in the following sections, the results corresponding to the constraints on its real part and its damping ratio separately.

C.1.1 Constraints on the Real Part of System Eigenvalues

An equivalent formulation of equation (C.6) is as

$$0 \leq \sigma \leq \frac{1}{2}\epsilon^2 \tag{C.8}$$

where ϵ is a preselected tolerance level and the variable σ is defined as

$$\sigma = \frac{1}{2}\sum_{i=1}^{n}[\max(\sigma_i - \sigma_{\max}, 0)]^2 \tag{C.9}$$

with $\sigma_{\max}$ being the desired maximum real part of the eigenvalues. Note that eigenvalues that satisfy the constraints in equation (C.6) do not contribute to the variable σ; only those eigenvalues that violate the constraints are accounted for in equation (C.9). Clearly, when the constraint in equation (C.8) is satisfied then the real parts of the active eigenvalues $\sigma_i (i = 1, ..., n)$ (i.e. those that contribute to σ in equation (C.9)) are within a tolerance $\pm\epsilon$ from the desired bound $\sigma_{\max}$. Note that the parameter σ is a continuously differentiable function with respect to the design parameters in the system matrix A. Section C.2 derives the sensitivity function $\frac{\partial \sigma}{\partial p}$ with respect to a parameter p in the system matrix A that is diagonalizable.

C.1.2 Constraints on the Damping Ratio of System Eigenvalues

An equivalent form of equation (C.7) is

$$0 \leq \zeta \leq \frac{1}{2}\epsilon^2 \tag{C.10}$$

where ϵ is a preselected tolerance level and the variable ζ is defined as

$$\zeta = \frac{1}{2}\sum_{i=1}^{n}[\max(\sigma_i + |\omega_i|\cot\alpha, 0)]^2 \tag{C.11}$$

with $\cos \alpha = \zeta_{\min}$ and $\sin \alpha = \sqrt{1 - \zeta_{\min}^2}$ where $\zeta_{\min}$ is the desired minimum damping ratio applied to all the system eigenvalues. Physically the constraint variable ζ is the sum of the square of the horizontal distance d_i for the eigenvalues with nonnegative imaginary parts (i.e. $\omega_i \geq 0$) that are located above the damping line $\zeta_{\min}$ (figure C.2). Any eigenvalue with nonnegative imaginary part that falls below the damping line does not contribute to the constraint variable ζ. Those eigenvalues with negative imaginary parts (i.e. $\omega_i < 0$) will contribute the same amount as their complex conjugate counterparts. When the constraint in equation (C.10) is satisfied, the damping ratio ζ_i of each active eigenvalue $\lambda_i (i = 1, ..., n)$ (i.e. one which contributes to ζ in equation (C.11)) will be bounded by

$$\zeta_{\min} \left(1 + \delta_- \left(\frac{\epsilon}{|\sigma_i|}, \zeta_{\min} \right) \right) \leq \zeta_i \leq \zeta_{\min} \left(1 + \delta_+ \left(\frac{\epsilon}{|\sigma_i|}, \zeta_{\min} \right) \right), (i = 1, ..., n)$$

(C.12)

where

$$\delta_- \left(\frac{\epsilon}{|\sigma_i|}, \zeta_{\min} \right) = \frac{1}{\sqrt{\cos^2 \alpha + \left(1 + \frac{\epsilon}{|\sigma_i|} \right)^2 \sin \alpha^2}} - 1 < 0 \qquad (C.13)$$

$$\delta_+ \left(\frac{\epsilon}{|\sigma_i|}, \zeta_{\min} \right) = \frac{1}{\sqrt{\cos^2 \alpha + \left(1 - \frac{\epsilon}{|\sigma_i|} \right)^2 \sin \alpha^2}} - 1 > 0 \qquad (C.14)$$

Figure C.3 shows relative levels of accuracies (i.e values of $\zeta / \zeta_{min} - 1$) achieved from the constraint equation (C.10) as a function of the ratio $\frac{\epsilon}{|\sigma_i|}$, i.e. plots of $\delta_\pm \left(\frac{\epsilon}{|\sigma_i|}, \zeta_{\min} \right)$. Thus for an actively constrained eigenvalue λ_i, the desired damping ratio $\zeta_{\min}$ is satisfied to within an acceptable level of accuracy, say 0.01, if the parameter ϵ is selected such that

$$\left| \delta_\pm \left(\frac{\epsilon}{|\sigma_i|}, \zeta_{\min} \right) \right| \leq 0.01 \qquad (C.15)$$

To ensure that all eigenvalues $\lambda_i (i = 1, ..., n)$ have the desired damping ratio $\zeta_{\min}$ to within a relative accuracy of at least 0.01, the parameter ϵ must be chosen based on the minimum value of $| \sigma_i | (i = 1, ..., n)$. Together with the constraint equation (C.8) for the real part of the eigenvalues, a reasonable estimate for the minimum of $| \sigma_i | (i = 1, ..., n)$ would be $| \sigma_{\max} |$.

C.2   Gradients of the Constraints with Respect to Parameters in the System Matrix

To apply the constraints of equations (C.8) and (C.10) into a control design problem using parameter optimization, it is often required that gradients of the constraint functions (e.g. σ and ζ) with respect to a system matrix parameter (e.g. element $(a_{ij})_{i,j=1,...,n}$) be supplied to the nonlinear optimization algorithm (in this case, NPSOL [Ref.8]). Determination of gradients using finite-difference approximation can be time-consumming and numerically inaccurate. Whenever possible, it is more efficient and accurate if expressions of constraint gradients can be derived and evaluated analytically.

Recall that constraint on real part of the system eigenvalues is formulated as a constraint on σ (equation (C.9)) where

$$\sigma = \frac{1}{2}\sum_{i=1}^{n}[\max(\sigma_i - \sigma_{\max},0)]^2 \tag{C.16}$$

Gradient of σ with respect to a parameter p in the system matrix is given by

$$\frac{\partial\sigma}{\partial p} = \sum_{i=1}^{n}\max(\sigma_i - \sigma_{\max},0)\frac{\partial\sigma_i}{\partial p} \tag{C.17}$$

Constraint on damping of the system eigenvalues are formulated as a single constraint on ζ (equation (C.11)) where

$$\zeta = \frac{1}{2}\sum_{i=1}^{n}[\max(\sigma_i + \mid\omega_i\mid\cot\alpha,0)]^2 \tag{C.18}$$

Gradient of ζ with respect to a parameter p in the system matrix is given by

$$\frac{\partial\zeta}{\partial p} = \sum_{i=1}^{n}\max(\sigma_i + \mid\omega_i\mid\cot\alpha,0)\left(\frac{\partial\sigma_i}{\partial p} + sgn(\omega_i)\frac{\partial\omega_i}{\partial p}\cot\alpha\right) \tag{C.19}$$

where $sgn(\cdot)$ is the sign function (i.e. $sgn(x) = 1$ if $x > 0$, $sgn(x) = 0$ if $x = 0$, and $sgn(x) = -1$ if $x < 0$).

C.2.1   Sensitivity Function of System Eigenvalues

In this section we derive analytically the sensitivity function of the system eigenvalues $\lambda_i, (i = 1,...,n)$ with respect to a parameter p in the system matrix, i.e. $\frac{\partial\lambda_i}{\partial p}$.

From the definition of system eigenvalues given in equation (C.2) we have

$$Av_i = \lambda_i v_i, (i = 1, ..., n) \tag{C.20}$$

Differentiating both sides of equation (C.20) with respect to a parameter p (where p is an element $(a_{ij})_{i,j=1,...,n}$ of the system matrix A) to yield

$$\frac{\partial A}{\partial p} v_i + A \frac{\partial v_i}{\partial p} = \frac{\partial \lambda_i}{\partial p} v_i + \lambda_i \frac{\partial v_i}{\partial p} \tag{C.21}$$

or

$$(A - \lambda_i I) \frac{\partial v_i}{\partial p} - \frac{\partial \lambda_i}{\partial p} v_i = -\frac{\partial A}{\partial p} v_i \tag{C.22}$$

Let T be a transformation that diagonalizes the system matrix A as

$$T^{-1}AT = \Lambda \tag{C.23}$$

$$= diag(\lambda_i)_{i=1,...,n} \tag{C.24}$$

Multiplying both sides of equation (C.22) by T^{-1} and after some manipulations we have

$$\begin{bmatrix} \lambda_1 & 0 & \cdot & \cdot & \cdot & \cdot & 0 \\ 0 & \cdot & & & & & \cdot \\ \cdot & 0 & \lambda_{i-1} & 0 & & & \cdot \\ \cdot\cdot & & 0 & 0 & 0 & & \cdot \\ \cdot & & & 0 & \lambda_{i+1} & 0 & \cdot \\ \cdot & & & & & \cdot & 0 \\ 0 & \cdot & \cdot & \cdot & \cdot & 0 & \lambda_n \end{bmatrix} T^{-1} \frac{\partial v_i}{\partial p} - T^{-1} v_i \frac{\partial \lambda_i}{\partial p}$$

$$= -T^{-1} \frac{\partial A}{\partial p} v_i \tag{C.25}$$

Clearly, one can solve for the sensitivity $\frac{\partial \lambda_i}{\partial p}$ from the ith row of equation (C.25) as

$$\frac{\partial \lambda_i}{\partial p} = -\frac{\left(T^{-1} \frac{\partial A}{\partial p} v_i\right)_i}{(T^{-1} v_i)_i} \tag{C.26}$$

where the notation $(\cdot)_i$ denotes the ith row of the enclosed quantity. Recall that the ith eigenvalue is $\lambda_i = \sigma_i + j\omega_i$, thus the sensitivities $\frac{\partial \sigma_i}{\partial p}$ and $\frac{\partial \omega_i}{\partial p}$ are simply the real and imaginary parts of $\frac{\partial \lambda_i}{\partial p}$ respectively. Note that the computation of the sensitivity function involves the determination of a transformation T consisting of system eigenvectors $v_i (i = 1, ..., n)$. For the case where some of the eigenvalues are repeated and the system does not have a complete set of eigenvectors corresponding to these eigenvalues, then the sensitivity function associated with these eigenvalues does not exist.

For a feedback controlled system, one is usually interested in obtaining the sensitivity of the closed-loop eigenvalues with respect to the controller design gain parameters. In the next section we will establish the relation between the closed-loop system matrix and the controller state matrices.

C.3 Sensitivity of the Closed-Loop System Matrix with Respect to Controller State Matrices

Consider a plant model with the following state equations

$$\dot{x}_p(t) = A_p x_p(t) + B_p u_p(t) \tag{C.27}$$
$$y_p(t) = C_p x_p(t) + D_p u_p(t) \tag{C.28}$$

where $x_p(t)$ is the plant state vector of dimension n, $u_c(t)$ the control input vector of dimension m and $y_p(t)$ the sensor output vector of dimension p. A linear time-invariant feedback controller for the above plant is of order r (where $r \leq n$) and has the following state-space description,

$$\dot{x}_c(t) = A_c x_c(t) + B_c u_c(t) \tag{C.29}$$
$$y_c(t) = C_c x_c(t) + D_c u_c(t) \tag{C.30}$$

where $x_c(t)$ is a controller state vector of dimension r and (A_c, B_c, C_c, D_c) are the controller state matrices of appropriate dimensions. Note that, in a feedback configuration, the plant sensor output vector $y_p(t)$ is connected to the input vector $u_c(t)$ of the controller, and the outputs $y_c(t)$ of the controller are the inputs $u_p(t)$ of the

plant. For convenience, we define a matrix K that contains in a compact form the quadruple (A_c, B_c, C_c, D_c) as follows,

$$K = \begin{bmatrix} D_c & C_c \\ B_c & A_c \end{bmatrix} \qquad (C.31)$$

In this formulation, when we refer to an element of the matrix K, we actually address one of the elements of the controller state matrices $A_c, B_c, C_c,$ and D_c.

With the feedback control loops closed and assuming that $D_c D_p = 0$, we obtain the following state model for the closed-loop system,

$$\begin{pmatrix} \dot{x}_p(t) \\ \dot{x}_c(t) \end{pmatrix} = \begin{bmatrix} A_p + B_p D_c C_p & B_p C_c \\ B_c(I + D_p D_c)C_p & A_c + B_c D_p C_c \end{bmatrix} \begin{pmatrix} x_p(t) \\ x_c(t) \end{pmatrix} \qquad (C.32)$$

$$= A_{closed} \begin{pmatrix} x_p(t) \\ x_c(t) \end{pmatrix} \qquad (C.33)$$

where A_{closed} is the closed-loop system matrix. Stability of the closed-loop system is determined by the eigenvalues of the matrix A_{closed}. The sensitivity of the matrix A_{closed} with respect to a parameter in the controller state matrix K (equation (C.31)) can be easily computed if we rewrite the matrix A_{closed} as follows,

$$A_{closed} = A_0 + (B_0 + I_0 K D_0) K C_0 \qquad (C.34)$$

where the matrices A_0, B_0, C_0, D_0 and I_0 are *independent* of the controller matrix K and they are given by

$$A_0 = \begin{bmatrix} A_p & 0 \\ 0 & 0 \end{bmatrix}_{(n+r)\times(n+r)} \qquad (C.35)$$

$$B_0 = \begin{bmatrix} B_p & 0 \\ 0 & I \end{bmatrix}_{(n+r)\times(m+r)} \qquad (C.36)$$

$$C_0 = \begin{bmatrix} C_p & 0 \\ 0 & I \end{bmatrix}_{(p+r)\times(n+r)} \qquad (C.37)$$

$$D_0 = \begin{bmatrix} D_p & 0 \\ 0 & 0 \end{bmatrix}_{(p+r)\times(m+r)} \qquad (C.38)$$

$$I_0 = \begin{bmatrix} 0 & 0 \\ 0 & I \end{bmatrix}_{(n+r)\times(m+r)} \tag{C.39}$$

Let p be the ij^{th} element of the controller matrix K (i.e. $p = k_{ij}$) then the sensitivity $\partial A_{closed}/\partial p$ is obtained by differentiating equation (C.34) with respect to p as

$$\frac{\partial A_{closed}}{\partial p} = (B_0 + I_0\Delta_{ij}D_0)\, KC_0 + (B_0 + I_0KD_0)\,\Delta_{ij}C_0 \tag{C.40}$$

where Δ_{ij} is a matrix of dimension $(m+r) \times (p+r)$ with zero entries except for the ij^{th} element where it is equal to unity. Finally sensitivity of the closed-loop eigenvalue with respect to a controller parameter p can be obtained using equation (C.40) and equation (C.26) for the system matrix A_{closed}.

Results presented in this appendix have been implemented in the design algorithm SANDY which combines the two types of nonlinear constraints given in equations (C.8) and (C.10) into a single inequality constraint. Precisely, the eigenvalue constraint is defined as

$$-\infty \le c_\lambda \le \frac{1}{2}\epsilon^2 \tag{C.41}$$

where c_λ is given by $c_\lambda = \frac{1}{2}\sum_{i=1}^{n} d_i^2$ with

$$d_i = \begin{cases} max(\sigma_i + \mid \omega_i \mid cot\alpha, 0) & , x_i \ge 0 \\ max(\sigma_i - \sigma_{\mathbf{max}}) & , x_i < 0 \end{cases} \tag{C.42}$$

and $x_i = \sigma_{max} + \mid \omega_i \mid cot\alpha$. Design specifications on the system eigenvalues are defined in the parameters $\sigma_{max} \ge 0$ and $0 < \alpha \le \pi/2$ where $cos\alpha = \zeta_{min}$.
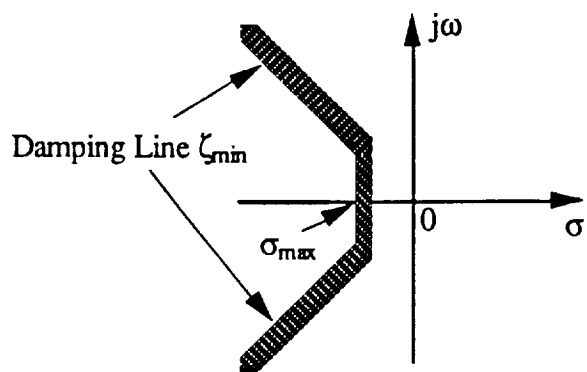
Figure C.1: Constraint Boundaries for System Eigenvalues
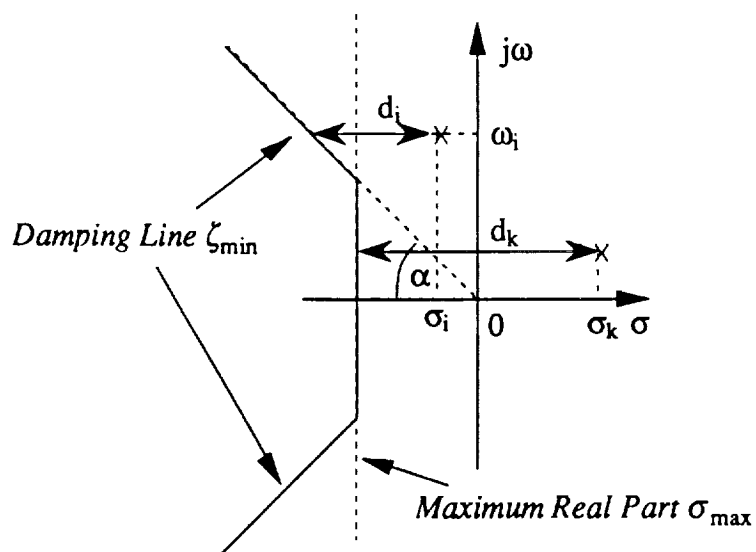
Figure C.2: Definition of Eigenvalue Real-Part and Damping Ratio Constraints
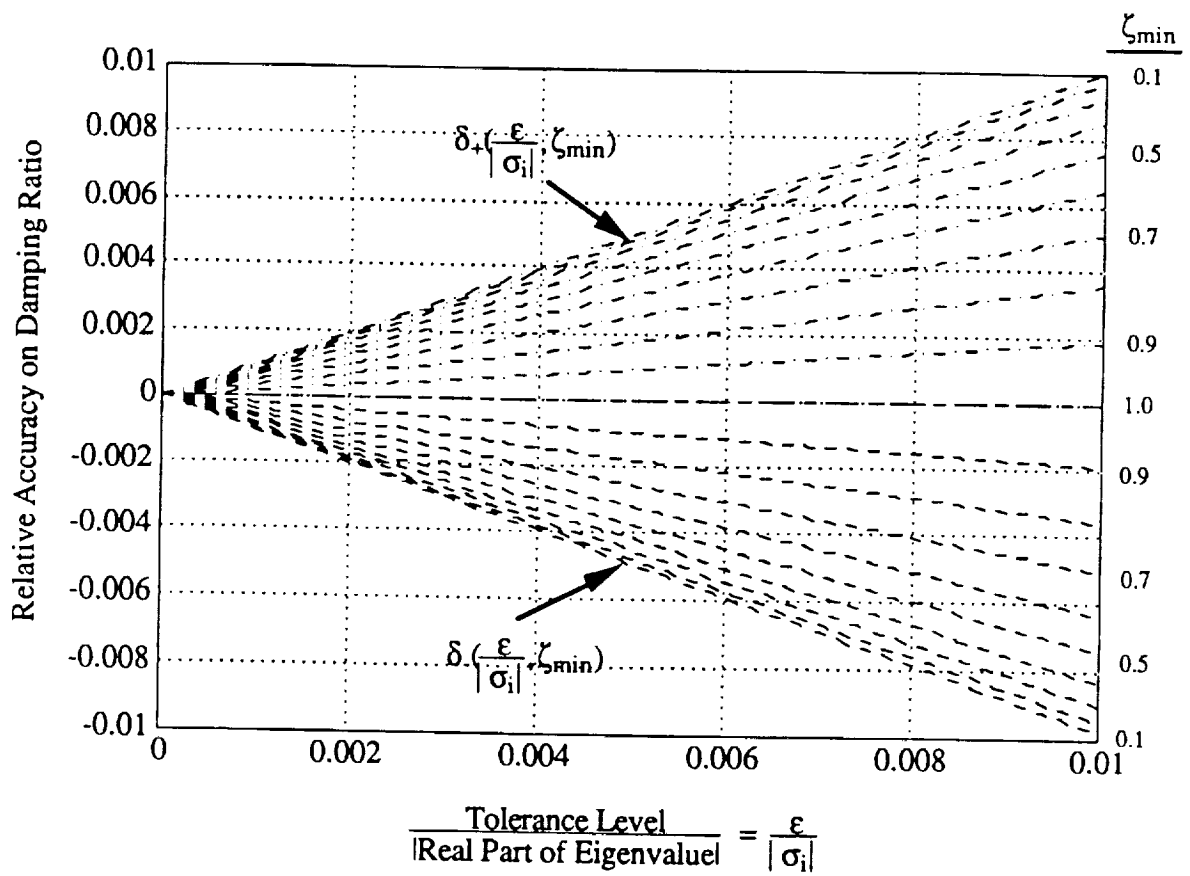
Figure C.3: Achieved Relative Accuracy on Damping Ratio Constraints

Appendix D

MULTIVARIABLE ROBUSTNESS MEASURES

Multivariable stability margins are defined in terms of maximum allowable variations of gain and phase in the feedback loops according to figure D.1 for multiplicative type uncertainties. The complex gain matrix K is given by

$$K = \left(k_{qr} e^{j\theta_{qr}} \right)_{q,r=1,\ldots,m} \tag{D.1}$$

where m is the number of feedback controls. Note that K is not a function of the complex frequency s. The border-line for closed-loop stability is when the return-difference transfer matrix of a nominally stable closed-loop system becomes singular at some frequency $s = j\omega$, i.e.

$$\det \left[I + G(j\omega)K \right] = 0 \tag{D.2}$$

D.1 Robustness Test I

For multiplicative type uncertainties as depicted in figure D.2, instability occurs when the return-difference matrix becomes singular for some value of $s = j\omega$, i.e.

$$\det \left[I + G(j\omega)(I + L(j\omega)) \right] = 0 \tag{D.3}$$

or

$$\det \left[G^{-1}(j\omega) + I + L(j\omega) \right] = 0 \tag{D.4}$$

Closed-loop stability is therefore guaranteed when

$$\bar{\sigma}\left(L(j\omega) \right) \leq \underline{\sigma}\left(I + G^{-1}(j\omega) \right) \tag{D.5}$$

for $\omega \geq 0$. The operators $\bar{\sigma}(\cdot)$ and $\underline{\sigma}(\cdot)$ denote the minimum and maximum singular values respectively. In terms of the complex gain matrix K of equation (D.1), the above bound becomes

$$\bar{\sigma}\left(K - I \right) \leq \underline{\sigma}\left(I + G^{-1}(j\omega) \right) \tag{D.6}$$

If the complex gain matrix is restricted to a diagonal matrix of the form

$$K = diag\left(k_{qq}e^{j\theta_{qq}}\right)_{q=1,\dots,m} \tag{D.7}$$

then the inequality bound reduces to

$$\max_{1\le q\le m} \sqrt{(1 - k_{qq})^2 + 2k_{qq}(1 - \cos\theta_{qq})} \le \min_{\omega}\underline{\sigma}\left(I + G^{-1}(j\omega)\right) \tag{D.8}$$

With this relation, gain and phase margins for type I uncertainties are easily computed from a plot of minimum singular values of the inverse return-difference matrix of the nominal system. Note that this test requires that the nominal loop gain matrix $G(j\omega)$ be nonsingular. If $G(j\omega)$ becomes singular at some frequency ω then this robustness test is not possible.

D.2 Robustness Test II

For multiplicative type uncertainties as depicted in figure D.3, instability occurs when the return-difference matrix becomes singular for some value of $s = j\omega$, i.e.

$$\det\left[I + G(j\omega)L(j\omega)\right] = 0 \tag{D.9}$$

or

$$\det\left[I + G(j\omega) + L^{-1}(j\omega) - I\right] = 0 \tag{D.10}$$

Closed-loop stability is therefore guaranteed when

$$\bar{\sigma}\left(L^{-1}(j\omega) - I\right) \le \underline{\sigma}(I + G(j\omega)) \tag{D.11}$$

for $\omega \ge 0$. In terms of the complex gain matrix K of equation (D.1), the above bound becomes

$$\bar{\sigma}\left(K^{-1} - I\right) \le \underline{\sigma}(I + G(j\omega)) \tag{D.12}$$

If the complex gain matrix is restricted to a diagonal matrix of the form

$$K = diag\left(k_{qq}e^{j\theta_{qq}}\right)_{q=1,\dots,m} \tag{D.13}$$

then the inequality bound reduces to

$$\max_{1\leq q\leq m} \sqrt{(1 - \frac{1}{k_{qq}})^2 + \frac{2}{k_{qq}}(1 - \cos\theta_{qq})} \leq \min_{\omega} \underline{\sigma}(I + G(j\omega)) \tag{D.14}$$

With this relation, the gain and phase margins for type II uncertainties are easily computed from a plot of minimum singular values of the return-difference matrix of the nominal system.

Both equations (D.8) and (D.14) will yield bounds which are applicable to simultanous gain and phase variations in every control loop. Stability margins associated with each test may be combined to produce less conservative bounds. For example, if the smallest $\underline{\sigma}(I + G(j\omega))$ is 0.7 and $\underline{\sigma}(I + G^{-1}(j\omega))$ is 0.6, then in the presence of phase uncertainties of ±30 degrees, the closed-loop system will tolerate simultaneous gain changes of −2.64 dB to 8.49 dB and −5.44 dB to 1.57 dB respectively. Remember that robustness test I requires a nonsingular loop system matrix $G(j\omega)$. If this is not the case, then robustness test I can not be used to improve the estimates of multivariable stability margins.

D.3 Effects of Scaling on Robustness Bounds

Estimates of multivariable stability margins of type I and type II computed from equations (D.8) and (D.14) can be improved by scaling the system matrices $G(j\omega)$, since singular values are not invariant under a similarity transformation. However, the characteristic equation of the nominal closed-loop system is unaffected by scale changes. This follows from the fact that, while $\det(I + RG(j\omega)R^{-1}) = 0$ is equivalent to $\det(I + G(j\omega)) = 0$ for any nonsingular transformation R, their singular value norms $\underline{\sigma}(I + RG(j\omega)R^{-1})$ and $\underline{\sigma}(I + G(j\omega))$ can be much different.

In fact, bounds on gain and phase variations determined from equations (D.8) and (D.14) can be improved by rescaling the loop transfer matrix $G(s)$. If the type of loop uncertainty is restricted to a diagonal complex gain matrix in equation (D.7) and we only consider diagonal scaling matrices $D = diag(d_i)_{i=1,...,m}$, then the left-hand side of equations (D.8) and (D.14) remain unchanged from the scaling of the return-difference and inverse return-difference transfer matrices. Increasing the minimum singular values through diagonal scaling will give less conservative estimates of the multivariable stability margins determined from equations (D.8) and (D.14).

D.4 Osborne's Method for Pre-Conditioning of Matrices

Reference 22 describes a method for pre-conditioning of matrices. The procedure involves the minimization of the euclidean (or Frobenius) norm of a square matrix through diagonal similarity transformations. The method is easily programmed for numerical solutions and is seen to converge quite rapidly. The euclidean norm of the matrix A is defined as

$$\|A\|_e^2 = \sum_{i=1}^{n} \sum_{j=1}^{n} |a_{ij}|^2 \tag{D.15}$$

The minimization problem becomes

$$\min_{D} \|DAD^{-1}\|_e^2 \tag{D.16}$$

over all real diagonal scaling matrices D. For simplicity, we can take each diagonal element d_j of $D = diag(d_1, ..., d_n)$ as a free variable. The product of DAD^{-1} is

$$\left(DAD^{-1}\right)_{ij} = \frac{d_i a_{ij}}{d_j} \tag{D.17}$$

Thus, as the element d_j varies, only the jth column and j^{th} row of the matrix DAD^{-1} are affected, leaving the jth diagonal element of the product unchanged. The square of the euclidean norm $\|DAD^{-1}\|_e^2$ can be rewritten to explicitly show the dependency on the single varying parameter d_j as

$$
\begin{aligned}
\|DAD^{-1}\|_e^2 &= \sum_{i=1}^{n} \sum_{j=1}^{n} \frac{d_i^2 a_{ij}^2}{d_j^2} \tag{D.18} \\
&= d_k^2 \sum_{\substack{j=1 \\ j \neq k}}^{n} \frac{|a_{kj}|^2}{d_j^2} + \frac{1}{d_k^2} \sum_{\substack{i=1 \\ i \neq k}}^{n} d_i^2 |a_{ik}|^2 + \left(\sum_{\substack{i=1 \\ i \neq k}}^{n} \sum_{\substack{j=1 \\ j \neq k}}^{n} \frac{d_i^2 |a_{ij}|^2}{d_j^2} + |a_{kk}|^2 \right) \tag{D.19} \\
&= d_k^2 R + \frac{1}{d_k^2} S + C \tag{D.20}
\end{aligned}
$$

This expression is minimized when

$$d_k^2 = \sqrt{\frac{S}{R}} \tag{D.21}$$

Therefore the euclidean norm of A may be minimized with respect to the element d_k of D in *one* step. Osborne's algorithm consists of stepping through each element d_k from $k = 1, ..., n$, and repeating the process over again until the norm $\|DAD^{-1}\|_e$ can no longer be improved and therefore has converged to the global minimum. It should be noted that the method is guaranteed to work only if the matrix A is in a form that is irreducible by permutation matrices. Otherwise, the algorithm would fail with either quantities S or R being equal to zero.

D.5 Improving the Multiloop Stability Margins through Diagonal Scaling

Our problem for improving the estimates of multivariable stability margins with diagonal scaling is stated as

$$\max_D \underline{\sigma}\left(D(I + G(j\omega))D^{-1}\right) \tag{D.22}$$

Recall that the minimum and maximum singular values are related by

$$\underline{\sigma}(A) = \frac{1}{\bar{\sigma}(A^{-1})} \tag{D.23}$$

so that our problem can be reformulated as

$$\min_D \bar{\sigma}\left(D(I + G(j\omega))^{-1}D^{-1}\right) \tag{D.24}$$

The maximum singular value of a matrix A is related to the euclidean norm of A as

$$\bar{\sigma}(A) \leq \|A\|_e \tag{D.25}$$

Hence, minimizing the euclidean norm of $D(I + G(j\omega))^{-1}D^{-1}$ would lower the upper bound on $\bar{\sigma}\left(D(I + G(j\omega))^{-1}D^{-1}\right)$ in equation (D.24). So if the loop transfer matrix is poorly scaled, Osborne's method provides a way for improving the estimates of the actual multivariable stability margins.
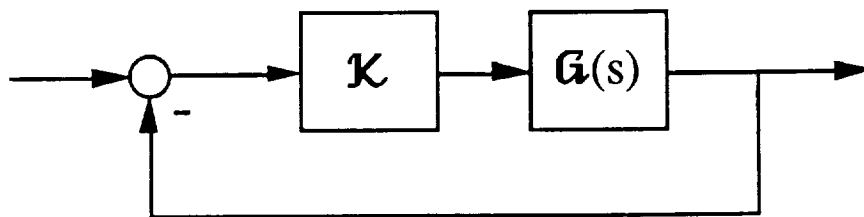
Figure D.1: Feedback System for Evaluation of Multivariable Stability Margins
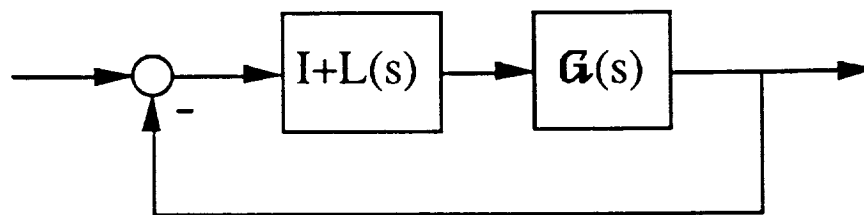
Figure D.2: Type I Multiplicative Perturbation where $L(s) = 0$ (nominal)
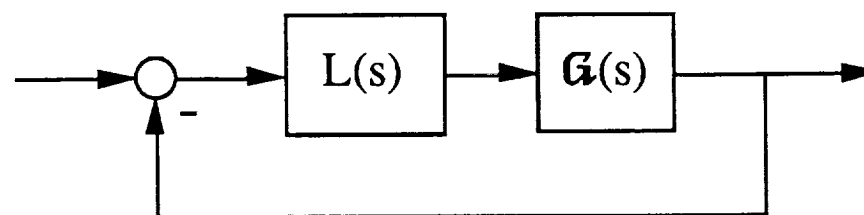
Figure D.3: Type II Multiplicative Perturbation where $L(s) = I$ (nominal)

Appendix E

TSRV B-737 DYNAMIC MODELS

Longitudinal aircraft rigid-body dynamic models are obtained for the NASA Langley Transport Systems Research Vehicle (TSRV). It is a highly modified Boeing 737-100 aircraft for research in advanced guidance, navigation, control and display concepts [Refs.12-14,24]. Linear dynamic models in the wind-axis are given in the form

$$\dot{x}_p(t) = A_p x_p(t) + B_p u_p(t) \tag{E.1}$$

State and control input vectors are

$$x_p^T(t) = \{u(t), \alpha(t), q(t), \theta(t)\} \tag{E.2}$$

and

$$u_p^T(t) = \{\delta_T(t), \delta_e(t)\} \tag{E.3}$$

respectively where

$$
\begin{aligned}
u(t) &= \text{forward velocity component (fps)} \\
\alpha(t) &= \text{angle of attack (rad)} \\
q(t) &= \text{pitch attitude rate (rad/sec)} \\
\theta(t) &= \text{pitch attitude (rad)} \\
\delta_T &= \text{total engine thrust (lbs)} \\
\delta_e &= \text{elevator control position (deg)}
\end{aligned}
$$

Two flight conditions were chosen for this investigation. One is an approach to landing condition and the other is a high-altitude cruise flight condition. Parameters for each flight condition are listed in tables E.1 and E.2 for trimmed flight. The state dynamic matrix A_p and control input matrix B_p for flight condition FLT1 are

$$
A_p = \begin{bmatrix}
-0.4697 \times 10^{-1} & 17.09 & 0 & -32.12 \\
-0.1524 \times 10^{-2} & -0.7136 & 0.9995 & 0.8295 \times 10^{-2} \\
-0.4397 \times 10^{-3} & -1.235 & -0.5020 & -0.3233 \times 10^{-3} \\
0 & 0 & 1.0 & 0
\end{bmatrix} \tag{E.4}
$$

$$B_p = \begin{bmatrix} 0.40177 \times 10^{-3} & 0 \\ -0.89059 \times 10^{-7} & -0.77001 \times 10^{-3} \\ 0.63002 \times 10^{-5} & -0.19737 \times 10^{-1} \\ 0 & 0 \end{bmatrix} \quad \text{(E.5)}$$

For flight condition FLT2, the matrices A_p and B_p are

$$A_p = \begin{bmatrix} -0.7055 \times 10^{-2} & 21.30 & 0 & -32.17 \\ -0.1275 \times 10^{-3} & -1.032 & 0.9976 & 0.8341 \times 10^{-14} \\ 0.3532 \times 10^{-4} & -6.948 & -1.009 & 0 \\ 0 & 0 & 1.0 & 0 \end{bmatrix} \quad \text{(E.6)}$$

$$B_p = \begin{bmatrix} 0.40210 \times 10^{-3} & 0 \\ -0.10185 \times 10^{-7} & -0.10562 \times 10^{-2} \\ 0.62982 \times 10^{-5} & -0.99133 \times 10^{-1} \\ 0 & 0 \end{bmatrix} \quad \text{(E.7)}$$

Control actuation dynamics are modeled as a continuous linear time-invariant system of the form

$$\dot{x}_{act}(t) = A_{act}x_{act}(t) + B_{act}u_{act}(t) \quad \text{(E.8)}$$

$$u_p(t) = C_{act}x_{act}(t) + D_{act}u_{act}(t) \quad \text{(E.9)}$$

where $x_{act}(t)$ contain the actuator model states and $u_{act}(t)$ the actuator command inputs. For both flight conditions, we use the following actuator dynamic model,

$$\begin{pmatrix} \dot{x}_1(t) \\ \dot{x}_2(t) \\ \dot{x}_3(t) \end{pmatrix} = \begin{bmatrix} -2 & 2 & 0 \\ 0 & -10 & 0 \\ 0 & 0 & -16 \end{bmatrix} \begin{pmatrix} x_1(t) \\ x_2(t) \\ x_3(t) \end{pmatrix} + \begin{bmatrix} 0 & 0 \\ 10 & 0 \\ 0 & 16 \end{bmatrix} \begin{pmatrix} \delta_{Tc}(t) \\ \delta_{ec}(t) \end{pmatrix} \quad \text{(E.10)}$$

$$\begin{pmatrix} \delta_T(t) \\ \delta_e(t) \end{pmatrix} = \begin{bmatrix} 1 & 0 & 0 \\ 0 & 0 & 1 \end{bmatrix} \begin{pmatrix} x_1(t) \\ x_2(t) \\ x_3(t) \end{pmatrix} + \begin{bmatrix} 0 & 0 \\ 0 & 0 \end{bmatrix} \begin{pmatrix} \delta_{Tc}(t) \\ \delta_{ec}(t) \end{pmatrix} \quad \text{(E.11)}$$

where

$\delta_{Tc}(t)$ = total thrust command (lbs)

$\delta_{ec}(t)$ = elevator position command (deg)

$\delta_T(t)$ = total thrust output (lbs)

$\delta_e(t)$ = elevator control position (deg)

Table E.1: TSRV B-737 Trim Parameters at Flight Condition FLT1

Parameter	Value
Altitude (ft)	1500
Gross Weight (lbs)	80000
Calibrated Airspeed (kts)	120
Center of Gravity Position	0.2
Flap Position (deg)	40
Flight-Path Angle (deg)	-3
Gear Position	down

Table E.2: TSRV B-737 Trim Parameters at Flight Condition FLT2

Parameter	Value
Altitude (ft)	25000
Gross Weight (lbs)	80000
Calibrated Airspeed (kts)	450
Center of Gravity Position	0.2
Flap Position (deg)	0
Flight-Path Angle (deg)	0
Gear Position	up

Appendix F

COMMAND PROCEDURES FOR DESIGN AND ANALYSIS

Command procedures to set up the design synthesis models and perform robustness analysis for the AFCS controller design are written for the control system analysis and design software $MATLAB$[1]. Command m-files for $MATLAB$ are used to develop the appropriate plant and controller models for use with the computer program $SANDY$ and to perform multivariable robustness analysis. SANDY command files listed here contain the actual design values used in the final optimized AFCS designs.

F.1 *MATLAB Command Files*

F.1.1 *Formulation of the Synthesis and Controller Models*

A $MATLAB$ function command file was used to compute state-space representations of the plant and controller models to be used as input data files to the computer program $SANDY$. A listing of this command file called **msystem** is given below.

```
function msystem(filename,filename1,filename2)
%//
%// system(filename,filename1,filename2)
%// computes the state-space representations of
%// the plant (B-737) and controller (TECS) and closed loop system
%// for optimization to step commands in the constrained parameter
%// optimization program SANDY.
%//
%//  Data Input: A737W  - Windaxis aircraft model (fps,rad,sec)
%//      B737W  - Windaxis aircraft model (fps,rad,sec,lbs,deg)
%// VTB0  - True airspeed (fps)
%// GRAVITY  - Gravitational acceleration (fpss)
%//              ALT      - Altitude (ft)
%//              LU       - Ugust factor at altitude (fps)
```

```
%//              LW        - Wgust factor at altitude (fps)
%//              kgw       - Aircraft gross weight (lbs)
%//              kti       - thrust integral gain
%//              ktp       - thrust proportional gain
%//              kei       - elevator integral gain
%//              kep       - elevator proportional gain
%//  kv  - Outer loop gain
%//  kh  - Outer loop altitude error gain
%//  Output Systems:
%//
%//      ***** Formulate the Plant State-Space Matrices *****
%//  System model  :  xpdot  = Ap*xp + Bp*u + Gp*w
%//                    yp     = Cp*xp + Dp*u + Omegap*w
%//where xp = [V(fps),Alpha(deg),Q(deg),Theta(deg),Xdth1(lbs),Xdth2,Xde3(deg),
%//            Xgustv(fps),Xgustw1(fps),Xgustw2,H(ft)]
%//       u  = [Dthc(lb),Dec(deg),Vc*(fps)]
%//       w  = [Etav(fps),Etaw(fps),Gammac(deg),Vdotc(ft/sec^2),Vc(fps),Hc(ft)]
%//       y  = [Gamma(rad),Vdot(g),Q(rad/sec),Theta(rad),(V-Vc)(fps),
%//            (Gamma-Gammac)(deg),(H-Hc)(ft),Gammac(deg),Vdotc(ft/sec^2),
%//            V(fps),Alpha(deg),Xdth1(lbs),Xde(deg),Xgustv(fps),
%//            Xgustw1(fps),H(ft),Nz(g)]
%//where: x  = [xIE,xIL,xVc]
%//       uc = [Gamma(rad),Vdot(g),Q(rad),Theta(rad),(V-Vc)(fps),
%//            (H-Hc)(ft), Gammac(deg),Vdotc(ft/sec^2)]
%//       yc = [Dthc(lbs/lbs),Dec(rad),Vc*(fps)]
%Create the Plant Model and Controller Design Gains
eval(['load ', filename]);
%Conversion Constants
r2d=180/pi; %  //Radians to degrees
d2r=pi/180; %  //Degrees to radians
%Dryden Turbulence Filters
alphau=vtb0/lu1;
numv=[sqrt(2*alphau)];% //numerator   coefs. for u-gust filter
denv=[1 alphau];      %  //denominator coefs. for u-gust filter
alphaw=vtb0/lw;
numw=sqrt(3*alphaw)*[1  alphaw/sqrt(3)];% //num. coefs. for w-gust filter
denw=[1  2*.95*alphaw alphaw^2];       % //den. coefs. for w-gust filter
w2alpha=r2d/vtb0;      % //conversion factor from w-gust to alpha-gust(deg)
[av,bv,cv,dv]=tf2ss(numv,denv);
[aw,bw,cw,dw]=tf2ss(numw,denw);
[agust,bgust,cgust,dgust]=append(av,bv,cv,dv,aw,bw,cw,dw);
% //State-Space Realization of u,w-gust Filters
%Gain Schedules
```

```
kgw=wg; %// Gross weight
kcas    = (200/vtb0)^2;%    //elevator gain schedule
%Actuator Dynamic Models
aact    = [-2       2      0; % //actuator state model
            0      -10     0; % //   x = [Xdth1,Xdth2,Xde1]
            0       0    -16];% //   u = [Dthc(lbs/lbs),Dec(rad)]
bact    = [ 0             0;         % //   y = [Dth(lbs),De(deg)]
          10*kgw         0;
            0     16*kcas*r2d];
cact    = [1    0    0;
           0    0    1];
dact    = 0*eye(2);
%Airplane Longitudinal Dynamics
a737    = a737w;
a737([2 3 4],:) = a737([2 3 4],:)*r2d;
a737(:,[2 3 4]) = a737(:,[2 3 4])*d2r;% //Convert A737w to fps and deg.
b737    = b737w;
b737([2 3 4],:) = b737([2 3 4],:)*r2d;% //Convert B737w to fps and deg.
ap      = [a737            b737*cact      a737(:,[1 2])*[1,0;0,w2alpha]*cgust;
           zeros(3,4)      aact           zeros(3,3);
           zeros(3,4)      zeros(3,3)     agust];
% Addition of the Altitude State
aplant = [ap zeros(10,1);
          0 -vtb0*d2r 0 vtb0*d2r 0 0 0 0 0 0 0];
bp      = [zeros(4,3);
           [bact,zeros(3,1)];
           zeros(4,3)];
gp      = [a737(:,[1,2])*dgust;
           zeros(3,2);
           bgust
           0 0];
bplant = [bp gp zeros(11,4)];
%//      y  = [Gamma(rad),Vdot(g),Q(rad/sec),Theta(rad),(V-Vc)(fps),
%//            (Gamma-Gammac)(deg),(H-Hc)(ft),Gammac(deg),Vdotc(ft/sec^2),
%//            V(fps),Alpha(deg),Xdth1(lbs),Xde(deg),Xgustv(fps),
%//            Xgustw1(fps),H(ft),Nz(g)]
cplant = [0 -d2r 0 d2r 0 0 0 0 0 0
          aplant(1,:)/gravity
          0 0 d2r 0 0 0 0 0 0 0 0
          0 0 0 d2r 0 0 0 0 0 0 0
          1 0 0 0 0 0 0 0 0 0 0
          0 -1 0 1 0 0 0 0 0 0 0
          0 0 0 0 0 0 0 0 0 0 1
```

```
              0 0 0 0 0 0 0 0 0 0 0
               0 0 0 0 0 0 0 0 0 0 0
              1 0 0 0 0 0 0 0 0 0 0
               0 1 0 0 0 0 0 0 0 0 0
              0 0 0 0 1 0 0 0 0 0 0
              0 0 0 0 0 0 1 0 0 0 0
              [zeros(2,7),cgust,zeros(2,1)]
              0 0 0 0 0 0 0 0 0 1
              vtb0/gravity*d2r*(aplant(4,:)-aplant(2,:)) ];
dplant = [zeros(17,9)];
dplant(5,3) = -1;dplant(5,8) = -1;
dplant(6,6)=-1;
dplant(7,9) = -1;
dplant(8,6) = 1;
dplant(9,7) = 1;
dplant(17,:) = vtb0/gravity*(bplant(4,:)-bplant(2,:));
%Save the Plant Synthesis Model into filename1
eval(['save ',filename1,' aplant bplant cplant dplant']);
%//
%//        ***** Formulate the Controller State-Space Matrices *****
%//   Initial
%//   System model  :  xcdot = Ac*xc + Bc*uc
%//                    yc    = Cc*xc + Dc*uc
%//where: x  = [xIE,xIL,xVc]
%//        uc = [Gamma(rad),Vdot(g),Q(rad),Theta(rad),(V-Vc)(fps),
%//             (H-Hc)(ft), Gammac(deg),Vdotc(ft/sec^2)]
%//        yc = [Dthc(lbs/lbs),Dec(rad),Vc*(fps)]
%//
acont = [zeros(3,3)];
bcont = [-1 -1 0 0 kv  kh  d2r  1/gravity
          1 -1 0 0 kv -kh -d2r  1/gravity
          0  0 0 0 0   0   0    1        ];
ccont = [kti 0   0
          0  kei 0
          0  0   k1 ];
dcont = [-ktp -ktp 0  0     0 0 0  0
          kep -kep kq ktheta 0 0 0  0
          0    0   0  0      0 0 k2 0 ];
%Save the Controller State model in filename2
eval(['save ',filename2,' acont bcont ccont dcont']);
```

F.1.2 Multivariable Robustness Analysis

Multivariable robustness measures described in Appendix C.3 involve computation of the minimum singular values of the return difference and inverse return difference transfer function matrices at different frequencies. *MATLAB* function files were devised for computing the minimum singular values of these transfer function matrices from the state-space representation of the broken-loop systems. Osborne's method [Ref.22] is used to improve the minimum singular values through diagonal scaling of the loop gain transfer function matrices. The *MATLAB* command files svdrtd and svdirtd are user-defined functions for computing the minimum singular values of the return-difference and inverse-return-difference transfer function matrices respectively. Their listings are shown below.

```
function [OMEGA,SIGMA]=svdrtd(A,B,C,D)
clg;
J=sqrt(-1);
[NIO,NIO]=size(D);
[NS,NS]=size(A);
DEL=0.00001;
NPTS=100;
OMEGA =logspace(-2,2,NPTS);
R = eye(NIO);
RoldIM1=eye(NIO);
for I=1:NPTS;
M = eye(NIO) + (C*inv(J*OMEGA(I)*eye(NS)-A)*B+D);
MI = inv(M);
RoldI = eye(NIO);
rk = 2;
k = 1;
while abs(rk-1) > DEL;
    rsum = 0.0;
    for l=1:NIO;rsum=rsum+abs(MI(k,l))^2.0;end;
    rsum = rsum - abs(MI(k,k))^2.0;
    csum = 0.0;
    for l=1:NIO;csum=csum+abs(MI(l,k))^2.0;end;
    csum = csum - abs(MI(k,k))^2.0;
    if rsum ~= 0.0;
        if csum ~= 0.0;
            rk = (csum/rsum)^0.25;
            R = eye(NIO);
            R(k,k) = rk;
```

```
        RoldI = RoldI*R;
      end;
   elseif rsum == 0.0;
      rk = 1.0;
      R = RoldIM1;
      RoldI = R;
   elseif csum == 0.0;
      rk = 1.0;
      R = RoldIM1;
      RoldI = R;
   end;
   M = R*M*inv(R);
   MI = inv(M);
   k=k+1;
   if k > NIO; k = 1;end;
end;
SIGMA(I)=min(svd(M));
RoldIM1=RoldI;
end
axis([-2,2,0,2]);
semilogx(OMEGA,SIGMA);
xlabel('Frequency (Rad/Sec)');
ylabel('Sigma');
grid;
title('Minimum Singular Value of the Return-Difference Matrix');
rmin=min(SIGMA)
%Multivariable stability margins
MIMOGM=[-20*log10(1+rmin),-20*log10(1-rmin)]
MIMOPM=[-acos(1-rmin^2/2)*180/pi,acos(1-rmin^2/2)*180/pi]

function [OMEGA,SIGMA]=svdirtd(A,B,C,D)
clg;
J=sqrt(-1);
[NIO,NIO]=size(D);
[NS,NS]=size(A);
DEL=0.00001;
NPTS=100;
OMEGA =logspace(-2,2,NPTS);
R = eye(NIO);
RoldIM1=eye(NIO);
for I=1:NPTS;
M = eye(NIO)- inv(C*inv(J*OMEGA(I)*eye(NS)-A)*B+D);
MI = inv(M);
RoldI = eye(NIO);
```

```
rk = 2;
k = 1;
while abs(rk-1) > DEL;
    rsum = 0.0;
    for l=1:NIO;rsum=rsum+abs(MI(k,l))^2.0;end;
    rsum = rsum - abs(MI(k,k))^2.0;
    csum = 0.0;
    for l=1:NIO;csum=csum+abs(MI(l,k))^2.0;end;
    csum = csum - abs(MI(k,k))^2.0;
    if rsum ~= 0.0;
        if csum ~= 0.0;
            rk = (csum/rsum)^0.25;
            R = eye(NIO);
            R(k,k) = rk;
            RoldI = RoldI*R;
        end;
    elseif rsum == 0.0;
        rk = 1.0;
        R = RoldIM1;
        RoldI = R;
    elseif csum == 0.0;
        rk = 1.0;
        R = RoldIM1;
        RoldI = R;
    end;
    M = R*M*inv(R);
    MI = inv(M);
    k=k+1;
    if k > NIO; k = 1;end;
end;
SIGMA(I)=min(svd(M));
RoldIM1=RoldI;
end
axis([-2,2,0,2]);
semilogx(OMEGA,SIGMA);
xlabel('Frequency (Rad/Sec)');
ylabel('Sigma');
grid;
title('Minimum Singular Value of the Inverse-Return-Difference Matrix');
rmin=min(SIGMA)
%Multivariable stability margins
MIMOGM=[20*log10(1-rmin),20*log10(1+rmin)]
MIMOPM=[-acos(1-rmin^2/2)*180/pi,acos(1-rmin^2/2)*180/pi]
```

F.2 SANDY Design Data Files

Data files for use with the computer program *SANDY* contain design information such as weighting matrices in the performance indices, linear constraints and nonlinear constraints. The *SANDY* data file for the optimized TECS inner-loop design in chapter 5 at flight condition FLT1 is shown in Appendix G, while the one for flight condition FLT2 is shown in Appendix H.

DESIGN DATA FILE FOR TECS INNER-LOOP AT FLIGHT CONDITION FLT1

'Nfcmax'	1	1		
		2000		
'Tf'	1	1		
		100		
'Tfctor'	1	1		
		2		
'Npm'	1	1		
		4		
'Wp'	4	1		
		1	1	1
		1		
'F'	40	10		

-0.04697	0.298276769165831	-4.00727596257898e-13
-0.560599755740579	0.00040177	0
8.5931e-14	-0.0234645506584104	0.0531038896468495
0.00423385423749794	-0.0873187679779375	-0.7136
0.9995	0.008295	-5.1027048276556e-06
0	-0.0441183231828685	-0.0436213679933638
-0.127046218711467	-0.0101291105986159	-0.0251929542519023
-1.235	-0.502	-0.0003233
0.000360974870088321	0	-1.13084680024971
-0.0125855088626523	-0.219873991183662	-0.0175300610836472
0	0	1
0	0	0
0	0	0
0	0	0
0	0	-2
2	0	0
0	0	0
0	0	0
0	-10	0
0	0	0
0	0	0
0	0	0

-16	0	0
0	0	0
0	0	0
0	0	-0.124782409638554
0	0	0
0	0	0
0	0	0
0	-0.262375813333333	-0.0190695477624178
0	0	0
0	0	0
0	0	1
0	-0.04697	0.298276769165831
-4.00727596257898e-13	-0.560599755740579	0.00040177
0	8.5931e-14	-0.0234645506584104
0.0531038896468495	0.00423385423749794	-0.0873187679779375
-0.7136	0.9995	0.008295
-5.1027048276556e-06	0	-0.0441183231828685
-0.0436213679933638	-0.127046218711467	-0.0101291105986159
-0.0251929542519023	-1.235	-0.502
-0.0003233	0.000360974870088321	0
-1.13084680024971	-0.0125855088626523	-0.219873991183662
-0.0175300610836472	0	0
1	0	0
0	0	0
0	0	0
0	0	0
-2	2	0
0	0	0
0	0	0
0	0	-10
0	0	0
0	0	0
0	0	0
0	-16	0
0	0	0
0	0	0
0	0	0
-0.124782409638554	0	0
0	0	0
0	0	0
0	0	-0.262375813333333
-0.0190695477624178	0	0
0	0	0

0	0	0
1	0	-0.04697
0.298276769165831	-4.00727596257898e-13	-0.560599755740579
0.00040177	0	8.5931e-14
-0.0234645506584104	0.0531038896468495	0.00423385423749794
-0.0873187679779375	-0.7136	0.9995
0.008295	-5.1027048276556e-06	0
-0.0441183231828685	-0.0436213679933638	-0.127046218711467
-0.0101291105986159	-0.0251929542519023	-1.235
-0.502	-0.0003233	0.000360974870088321
0	-1.13084680024971	-0.0125855088626523
-0.219873991183662	-0.0175300610836472	0
0	1	0
0	0	0
0	0	0
0	0	0
0	-2	2
0	0	0
0	0	0
0	0	0
-10	0	0
0	0	0
0	0	0
0	0	-16
0	0	0
0	0	0
0	0	0
0	-0.124782409638554	0
0	0	0
0	0	0
0	0	0
-0.262375813333333	-0.0190695477624178	0
0	0	0
0	0	0
0	1	0
-0.04697	0.298276769165831	-4.00727596257898e-13
-0.560599755740579	0.00040177	0
8.5931e-14	-0.0234645506584104	0.0531038896468495
0.00423385423749794	-0.0873187679779375	-0.7136
0.9995	0.008295	-5.1027048276556e-06
0	-0.0441183231828685	-0.0436213679933638
-0.127046218711467	-0.0101291105986159	-0.0251929542519023
-1.235	-0.502	-0.0003233

```
   0.000360974870088321                   0      -1.13084680024971
  -0.0125855088626523   -0.219873991183662   -0.0175300610836472
                    0                    0                     1
                    0                    0                     0
                    0                    0                     0
                    0                    0                    -2
                    2                    0                     0
                    0                    0                     0
                    0                    0                     0
                    0                  -10                     0
                    0                    0                     0
                    0                    0                     0
                    0                    0                     0
                  -16                    0                     0
                    0                    0                     0
                    0                    0                     0
                    0                    0      -0.124782409638554
                    0                    0                     0
                    0                    0                     0
                    0                    0                     0
                    0   -0.262375813333333   -0.0190695477624178
                    0                    0                     0
                    0                    0                     0
                    0                    0                     1
                    0

 'G'          40    3
                    0                    0                     0
                    0                    0                     0
                    0                    0                     0
                    0                    0                     0
                    0                    0                     0
               800000                    0                     0
                    0    854.633071305922                     0
                    0                    0                     0
                    0                    0                     0
                    0                    0                     0
                    0                    0                     0
                    0                    0                     0
                    0                    0                     0
                    0                    0                     0
                    0                    0                     0
               800000                    0                     0
```

0	854.633071305922	0
0	0	0
0	0	0
0	0	0
0	0	0
0	0	0
0	0	0
0	0	0
0	0	0
800000	0	0
0	854.633071305922	0
0	0	0
0	0	0
0	0	0
0	0	0
0	0	0
0	0	0
0	0	0
0	0	0
800000	0	0
0	854.633071305922	0
0	0	0
0	0	0
0	0	0

'Gam'   40   6

0	0	0
0	0	0
0	0	0
0	0	0
0	0	0
0	0	0
0	0	0
0	0	0
0	0	0
0	0	0
800000	0	0
0	0	0
0	854.633071305922	0
0	0	0
0	0	1
0	0	0
0	0	0
1	0	0

0	0	0
0	0	0
0	0	0
0	0	0
0	0	0
0	0	0
0	0	0
0	0	0
0	0	0
0	0	0
0	0	0
0	0	0
800000	0	0
0	0	0
0	854.633071305922	0
0	0	0
0	0	1
0	0	0
0	0	0
1	0	0
0	0	0
0	0	0
0	0	0
0	0	0
0	0	0
0	0	0
0	0	0
0	0	0
0	0	0
0	0	0
0	0	0
0	0	0
800000	0	0
0	0	0
0	854.633071305922	0
0	0	0
0	0	1
0	0	0
0	0	0
1	0	0
0	0	0
0	0	0
0	0	0

0	0	0
0	0	0
0	0	0
0	0	0
0	0	0
0	0	0
0	0	0
0	0	0
0	0	0
800000	0	0
0	0	0
0	854.633071305922	0
0	0	0
0	0	1
0	0	0
0	0	0
1	0	0
0	0	0
0	0	0

'Hs'   32   10

0	-0.0174532925199433	0
0.0174532925199433	0	0
0	0	0
0	-0.00145960223741454	0.00926901085039872
-1.24526909962057e-14	-0.0174207506445177	1.24850839030454e-05
0	2.67032318210068e-15	-0.000729165651286837
0.00165021409716748	0.00013156787562144	0
0	0.0174532925199433	0
0	0	0
0	0	0
0.0174532925199433	0	0
0	0	0
0	1	0
0	0	0
0	0	0
0	0	0
0	0	0
0	0	0
0	0	0
0	0	0
0	0	0

0	0	0
0	0	0
0	0	0
0	0	0
-0.0174532925199433	0	0.0174532925199433
0	0	0
0	0	0
-0.00145960223741454	0.00926901085039872	-1.24526909962057e-14
-0.0174207506445177	1.24850839030454e-05	0
2.67032318210068e-15	-0.000729165651286837	0.00165021409716748
0.00013156787562144	0	0
0.0174532925199433	0	0
0	0	0
0	0	0
0	0	0.0174532925199433
0	0	0
0	0	0
1	0	0
0	0	0
0	0	0
0	0	0
0	0	0
0	0	0
0	0	0
0	0	0
0	0	0
0	0	0
0	0	0
0	0	-0.0174532925199433
0	0.0174532925199433	0
0	0	0
0	0	-0.00145960223741454
0.00926901085039872	-1.24526909962057e-14	-0.0174207506445177
1.24850839030454e-05	0	2.67032318210068e-15
-0.000729165651286837	0.00165021409716748	0.00013156787562144
0	0	0.0174532925199433
0	0	0
0	0	0
0	0	0
0	0.0174532925199433	0
0	0	0

0	0	1
0	0	0
0	0	0
0	0	0
0	0	0
0	0	0
0	0	0
0	0	0
0	0	0
0	0	0
0	0	0
0	0	0
0	0	0
0	0	0
0	-0.0174532925199433	0
0.0174532925199433	0	0
0	0	0
0	-0.00145960223741454	0.00926901085039872
-1.24526909962057e-14	-0.0174207506445177	1.24850839030454e-05
0	2.67032318210068e-15	-0.000729165651286837
0.00165021409716748	0.00013156787562144	0
0	0.0174532925199433	0
0	0	0
0	0	0
0	0	0
0.0174532925199433	0	0
0	0	0
0	1	0
0	0	0
0	0	0
0	0	0
0	0	0
0	0	0
0	0	0
0	0	0
0	0	0
0	0	0
0	0	0
0	0	0
0	0	0
0	0	

'Dsu'   32   3

0	0	0

0	0	0
0	0	0
0	0	0
0	0	-1
0	0	0
0	0	0
0	0	0
0	0	0
0	0	0
0	0	0
0	0	0
0	0	-1
0	0	0
0	0	0
0	0	0
0	0	0
0	0	0
0	0	0
0	0	0
0	0	0
0	0	-1
0	0	0
0	0	0
0	0	0
0	0	0
0	0	0
0	0	0
0	0	0
0	0	0
0	0	-1
0	0	0
0	0	0
0	0	0

'Dsw'   32   6

0	0	0
0	0	0
0	0	0
0	0	0
0	0	0
0	0	0
0	0	0
0	0	0
0	0	0
0	0	0
0	0	0

0	0	0
0	0	0
0	1	0
0	0	0
0	0	1
0	0	0
0	0	0
0	0	0
0	0	0
0	0	0
0	0	0
0	0	0
0	0	0
0	0	0
0	0	0
0	1	0
0	0	0
0	0	1
0	0	0
0	0	0
0	0	0
0	0	0
0	0	0
0	0	0
0	0	0
0	0	0
0	0	0
0	0	0
0	0	0
0	1	0
0	0	0
0	0	1
0	0	0
0	0	0
0	0	0
0	0	0
0	0	0

0	0	0
0	0	0
0	0	0
0	0	0
0	0	0
0	0	0
0	0	0
0	1	0
0	0	0
0	0	1

'Hc'   8   10

1	0	0
0	0	0
0	0	0
0	0	-1
0	1	0
0	0	0
0	0	1
0	0	0
0	0	0
0	0	0
0	-1	0
1	0	0
0	0	0
0	1	0
0	0	0
0	0	0
0	0	0
-1	0	1
0	0	0
0	0	0
1	0	0
0	0	0
0	0	0
0	0	-1
0	1	0
0	0	0
0	0	

'Dcu'   8   3

0	0	-1
0	0	0
0	0	-1
0	0	0

			0	0	-1
			0	0	0
			0	0	-1
			0	0	0
'Dcw'	8	6			
			0	0	0
			0	0	0
			0	0	0
			0	-1	0
			0	0	0
			0	0	0
			0	0	0
			0	-1	0
			0	0	0
			0	0	0
			0	0	0
			0	-1	0
			0	0	0
			0	0	0
			0	0	0
			0	-1	0
'Wspec'	24	6			
			0	0	0
			0	0	1
			0	0	0
			0	0	1
			0	0	0
			0	0	1
			0	0	0
			0	0	1
			0	0	1.2
			1	1.2	0
			0	0	1.2
			0	1	1.2
			0	1	0
			0	1	0.2
			0	0	0
			0	0	1
			0	0	0
			0	0	1
			0	0	0
			0	0	1
			0	0	0

```
                    0                   0                   1
                    0                   0                   0
                    0                   0                   1
                    0                   0                   0
                    0                   0                   1
                    0                0.16                   0
                    0                   1                   2
                    0                   0                   0
                    0                   0                   1
                    0                   0                   0
                    0                   0                   1
                    0                   0                   0
                    0                   0                   1
                    0                   0                   0
                    0                   0                   1
                    0                   0                   0
                    0                   0                   1
                    0                   0                   0
                    0                   0                   1
                    0                   0                 6.6
                    0                   0                   1
                    0                   0                 6.3
                    0                   0                   1
                    0                   0                   0
                    0                   0                   1
                    0                   0                   0
                    0                   0                   1
'Alpha'       4   1
                    0                   0                   0
                    0
'Sigmamax'    4   1
                    0                   0                   0
                    0
'Zetamin'     4   1
                  0.7     0                                 0
                  0
'Q'           8   2
                    1                   0                   0
                    2                   0                   0
                    0                   0                   0
                    0                   0                   0
                    0                   0                   0
                    0
```

```
'R'              12    3
                        0                      0                      0
                        0                      0                      0
                        0                      0                      0
                       10                      0                      0
                        0                      0                      0
                        0                      0                      0
                        0                      0                      0
                        0                      3                      0
                        0                      0                      0
                        0                      0                      0
                        0                      0                      0
                        0                      0                      0
'nDircu'          4    1
                        0                      0                      0
                        2
'Dircu'           2    3
                        1                      0               0.000756
                        2                      0                6.735e-4
'nDircy'          4    1
                        0                      0                      0
                        1
'Dircy'           1    3
  1   0    5.1223e-1
'A'               3    3
     0.000000000000000D+00   0.000000000000000D+00   0.000000000000000D+00
     0.000000000000000D+00   0.000000000000000D+00   0.000000000000000D+00
     0.000000000000000D+00   0.000000000000000D+00   0.000000000000000D+00
'B'               3    8
    -1.000000000000000D+00  -1.000000000000000D+00   0.000000000000000D+00
     0.000000000000000D+00   0.000000000000000D+00   0.000000000000000D+00
     1.745329251994330D-02   3.107520198881290D-02
     1.000000000000000D+00  -1.000000000000000D+00   0.000000000000000D+00
     0.000000000000000D+00   0.000000000000000D+00  -0.000000000000000D+00
    -1.745329251994330D-02   3.107520198881290D-02
     0.000000000000000D+00   0.000000000000000D+00   0.000000000000000D+00
     0.000000000000000D+00   0.000000000000000D+00   0.000000000000000D+00
     0.000000000000000D+00   1.000000000000000D+00
'C'               3    3
     3.498961631412376D-01   0.000000000000000D+00   0.000000000000000D+00
     0.000000000000000D+00   2.403685052903295D+00   0.000000000000000D+00
     0.000000000000000D+00   0.000000000000000D+00   9.194135380113152D-01
'D'               3    8
```

```
       -9.694232982519398D-02   -9.694232982519398D-02    0.000000000000000D+00
        0.000000000000000D+00    0.000000000000000D+00    0.000000000000000D+00
        0.000000000000000D+00    0.000000000000000D+00
        3.375954098020312D+00   -3.375954098020312D+00    3.007108016451161D+00
        3.124000504141355D+00    0.000000000000000D+00    0.000000000000000D+00
        0.000000000000000D+00    0.000000000000000D+00
        0.000000000000000D+00    0.000000000000000D+00    0.000000000000000D+00
        0.000000000000000D+00    0.000000000000000D+00    0.000000000000000D+00
       -1.633243449039959D-01    0.000000000000000D+00
'nAid'          1   1
                    0
'Aid'           0   0
'nBid'          1   1
                    0
'Bid'           0   0
'nCid'          1   1
                    3
'Cid'           3   5
                    1              1              1
                   -5              5              2
                    2              1             -5
                    5              3              3
                    1              0.85           1
'nDid'          1   1
                    7
'Did'           7   5
                    1              1              1
                   -5              5              1
                    2              1             -5
                    5              2              1
                    1             -5              5
                    2              2              1
                   -5              5              2
                    3              1            -10
                   10              2              4
                    1            -10             10
3 7             1
-1 1
'Nclin'         1   1
                    2
'nLincoef'      2   1
                    2              2
'Lincoef'       4   4
```

```
                         1              100                1
                         1               -1              100
                         1                2                1
                       100                2                1
                         1              100                2
                         2
'Linbnds'     2    2
                         0                0                0
                         0
'Nudnlc'      1    1
                         0
```

Appendix H

DESIGN DATA FILE FOR TECS INNER-LOOP AT FLIGHT CONDITION FLT2

'Nfcmax'	1	1
		1000
'Tf'	1	1
		100
'Tfctor'	1	1
		2
'Npm'	1	1
		4
'Wp'	4	1

1	1	1
1		

'F' 40 10

-0.007055	0.371755130674792	-5.74387856831334e-13
-0.561472420366576	0.0004021	0
1.8924e-13	-0.00655643326711755	0.0320809006871565
0.00799829068925111	-0.007305211887918	-1.032
0.9976	8.341e-15	-5.83557514340744e-07
0	-0.0605158023217175	-0.00678896303972901
-0.0890572497252435	-0.0222034218500884	0.00202368693240207
-6.948	-1.009	0
0.000360860278529295	0	-5.67990251047039
0.00188067587892728	-0.599583111522279	-0.149485828502339
0	0	1
0	0	0
0	0	0
0	0	0
0	0	-2
2	0	0
0	0	0
0	0	0
0	-10	0
0	0	0
0	0	0
0	0	0

-16	0	0
0	0	0
0	0	0
0	0	-0.431828457142857
0	0	0
0	0	0
0	0	0
0	-0.820474068571428	-0.18647581639838
0	0	0
0	0	0
0	0	1
0	-0.007055	0.371755130674792
-5.74387856831334e-13	-0.561472420366576	0.0004021
0	1.8924e-13	-0.00655643326711755
0.0320809006871565	0.00799829068925111	-0.007305211887918
-1.032	0.9976	8.341e-15
-5.83557514340744e-07	0	-0.0605158023217175
-0.00678896303972901	-0.0890572497252435	-0.0222034218500884
0.00202368693240207	-6.948	-1.009
0	0.000360860278529295	0
-5.67990251047039	0.00188067587892728	-0.599583111522279
-0.149485828502339	0	0
1	0	0
0	0	0
0	0	0
-2	2	0
0	0	0
0	0	0
0	0	-10
0	0	0
0	0	0
0	0	0
0	-16	0
0	0	0
0	0	0
0	0	0
-0.431828457142857	0	0
0	0	0
0	0	0
0	0	-0.820474068571428
-0.18647581639838	0	0
0	0	0

0	0	0
1	0	-0.007055
0.371755130674792	-5.74387856831334e-13	-0.561472420366576
0.0004021	0	1.8924e-13
-0.00655643326711755	0.0320809006871565	0.00799829068925111
-0.007305211887918	-1.032	0.9976
8.341e-15	-5.83557514340744e-07	0
-0.0605158023217175	-0.00678896303972901	-0.0890572497252435
-0.0222034218500884	0.00202368693240207	-6.948
-1.009	0	0.000360860278529295
0	-5.67990251047039	0.00188067587892728
-0.599583111522279	-0.149485828502339	0
0	1	0
0	0	0
0	0	0
0	0	0
0	-2	2
0	0	0
0	0	0
0	0	0
-10	0	0
0	0	0
0	0	0
0	0	-16
0	0	0
0	0	0
0	0	0
0	-0.431828457142857	0
0	0	0
0	0	0
0	0	0
-0.820474068571428	-0.18647581639838	0
0	0	0
0	0	0
0	1	0
-0.007055	0.371755130674792	-5.74387856831334e-13
-0.561472420366576	0.0004021	0
1.8924e-13	-0.00655643326711755	0.0320809006871565
0.00799829068925111	-0.007305211887918	-1.032
0.9976	8.341e-15	-5.83557514340744e-07
0	-0.0605158023217175	-0.00678896303972901
-0.0890572497252435	-0.0222034218500884	0.00202368693240207
-6.948	-1.009	0

0.000360860278529295	0	-5.67990251047039
0.00188067587892728	-0.599583111522279	-0.149485828502339
0	0	1
0	0	0
0	0	0
0	0	-2
2	0	0
0	0	0
0	0	0
0	-10	0
0	0	0
0	0	0
0	0	0
-16	0	0
0	0	0
0	0	0
0	0	-0.431828457142857
0	0	0
0	0	0
0	0	0
0	-0.820474068571428	-0.18647581639838
0	0	0
0	0	0
0	0	1
0		

'G'   40   3

0	0	0
0	0	0
0	0	0
0	0	0
0	0	0
800000	0	0
0	64.2101954444935	0
0	0	0
0	0	0
0	0	0
0	0	0
0	0	0
0	0	0
0	0	0
0	0	0
800000	0	0

0	64.2101954444935	0
0	0	0
0	0	0
0	0	0
0	0	0
0	0	0
0	0	0
0	0	0
0	0	0
800000	0	0
0	64.2101954444935	0
0	0	0
0	0	0
0	0	0
0	0	0
0	0	0
0	0	0
0	0	0
0	0	0
800000	0	0
0	64.2101954444935	0
0	0	0
0	0	0
0	0	0

'Gam'   40   6

0	0	0
0	0	0
0	0	0
0	0	0
0	0	0
0	0	0
0	0	0
0	0	0
0	0	0
0	0	0
800000	0	0
0	0	0
0	64.2101954444935	0
0	0	0
0	0	1
0	0	0
0	0	0
1	0	0

0		0	0
0		0	0
0		0	0
0		0	0
0		0	0
0		0	0
0		0	0
0		0	0
0		0	0
0		0	0
0		0	0
0		0	0
800000		0	0
0		0	0
0	64.2101954444935	0	0
0		0	0
0		0	1
0		0	0
0		0	0
1		0	0
0		0	0
0		0	0
0		0	0
0		0	0
0		0	0
0		0	0
0		0	0
0		0	0
0		0	0
0		0	0
800000		0	0
0		0	0
0	64.2101954444935	0	0
0		0	0
0		0	1
0		0	0
0		0	0
1		0	0
0		0	0
0		0	0
0		0	0

0	0	0
0	0	0
0	0	0
0	0	0
0	0	0
0	0	0
0	0	0
0	0	0
0	0	0
800000	0	0
0	0	0
0	64.2101954444935	0
0	0	0
0	0	1
0	0	0
0	0	0
1	0	0
0	0	0
0	0	0

```
'Hs'          32    10
```

0	-0.0174532925199433	0
0.0174532925199433	0	0
0	0	0
0	-0.000219235550031075	0.0115523657760967
-1.78492186709551e-14	-0.017447868874039	1.24953387197017e-05
0	5.88067122436296e-15	-0.000203742488101851
0.000996920468836435	0.00024854849873372	0
0	0.0174532925199433	0
0	0	0
0	0	0
0	0	0
0.0174532925199433	0	0
0	0	0
0	1	0
0	0	0
0	0	0
0	0	0
0	0	0
0	0	0
0	0	0
0	0	0
0	0	0
0	0	0

0	0	0
0	0	0
0	0	0
0	0	0
-0.0174532925199433	0	0.0174532925199433
0	0	0
0	0	0
-0.000219235550031075	0.0115523657760967	-1.78492186709551e-14
-0.017447868874039	1.24953387197017e-05	0
5.88067122436296e-15	-0.000203742488101851	0.000996920468836435
0.00024854849873372	0	0
0.0174532925199433	0	0
0	0	0
0	0	0
0	0	0.0174532925199433
0	0	0
0	0	0
1	0	0
0	0	0
0	0	0
0	0	0
0	0	0
0	0	0
0	0	0
0	0	0
0	0	0
0	0	0
0	0	0
0	0	0
0	0	-0.0174532925199433
0	0.0174532925199433	0
0	0	0
0	0	-0.000219235550031075
0.0115523657760967	-1.78492186709551e-14	-0.017447868874039
1.24953387197017e-05	0	5.88067122436296e-15
-0.000203742488101851	0.000996920468836435	0.00024854849873372
0	0	0.0174532925199433
0	0	0
0	0	0
0	0	0
0	0.0174532925199433	0
0	0	0

0	0	1
0	0	0
0	0	0
0	0	0
0	0	0
0	0	0
0	0	0
0	0	0
0	0	0
0	0	0
0	0	0
0	0	0
0	0	0
0	0	0
0	-0.0174532925199433	0
0.0174532925199433	0	0
0	0	0
0	-0.000219235550031075	0.0115523657760967
-1.78492186709551e-14	-0.017447868874039	1.24953387197017e-05
0	5.88067122436296e-15	-0.000203742488101851
0.000996920468836435	0.00024854849873372	0
0	0.0174532925199433	0
0	0	0
0	0	0
0.0174532925199433	0	0
0	0	0
0	1	0
0	0	0
0	0	0
0	0	0
0	0	0
0	0	0
0	0	0
0	0	0
0	0	0
0	0	0
0	0	

'Dsu'   32   3

0	0	0

0	0	0
0	0	0
0	0	0
0	0	-1
0	0	0
0	0	0
0	0	0
0	0	0
0	0	0
0	0	0
0	0	0
0	0	-1
0	0	0
0	0	0
0	0	0
0	0	0
0	0	0
0	0	0
0	0	0
0	0	-1
0	0	0
0	0	0
0	0	0
0	0	0
0	0	0
0	0	0
0	0	0
0	0	-1
0	0	0
0	0	0
0	0	0

'Dsw'   32   6

0	0	0
0	0	0
0	0	0
0	0	0
0	0	0
0	0	0
0	0	0
0	0	0
0	0	0
0	0	0
0	0	0

0	0	0
0	0	0
0	1	0
0	0	0
0	0	1
0	0	0
0	0	0
0	0	0
0	0	0
0	0	0
0	0	0
0	0	0
0	0	0
0	0	0
0	0	0
0	0	0
0	0	0
0	0	0
0	1	0
0	0	0
0	0	1
0	0	0
0	0	0
0	0	0
0	0	0
0	0	0
0	0	0
0	0	0
0	0	0
0	0	0
0	0	0
0	0	0
0	0	0
0	0	0
0	0	0
0	1	0
0	0	0
0	0	1
0	0	0
0	0	0
0	0	0
0	0	0
0	0	0
0	0	0

0	0	0
0	0	0
0	0	0
0	0	0
0	0	0
0	0	0
0	0	0
0	1	0
0	0	0
0	0	1

'Hc'   8   10

1	0	0
0	0	0
0	0	0
0	0	-1
0	1	0
0	0	0
0	0	1
0	0	0
0	0	0
0	0	0
0	-1	0
1	0	0
0	0	0
0	1	0
0	0	0
0	0	0
0	0	0
-1	0	1
0	0	0
0	0	0
1	0	0
0	0	0
0	0	0
0	0	-1
0	1	0
0	0	0
0	0	

'Dcu'   8   3

0	0	-1
0	0	0
0	0	-1
0	0	0

			0	0	-1
			0	0	0
			0	0	-1
			0	0	0
'Dcw'	8	6			
			0	0	0
			0	0	0
			0	0	0
			0	-1	0
			0	0	0
			0	0	0
			0	0	0
			0	-1	0
			0	0	0
			0	0	0
			0	0	0
			0	-1	0
			0	0	0
			0	0	0
			0	0	0
			0	-1	0
'Wspec'	24	6			
			0	0	0
			0	0	1
			0	0	0
			0	0	1
			0	0	0
			0	0	1
			0	0	0
			0	0	1
			0	0	1.2
			1	1.2	0
			0	0	1.2
			0	1	1.2
			0	1	0
			0	1	0.2
			0	0	0
			0	0	1
			0	0	0
			0	0	1
			0	0	0
			0	0	1
			0	0	0

		0	0	1
		0	0	0
		0	0	1
		0	0	0
		0	0	1
		0	0.16	0
		0	1	2
		0	0	0
		0	0	1
		0	0	0
		0	0	1
		0	0	0
		0	0	1
		0	0	0
		0	0	1
		0	0	0
		0	0	1
		0	0	0
		0	0	1
		0	0	4.7
		0	0	1
		0	0	4.7
		0	0	1
		0	0	0
		0	0	1
		0	0	0
		0	0	1
'Alpha'	4	1		
		0	0	0
		0		
'Sigmamax'	4	1		
		0	1	1
		1		
'Zetamin'	4	1		
		0.6	0	0
		0		
'Q'	8	2		
		2	0	0
		2	0	0
		0	0	0
		0	0	0
		0	0	0
		0		

```
'R'              12    3
                        0                    0                    0
                        0                    0                    0
                        0                    0                    0
                       20                    0                    0
                        0                    0                    0
                        0                    0                    0
                        0                    0                    0
                        0                    6                    0
                        0                    0                    0
                        0                    0                    0
                        0                    0                    0
                        0                    0                    0
'nDircu'          4    1
                        0                    0                    0
                        2
'Dircu'           2    3
                        1                    0           1.80370E-05
                        2                    0           2.75000E-03
'nDircy'          4    1
                        0                    0                    0
                        0
'Dircy'           0    0
'A'               3    3
     0.000000000000000D+00    0.000000000000000D+00    0.000000000000000D+00
     0.000000000000000D+00    0.000000000000000D+00    0.000000000000000D+00
     0.000000000000000D+00    0.000000000000000D+00    0.000000000000000D+00
'B'               3    8
    -1.000000000000000D+00   -1.000000000000000D+00    0.000000000000000D+00
     0.000000000000000D+00    0.000000000000000D+00    0.000000000000000D+00
     1.745329251994330D-02    3.107520198881290D-02
     1.000000000000000D+00   -1.000000000000000D+00    0.000000000000000D+00
     0.000000000000000D+00    0.000000000000000D+00   -0.000000000000000D+00
    -1.745329251994330D-02    3.107520198881290D-02
     0.000000000000000D+00    0.000000000000000D+00    0.000000000000000D+00
     0.000000000000000D+00    0.000000000000000D+00    0.000000000000000D+00
     0.000000000000000D+00    1.000000000000000D+00
'C'               3    3
     3.834893369818892D-01    0.000000000000000D+00    0.000000000000000D+00
     0.000000000000000D+00    2.336031819451096D+00    0.000000000000000D+00
     0.000000000000000D+00    0.000000000000000D+00    9.059807189192843D-01
'D'               3    8
    -1.418948652779962D-01   -1.418948652779963D-01    0.000000000000000D+00
```

```
    0.0000000000000000D+00    0.0000000000000000D+00    0.0000000000000000D+00
    0.0000000000000000D+00    0.0000000000000000D+00
    3.431203419266172D+00   -3.431203419266172D+00    2.978752933689066D+00
    3.118447290949190D+00    0.0000000000000000D+00    0.0000000000000000D+00
    0.0000000000000000D+00    0.0000000000000000D+00
    0.0000000000000000D+00    0.0000000000000000D+00    0.0000000000000000D+00
    0.0000000000000000D+00    0.0000000000000000D+00    0.0000000000000000D+00
   -9.500731826474930D-02    0.0000000000000000D+00

'nAid'       1   1
                    0
'Aid'        0   0
'nBid'       1   1
                    0
'Bid'        0   0
'nCid'       1   1
                    3
'Cid'        3   5
                    1                1                1
                    0               20                2
                    2                1                0
                   20                3                3
                    1             0.85                1
'nDid'       1   1
                    7
'Did'        7   5
                    1                1                1
                  -20                0                1
                    2                1              -20
                    0                2                1
                    1                0               20
                    2                2                1
                  -20                0                2
                    3                1                0
                   20                2                4
                    1                0               20
                    3                7                1
                  -10               10
'Nclin'      1   1
                    6
'nLincoef'   6   1
                    2                2                2
                    2                2                2
'Lincoef'   12   4
```

```
                   1                      99                         1
                   1       +2.70263012146753                       100
                   1                       1
                   1
                 100                       1                         1
                  -1                     100                         1
                   2
                   1                      99
                   2                       2        -0.68081997305502
                 100                       2                         1

                   1                     100                         2
                   1                       1                       100
                   2                       2
  -0.86813650189418
                 100                       2                         1
                   1                     100                         2
                   3
  -0.90884943557678                     100
                   2                       1                         1
                 100                       2                         4
'Linbnds'     6     2
                   0                       0                         0
                   0                       0                         0
                   0                       0                         0
                   0                       0                         0
'Nudnlc'      1     1
                   0
```